



Universidade de  
Aveiro  
2019

Departamento de Química

**JOHANNA  
MADEIRA  
SIMÕES**

**REMOÇÃO DE PURINAS E ÁCIDOS  
NUCLEICOS UTILIZANDO MATERIAIS  
FUNCIONALIZADOS COM LÍQUIDOS  
IÓNICOS**

**PURINES AND NUCLEIC ACIDS REMOVAL  
WITH MATERIALS FUNCTIONALIZED WITH  
IONIC LIQUIDS**





Universidade de  
Aveiro  
2019

Departamento de Química

**JOHANNA  
MADEIRA  
SIMÕES**

**REMOÇÃO DE PURINAS E ÁCIDOS NUCLEICOS  
UTILIZANDO MATERIAIS FUNCIONALIZADOS COM  
LÍQUIDOS IÓNICOS**

**PURINES AND NUCLEIC ACIDS REMOVAL WITH  
MATERIALS FUNCTIONALIZED WITH IONIC  
LIQUIDS**

Dissertação apresentada à Universidade de Aveiro para cumprimento dos requisitos necessários à obtenção do grau de Mestre em Biotecnologia, realizada sob a orientação científica da Doutora Mara Guadalupe Freire Martins, Investigadora Coordenadora do Departamento de Química da Universidade de Aveiro, e coorientação da Doutora Márcia Carvalho Neves, investigadora de pós-doutoramento do Departamento de Química da Universidade de Aveiro.



## **O júri**

**Presidente**

**Professora Doutora Ana Maria Rebelo Barreto Xavier**  
Professora Auxiliar, Departamento de Química, Universidade de Aveiro

**Doutora Raquel Oliveira Cristóvão**  
Investigadora de Pós-Doutoramento, Faculdade de Engenharia da Universidade do Porto

**Doutora Márcia Carvalho Neves**  
Investigadora Auxiliar, Departamento de Química, Universidade de Aveiro



## Agradecimentos

A realização desta dissertação foi uma verdadeira aventura que me permitiu evoluir tanto a nível pessoal, como a nível intelectual. Este crescimento não teria sido possível sem o contributo de um grupo de pessoas muito especial, ao qual eu não poderia deixar de agradecer.

Em primeiro lugar, agradeço à minha orientadora, à Doutora Mara Freire, por me ter dado a oportunidade e confiança para trabalhar neste projeto e com este grupo fantástico que lidera. Pelo conhecimento transmitido, pela sua orientação e por toda a sua gentileza, um muito, muito obrigada.

Quero também exprimir a minha enorme gratidão à Doutora Márcia Neves, por todos os ensinamentos, pelo apoio constante, compreensão e paciência ao longo deste ano. Pela alegria, que tanto a caracteriza, motivação e confiança demonstradas, que foram fundamentais para a realização deste trabalho, um sincero obrigada.

Ao Doutor Augusto Pedro e à Leonor Castro, estou imensamente grata pela ajuda no protocolo da extração de DNA. Eles foram peças fundamentais para que esta tese pudesse ser completada.

A todo o grupo do PATH agradeço por me ter recebido tão bem. Especialmente à Rita Teles, Maria João Quental, Marguerita, Ana Rufino, Alexandre Santiago, Bobi, João Nunes, Andreia Fernandes, Teresa Dinis, Emanuel Capela e aos “visitantes” Nuno Silva, Rita Carapito e Abel Muñiz, um muito obrigada por toda a boa disposição, assim como pelo conhecimento transmitido sobre os métodos de laboratório que me ajudaram imenso no decorrer desta dissertação. Não poderia ter pedido melhores parceiros de laboratório!

Às “Pathinhas” (Maria Santos, Catarina Almeida e Jéssica Bairos), que se tornaram o sinónimo de grandes amizades, agradeço do fundo do coração por toda a camaradagem em todos os bons e menos bons momentos. Ao meu irmão, Philippe Simões, e à minha amiga, Mariana Correia, pela amizade e pela paciência de passar o “lápiz azul” no inglês do documento, o meu grande obrigada.

Aos meus amigos condeixenses, aveirenses e portuenses presto o meu grande agradecimento por todo o suporte, por não me deixarem ir abaixo nunca e por todo o encorajamento.

Por último, mas não menos importante, aos meus pais, a quem devo tudo. Por estarem sempre lá, por todo o apoio, dedicação e por nunca me deixarem baixar os braços. Por acreditarem em mim, um enorme obrigada.

A todos um grande obrigada!





## Palavras-chave

Materiais funcionalizados com líquidos iônicos, Adsorção, Remoção de DNAs  
Gota,

## Resumo

Os ácidos nucleicos e as purinas estão presentes em muitas bebidas fermentadas, nomeadamente na cerveja. Estes compostos são essencialmente provenientes do ADN do malte e da levedura responsável pela fermentação da cerveja. Estes, quando ingeridos por seres humanos, são catabolizados em ácido úrico, contribuindo para o aumento do seu nível sérico, a hiperuricemia, um fator de risco da gota. Esta doença causa inflamação e dor intensa e pode ser aguda ou crónica. Por esse motivo, no tratamento da gota, recomenda-se uma dieta com restrições de cerveja.

É por isso relevante desenvolver metodologias que consigam remover as purinas e os seus os precursores da cerveja. Neste sentido, surgiu os Líquidos Iônicos Suportados (LIS) que foram, então, estudados para adsorver compostos de purina e ADN de *Saccharomyces cerevisiae* a partir de soluções aquosas.

Cinco LIS com diferentes catiões e com o anião cloreto foram sintetizados e caracterizados usando várias técnicas: análise elementar, espectroscopia de infravermelho por transformada de Fourier com refletância total atenuada, ressonância magnética nuclear de  $^{13}\text{C}$  em estado sólido, potencial zeta, método de isotérmica BET E BJH para a caracterização de área de superfície e da estrutura de poros e, por fim, microscopia eletrónica de varrimento. De seguida, os materiais foram utilizados em ensaios de adsorção de purinas, de ADN e de um aminoácido- a tirosina.

Os LIS não demonstraram capacidade de remover purinas. Por outro lado, o ADN extraído de *Saccharomyces cerevisiae* foi utilizado para ensaios de adsorção. Os dados demonstraram que a adsorção de ADN é instantânea, não tendo sido possível ajustar modelos cinéticos aos dados experimentais. Dos cinco LIS sintetizados, três deles ( $[\text{Si}][\text{C}_3\text{C}_1\text{Im}]\text{Cl}$ ;  $[\text{Si}][\text{N}_{3114}]\text{Cl}$  e  $[\text{Si}][\text{N}_{3222}]\text{Cl}$ ) mostraram capacidade de remoção do ADN, sendo que o  $[\text{Si}][\text{C}_3\text{C}_1\text{Im}]\text{Cl}$  demonstrou ser o mais eficaz, com capacidade de remoção de 43,32  $\mu\text{g}$  por mg de material. Estes LIS não demonstraram capacidade de remoção de aminoácidos, fornecendo uma pequena prova de seletividade.

Mais estudos precisam de ser realizados, a fim de identificar materiais mais promissores que podem ser usados para remover compostos de purina e ADN da cerveja, a fim de evitar restrições devido a condições de hiperuricemia e gota.



**Keywords**

Materials functionalized with ionic liquids, Liquids, Adsorption, DNA removal, Gout

**Abstract**

Purines and nucleic acid are present in several fermented beverages, including beer. These compounds essentially come from malt and yeast DNA. When ingested by humans they are catabolized into uric acid, contributing to its serum level increase leading to hyperuricemia, a risk factor of gout. This disease causes inflammation and intense pain and can be acute or chronic. For this reason, in the treatment of gout, it is recommended a diet with beer restrictions.

Therefore, it is relevant to develop methodologies that can remove purines and their precursors from beer, in this way the Supported Ionic Liquids (SIL) that are studied for the adsorption of purine compounds and DNA *Saccharomyces cerevisiae* from aqueous solutions. Five SILs with different cations and chloride as counter ion were synthesized and characterized using several techniques: Elemental analysis, Fourier-Transform Infrared spectroscopy with attenuated Total Reflectance, Solid-State  $^{13}\text{C}$  NMR, point of zero charges, Surface area and pore structure characterization and Scanning electron microscope. Then the materials are used for purines, DNA and amino acids assays- Tyrosine.

SILs demonstrate no capacity to remove purines. On the other hand, the DNA extracted from *Saccharomyces cerevisiae* was used to performed adsorption assay. The data demonstrate that DNA adsorption is instantaneous, in this way, the models of kinetics are not applicable. Of the five synthesized SILs,  $[\text{Si}][\text{C}_3\text{C}_1\text{Im}]\text{Cl}$ ;  $[\text{Si}][\text{N}_{3114}]\text{Cl}$  and  $[\text{Si}][\text{N}_{3222}]\text{Cl}$  showed the ability to remove DNA.  $[\text{Si}][\text{C}_3\text{C}_1\text{Im}]\text{Cl}$  demonstrates to be the most efficient for DNA removal with a capacity of removal  $43.32 \mu\text{g}$  per mg of material.

These SILs don't demonstrate the adsorbed capacity for this amino acid removal, giving a little proof of selectivity.

Further studies are being carried out in order to identify more promising materials that can be used to remove purine compounds and DNA from beer to avoid beer restrictions due to hyperuricemia and gout conditions.



## Index

Index .....	i
List of Figures.....	v
List of tables .....	vii
List of annex Table .....	ix
List of abbreviations .....	xi
List of synthesized materials .....	xv
I - Introduction.....	1
1.1. Fermented drinks .....	3
1.2. DNA and beer purines .....	8
1.2.1. Purines origin .....	8
1.2.2. Types of purines .....	9
1.2.3. Beer as a strong source of purines.....	11
1.3. Gout disease .....	17
1.3.1. Pathogenesis .....	17
1.3.2. Epidemiology .....	18
1.3.3. Treatment and diet.....	19
1.4. Purines removal .....	20
1.4.1. Solid-phase extraction .....	21
1.4.2. Supported ionic liquids as alternative adsorbent materials .....	23
1.5. Scope and objectives.....	29
II- Experimental section .....	31
2.1. Materials .....	33
2.2. SILs synthesis .....	34
2.3. Supported Ionic liquids characterization .....	36
2.3.1. Elemental analysis.....	36

2.3.2.	Fourier-transform infrared spectroscopy (FTIR) with Attenuated total reflectance	36
2.3.3.	Solid state <sup>13</sup> C nuclear magnetic resonance (Solid state <sup>13</sup> C NMR)	36
2.3.4.	Point zero charge	37
2.3.5.	Surface area and pore structure characterization	37
2.3.6.	Scanning electron microscope (SEM)	37
2.4.	Saccharomyces cerevisiae DNA extraction	37
2.5.	Adsorption assays	38
2.5.1.	Purines adsorption assays	39
2.5.2.	DNA adsorptions assays	39
2.5.2.1.	DNA Kinetics	40
2.5.2.2.	DNA Isotherm	41
2.5.3.	Error analysis of the data	43
III -	Results and discussion	45
3.1.	Materials synthesis and characterization	47
3.1.1.	Elemental analysis	47
3.1.2.	FTIR-ATR	49
3.1.3.	Solid-state <sup>13</sup> C NMR	50
3.1.4.	Zeta Potential (ZP)	53
3.1.5.	Brunauer-Emmett-Teller	55
3.1.6.	Scanning electron microscope (SEM)	56
3.1.7.	Purines adsorption	58
3.1.8.	DNA adsorption	62
3.1.8.1.	Kinetics determination assays	63
3.1.8.2.	Isothermal DNA assay	68
3.1.9.	Selective assays	73

IV-Conclusions and future work .....	75
V- Bibliography.....	79
Annexes .....	1
A. Properties of molecules.....	2
B. Purine calibration curves .....	4
C. Proprieties of cation precursor .....	6
D. DNA Kinetic assays.....	7
E. DNA isotherms assays .....	10





## List of Figures

<b>Figure 1</b> - Scheme of brewing process .....	6
<b>Figure 2</b> - Formation of beer compounds by yeast metabolism during fermentation .....	7
<b>Figure 3</b> – Helicoidal structure and chemical structure of DNA. ....	9
<b>Figure 4</b> – Base purine structure. ....	9
<b>Figure 5</b> - Several structures of purines. ....	10
<b>Figure 6</b> - Outline of the De novo synthetic pathway for purines .....	12
<b>Figure 7</b> - Overview of the breakdown of purines to uric acid. ....	15
<b>Figure 8</b> - Proposed mechanism for adenine nucleotide degradation during ethanol metabolism. ....	16
<b>Figure 9</b> – Purines metabolism (summary of chapter 3). ....	17
<b>Figure 10</b> - Schematic diagram showing the progression of gout from stage 1 (asymptomatic hyperuricaemia), 2 (acute), 3 (intercritical), to 4 (chronic tophaceous) .....	18
<b>Figure 11</b> - Structure of some cations and anions that could be used to form ILs. ....	24
<b>Figure 12</b> - Schematic illustration of synthesis of ionic liquid-modified polymer. ....	27
<b>Figure 13</b> - Molecular structures of caffeine and theophylline. ....	28
<b>Figure 14</b> - Preparation of the functionalized silica with propylmethylimidazolium chloride. ....	34
<b>Figure 15</b> – FTIR-ATR spectra of silica, [Si][C <sub>3</sub> ]Cl and SILs. ....	50
<b>Figure 16</b> - Solid-state <sup>13</sup> C NMR spectrum of [Si][C <sub>3</sub> ]Cl. ....	51
<b>Figure 17</b> - Solid-state <sup>13</sup> C NMR spectrum of [Si][C <sub>3</sub> C <sub>1</sub> Im]Cl. ....	51
<b>Figure 18</b> - Solid-state <sup>13</sup> C NMR spectrum of [Si][N <sub>3114</sub> ]Cl. ....	52
<b>Figure 19</b> - Solid-state <sup>13</sup> C NMR spectrum of [Si][N <sub>3222</sub> ]Cl. ....	52
<b>Figure 20</b> - Solid-state <sup>13</sup> C NMR spectrum of [Si][N <sub>3444</sub> ]Cl and [Si][N <sub>3888</sub> ]Cl .....	53
<b>Figure 21</b> - Potential zeta as a function of pH values for all synthesized SIL. ....	54
<b>Figure 22</b> - SEM images of Silica. ....	56
<b>Figure 23</b> - SEM images of [Si][C <sub>3</sub> C <sub>1</sub> Im]Cl. ....	56
<b>Figure 24</b> - SEM images of [Si][N <sub>3114</sub> ]Cl. ....	56
<b>Figure 25</b> - SEM images of [Si][N <sub>3222</sub> ]Cl. ....	57
<b>Figure 26</b> - SEM images of [Si][N <sub>3444</sub> ]Cl. ....	57
<b>Figure 27</b> - SEM images of [Si][N <sub>3888</sub> ]Cl. ....	57

<b>Figure 28</b> - Adenine adsorption assays, after 24 hours in contact with SILs synthesized. This absorbance corresponds 2 times of dilution concentration.....	58
<b>Figure 29</b> - Adenosine adsorption assays, after 24 hours in contact with SILs synthesized. This absorbance corresponds to 2 times of dilution concentration. ....	59
<b>Figure 30</b> - Inosine adsorption assays, after 24 hours in contact with SILs synthesized. This absorbance corresponds 2 times of dilution concentration.....	59
<b>Figure 31</b> - Guanosine adsorption assays, after 24 hours in contact with SILs synthesized. This absorbance corresponds 2 times of dilution concentration.....	60
<b>Figure 32</b> – Charge of the compounds tested as a function of pH, based on pK <sub>a</sub> .....	61
<b>Figure 33</b> – DNA adsorption assays, after 1 hour in contact with SILs. ....	62
<b>Figure 34</b> – Adsorption efficiencys of DNA with diferentes SILs, using an initial concentration of 27.25 ug/mL .....	63
<b>Figure 35</b> – DNA kinetic assay with [Si][C <sub>3</sub> C <sub>1</sub> Im]Cl with representation of pseudo-first order (PFO) and pseudo-second order (PSO) kinetic models for [Si][C <sub>3</sub> C <sub>1</sub> Im]Cl. ....	64
<b>Figure 36</b> - Experimental values of q <sub>t</sub> (μg/mg) of DNA as a function of time (min) and representation of pseudo-first order (PFO) and pseudo-second order (PSO) kinetic models for [Si][N <sub>3114</sub> ]Cl.....	65
<b>Figure 37</b> - DNA kinetic assay with [Si][N <sub>3222</sub> ]Cl. ....	65
<b>Figure 38</b> - Adsorption isotherms of DNA onto SILs at room temperature: A) [Si][C <sub>3</sub> C <sub>1</sub> Im]Cl; B) [Si][N <sub>3114</sub> ]Cl and C) [Si][ Propyl dimethyl butylamine chloride N <sub>3222</sub> ]Cl .....	69
<b>Figure 39</b> – Tyrosine adsorption assays, after 30 minutes contact with SILs .....	73

## List of tables

<b>Table 1</b> – Differences between Lager and Ale beer.....	4
<b>Table 2</b> - Chemical composition of beer, adapted from Buiatti <i>et al.</i> <sup>8</sup> .....	7
<b>Table 3</b> - Structure of guanine and its nucleosides and nucleotides .....	10
<b>Table 4</b> - Standard nomenclature of the major nucleic acid bases, nucleosides, and nucleotides.....	11
<b>Table 5</b> - Review of literature on purine removal materials. ....	21
<b>Table 6</b> - ILs in the food industry .....	25
<b>Table 7</b> - Extraction and Separation of Small and Extractable Organic Compounds Using IL-Modified Materials in SPE. ....	26
<b>Table 8</b> – Reagents used in the synthesis of the materials and preparation of solutions and their respective purity and providers. ....	33
<b>Table 9</b> - Source of the cation and representation of the corresponding SIL. ....	35
<b>Table 10</b> –SILs elemental analysis. ....	47
<b>Table 11</b> – SILs Bounding amount. ....	49
<b>Table 12</b> - Table with PZC values for silica, [Si][C <sub>3</sub> ]Cl and each SIL.....	54
<b>Table 13</b> - BET surface area ( $S_{BET}$ ), pore surface area (A), pore volume (V) and pore size diameter (Dp) of silica, [Si][C <sub>3</sub> ]Cl and SILs. ....	55
<b>Table 14.</b> $q_t$ values ( $\mu\text{g}/\text{mg}$ ) corresponding to the primary study of DNA adsorption. .	62
<b>Table 15</b> - Kinetic parameters for the pseudo-first-order (PPO) and pseudo-second-order (PSO) models for the different synthesized SIL.....	66
<b>Table 16</b> - Parameters and correlation coefficients obtained with the Langmuir, Freundlich and Sips models regarding the adsorption isotherms of DNA onto the three SILs.....	70
<b>Table 17</b> - The maximum capacities of DNA adsorption/extraction by various materials reported in the literature .....	72



## List of annex Table

<b>Tab. 1</b> – Purines properties (structure, molecular formula, and weight, CAS, Water solubility, melting point Log $K_{ow}$ and pKa (Strongest acid and strongest basic)); adapted from .....	2
<b>Tab. 2</b> – Amino acids properties (structure, molecular formula, an weight, CAS, Water solubility, melting point Log $K_{ow}$ and pKa (Strongest acid and strongest basic)) .....	3
<b>Tab. 3</b> - Values used of Volume (V), Molar mass (M), density and % of w/w.....	6
<b>Tab. 4</b> – Adsorption time (minutes) used for kinetics assay with [Si][C <sub>3</sub> C <sub>1</sub> Im]Cl and respective results: absorbance obtained (with FD = 2),% removal efficient (%) and amount of ug DNA adsorbed per gram of material. ....	7
<b>Tab. 5</b> - Adsorption time (minutes) used for kinetics assay with [Si][N <sub>3114</sub> ]Cl and respective results: absorbance obtained (with FD = 2).% removal efficient (%) and amount of ug DNA adsorbed per gram of material. ....	8
<b>Tab. 6</b> - Adsorption time (minutes) used for kinetics assay with [Si][N <sub>3222</sub> ]Cl and respective results: absorbance obtained (with FD = 2).% removal efficient (%) and amount of ug DNA adsorbed per gram of material. ....	9
<b>Tab. 7</b> - Equilibrium concentration of DNA after adsorption ( $C_e$ ), the concentration of adsorbate in the solid phase ( $q_e$ ), at room temperature. ....	10



## List of abbreviations

<b>ADP</b>	Adenosine diphosphate
<b>AMP</b>	Adenosine monophosphate
<b>APPRT</b>	Adenine phosphoribosyltransferase
<b>APRT</b>	Amidophosphoribosyl transferase
<b>ATP</b>	Adenosine triphosphate
<b>AE</b>	Adsorption efficiency
<b>BA</b>	Bounding amount
<b>BET</b>	Brunaver-Emmett-Teller
<b>BJH</b>	Barrett-Joyner-Halenda
<b>CE</b>	Capillary electrophoresis
<b>C<sub>e</sub></b>	Concentration of adsorbate at equilibrium
<b>CEC</b>	Capillary electrochromatography
<b>C<sub>i</sub></b>	Initial concentration of adsorbate
<b>cGMP</b>	Cyclic guanosine monophosphate
<b>CPMAS</b>	Cross-Polarization Magic Angle Spinning
<b>dAMP</b>	Deoxyadenosine 5'-monophosphate
<b>dGMP</b>	Deoxyguanosine 5'-monophosphate
<b>DNA</b>	Deoxyribonucleic acid
<b>DNase</b>	Deoxyribonucleic acid nuclease
<b>FDA</b>	Food and Drug Administration
<b>FD</b>	Factor dilution
<b>FTIR-ATR</b>	Fourier-transform infrared spectroscopy with Attenuated total reflectance
<b>GC</b>	Gas Chromatography
<b>GTP</b>	Guanosine triphosphate
<b>HGPPRT</b>	Hypoxanthine-guanine phosphoribosyltransferase
<b>HPLC</b>	High-performance liquid chromatography
<b>IL</b>	Ionic Liquids
<b>IMP</b>	Inosine monophosphate
<b>k<sub>1</sub></b>	Pseudo-first-order constant

<b>k<sub>2</sub></b>	Pseudo-second-order constant
<b>k<sub>F</sub></b>	Freundlich constant associated the bonding energy of sorption
<b>k<sub>L</sub></b>	Langmuir constant associated the bonding energy of sorption
<b>k<sub>s</sub></b>	Sips constant associated the bonding energy of sorption
<b>LC</b>	Liquid Chromatography
<b>logk<sub>ow</sub></b>	n-octanol/water partition coefficient
<b>MSU</b>	Monovalent Sodium Salt Urate
<b>n<sub>f</sub></b>	Freundlich constant
<b>n<sub>s</sub></b>	Sips constant
<b>NMR</b>	Nuclear magnetic resonance
<b>PFO</b>	Pseudo First Order
<b>PIL</b>	Polymeric ionic liquid
<b>PNP</b>	Purine nucleoside phosphorylase
<b>PPi</b>	Pyrophosphate
<b>PRPP</b>	5-phosphoribosyl-1-pyrophosphate
<b>PRPPS</b>	Phosphoribosylpyrophosphate Synthetase.
<b>PSAC</b>	Pitch-based spherical activated carbon
<b>PSO</b>	Pseudo Second Order
<b>PZC</b>	Point of zero charges
<b>q<sub>e</sub></b>	Equilibrium concentration of adsorbate in solid phase
<b>q<sub>máx</sub></b>	Maximum monolayer coverage capacity of the adsorbent
<b>q<sub>t</sub></b>	Concentration of adsorbate in solid phase at time t
<b>RNA</b>	Ribonucleic acid
<b>RNAse</b>	Ribonucleic acid nuclease
<b>S<sub>BET</sub></b>	Surface area
<b>SEM</b>	Scanning electron microscopy
<b>SIL</b>	Supported Ionic Liquids
<b>SPE</b>	Solid-phase extraction
<b>SPME</b>	Solid-phase microextraction
<b>Tris-HCL</b>	Tris(hydroxymethyl)aminomethane hydrochloride
<b>UA</b>	Uric acid
<b>UV-Vis</b>	Ultra - visible and visible



<b>XMP</b>	Xanthosine monophosphate
<b>XO</b>	Xanthine oxidase
<b>ZP</b>	Zeta Potential



## List of synthesized materials

[Si][C <sub>3</sub> ]Cl	3-chloropropylsilane
[Si][C <sub>3</sub> C <sub>1</sub> Im]Cl	Propylmethylimidazolium chloride
[Si][N <sub>3114</sub> ]Cl	Propyldimethylbutylamine chloride
[Si][N <sub>3222</sub> ]Cl	Propyltriethylamine chloride
[Si][N <sub>3444</sub> ]Cl	Propyltributylamine chloride
[Si][N <sub>3888</sub> ]Cl	Propyl trioctylamine chloride



# **I - Introduction**



## 1.1. Fermented drinks

Alcoholic beverages have been used in human societies since prehistoric times<sup>1,2</sup>. As with the discovery of other foods, it can be assumed that alcoholic beverages were discovered by accident<sup>3</sup>. As for definition, alcoholic beverages are drinks that contain the chemical compound of ethyl alcohol (or ethanol), a colorless and flammable liquid<sup>4,5</sup>.

Ethanol for human consumption is exclusively obtained by the alcoholic fermentation of the sugar- or starch-containing material, like grains, fruits, honey, and others<sup>4</sup>. The use of synthetic ethanol manufactured from the hydration of ethylene for food purposes is not permitted in most parts of the world<sup>4</sup>.

The categorization of alcoholic beverages is usually based on production methods and ethanol content and is divided into spirits distilled beverages and fermented beverages<sup>4</sup>. Spirits distilled beverages are produced by the distillation of ethanol after fermentation, and its alcohol content is higher than in fermented beverages<sup>4,6</sup>. Fermented drinks are a type of alcoholic beverage that is prepared only through the fermentation process and has low alcohol content<sup>4,6</sup>. An example of fermented beverages is beer<sup>7</sup>.

The name beer originates from the Latin term *biber* and the earliest evidence of its production dates to, approximately 6000 BC in the Mesopotamian and ancient Egypt regions<sup>8</sup>. This drink is not only the oldest alcoholic beverage but also the most important in terms of the number of volumes produced worldwide<sup>1,8</sup>. Beer is the third most popular drink worldwide after tea and coffee, being the most preferred alcoholic beverage<sup>9</sup>. In addition, it is increasingly popular due to the diverse positive effects on health<sup>1,10-12</sup>. Over centuries, pieces of evidence have shown its beneficial effect in preventing cardiovascular, neurodegenerative, osteoporotic, gynecological and neoplastic diseases<sup>13</sup>.

Portuguese legislation defines beer, such as: “a drink obtained by alcoholic fermentation, by means selected **yeasts** from the genus *Saccharomyces*, of a wort made from cereal malt, **mainly barley**, which **hop flowers** and potable **water** have been added”<sup>14</sup>.

There are several classifications for distinguishing the different types of beers. Such as alcohol content (alcohol-free, low, medium or high alcohol content); color (light or dark); content of the primitive extract (weak, normal, extra and strong) and especially the type of fermentation<sup>15</sup>. According to the type of fermentation<sup>15</sup>, beer can be classified into two groups covering practically all types of commercial beers, Lager and Ale, being the Lager the most common<sup>15</sup>. The main differences between Lager and Ale beer are represented in Table 1.

**Table 1** – Differences between Lager and Ale beer.

	<b>Lager beer</b>	<b>Ale beer</b>
<b>Yeast genus</b>	<i>Saccharomyces pastorianus</i> <sup>16</sup>	<i>Saccharomyces cerevisiae</i> <sup>16</sup>
<b>Time of fermentation</b>	7-12 days <sup>16</sup>	5-7 days <sup>16</sup>
<b>Temperature of fermentation</b>	5-10 °C <sup>16</sup>	15 - 27 °C <sup>16</sup>
<b>Yeast flocculation</b>	Bottom of the fermentation tank <sup>16</sup>	Top of the fermentation tank <sup>16</sup>
<b>Alcoholic content</b>	4 to 5% <sup>16</sup>	3 to 10% <sup>16</sup>
<b>Characteristics of beer</b>	Gilded, transparent, light and with good foam <sup>16</sup>	Dense, fruity beer <sup>16</sup>

The ingredients of beer are malt, yeast, hops, water, and sometimes other starch adjuncts like rice and syrup<sup>15</sup>. Brewing lies in converting natural food materials (barley) into a pleasing beverage (beer)<sup>17</sup>. The brewing beer process contains several steps, including:

- **Malting:** several stages (milling, stepping, germination and kilning) that convert raw grain barley into malt<sup>18</sup>. As an ingredient, malt provides saccharides, proteins, free amino nitrogen, and enzymes<sup>16,18</sup>. In addition, it is a major contributor to the final color and body characteristics of the beer<sup>16</sup>. To produce malt, barley grains are first steeped in aerated water and then germinated at 15–20 °C for 3–7 days<sup>16</sup>. After the barley germinates, the sprouts are removed, leaving a medium rich with  $\alpha$  and  $\beta$ -amylase, proteases, and their respective substrates<sup>16</sup>. The malt is kilned, under controlled temperatures, to remove the water without inactivating the desired enzymes<sup>16</sup>.

- **Mashing:** occurs when the malt is mixed with boiling water followed by a resting period at a temperature between a 40 °C and 75 °C (to enhance amylases and proteases activity)<sup>16</sup>. At this time, occurs the hydrolyze of starch, protein and  $\beta$ -glucans, to release simple sugars (maltose, maltotriose and smaller amounts of sucrose, glucose and fructose) as substrate, and other nutrients that can be assimilated by the yeast<sup>19</sup>: Within a few hours, the process is complete, and the temperature is increased to at least 75 °C to inactivate the enzymes<sup>16</sup>. In the end, is obtained the wort, that contains the soluble compounds<sup>16</sup>.

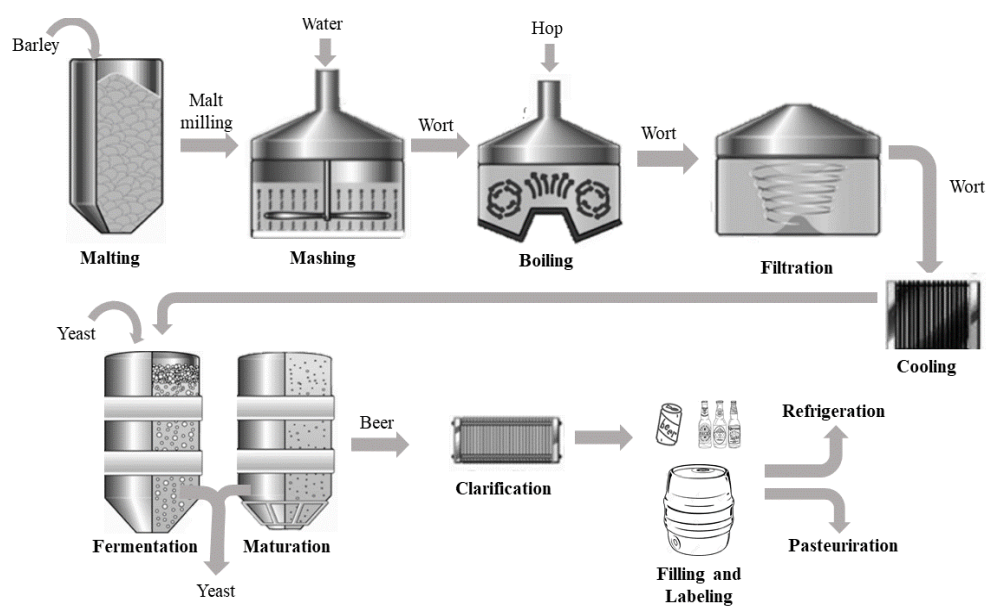


- **Wort processing:** boiling, filtration, and cooling<sup>16</sup>. The wort is transferred into a heating tank, hops are added before the mixture is boiled (1-2 hours)<sup>16,20</sup>. The hop is the flower of a plant called *Humulus lupulus*<sup>15</sup>. As an ingredient, it makes a great contribution to the aroma, flavor, and stability of beer<sup>15</sup>. Objectives of boiling of the wort are: kill all the vegetative microorganisms and inactivate enzymes remaining after mashing; enhance extraction of essential oils from the hops and remove undesirable volatiles<sup>16</sup>. After boiling, the wort is separated from the spent hops, cooled rapidly, and placed into a fermentation vessel<sup>16</sup>.

- **Fermentation and maturation (second fermentation):** fermentation is the crucial step to obtain beer<sup>20</sup>. In fermentation, the wort is inoculated with brewers' yeast<sup>16,20</sup>. The yeast produces alcohol, carbon dioxide, and some additional flavor constituents. Fermentation occurs at a controlled temperature for 5-15 days, it depends on the pretended beer type (Table 1)<sup>16,20</sup>. In traditional brewing, maturation of the beer occurs during storage at 0 °C for several days<sup>16</sup>. This step allows the beer to develop its final flavor, color, and body characteristics<sup>16</sup>.

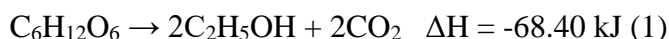
- **Finished process:** beer suffers several processing phases in preparation for distribution to the consumer - clarification, packaging, and pasteurization<sup>16,20</sup>. Clarification occurs to suspended solids precipitate and yeast flocculate<sup>16</sup>. After that, beer can be packed inside bottles, cans or kegs<sup>16</sup>. Lastly, packaged beer may or may not be pasteurized<sup>16</sup>. If it is not pasteurized, it must be stored under refrigeration temperatures to maintain quality<sup>16</sup>.

Figure 1 demonstrates the stages of beer production.



**Figure 1** - Scheme of brewing process, adapted from Wunderlich, Zürcher, & Back<sup>129</sup>

Fermentation is one of the most effective methods of processing beverages acceptable to man, and the most crucial step to obtain beer<sup>21</sup>. This oldest biotechnological process enhances the nutritional quality of raw ingredients by improving the digestibility of nutrients and inactivating anti-nutritional factors<sup>21</sup>. During fermentation, the most important reaction is the conversion of wort sugars into ethanol and carbon dioxide by yeasts, which happens in anaerobic conditions<sup>20</sup>. This conversion is represented by the overall Gay-Lussac exothermic reaction (Equation 1)<sup>20</sup>:



This reaction demonstrates the start and end compounds of the alcoholic fermentation. Fermentable sugars of the wort (maltose, maltotriose and smaller amounts of sucrose) are hydrolyzed to glucose<sup>20,22</sup>. During the glycolic pathway, glucose is converted into pyruvate<sup>20,22</sup>. In the next step, pyruvate suffers decarboxylation, resulting in carbon dioxide (CO<sub>2</sub>, responsible for beer carbonation) and acetaldehyde<sup>20,22</sup>. Later, acetaldehyde is reduced to ethanol<sup>20,22</sup>. The main products of the fermentation are ethanol and carbon dioxide. As a result, they are the major constituents of the beer besides water. Though, yeast metabolism results in several by-products (Figure 2), which are present in the final beer at low

concentrations and have a very important contribution to the aroma and flavor profile of beers<sup>20,23</sup>.

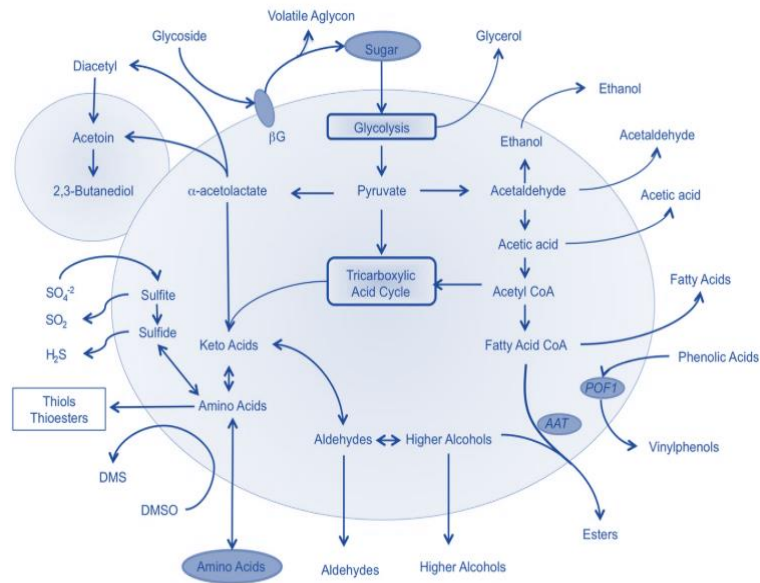


**Figure 2** - Formation of beer compounds by yeast metabolism during fermentation, from Bokulich *et al.* 2013<sup>22</sup>.

The composition of beer is represented in Table 2. These compounds are the result of all process of brewing.

**Table 2-** Chemical composition of beer, adapted from Buiatti *et al.*<sup>8</sup>.

Substances	Concentration	Source or agent
Water	90-94%	-
Ethanol	3-5% v/v	Yeast, malt
Carbohydrates	1-6% w/v	Malt
Carbon dioxide	3,5-4,5 g/L	Yeast, malt
Inorganic salts	500-4000 mg/L	Water, malt
Phenolic compounds	150-350 mg/L	Malts, hops
Organic acids	50-250 mg/L	Yeast, malt
Higher Alcohols	100-300 mg/L	Yeast, malt
Aldehydes	30-40 mg/L	Yeast, hops
Esters	25-40 mg/L	Yeast, malt, hops
Sulfur compounds	1-10 mg/L	Yeast, malt, hops

Hop derivates	20-60 mg/L	Hops
Vitamin B compounds	5-10 mg/L	Yeast, malt
Total nitrogen content	300-1000 mg/L	Yeast, malt

The compounds represented in Table 2 are very significant for the profile of the beer. However, in this work, the focus is nitrogen content, which is derived from malt and Yeast metabolism and it includes amino acids, peptides, polypeptides, nucleic acids, and their derivatives, amines and heterocyclic compounds<sup>24</sup>. Especially, products derived from the degradation of nucleic acids, which include purine compounds (free bases, nucleotides, and nucleosides), that come from Malt and Yeast deoxyribonucleic acid (DNA)<sup>24,25</sup>.

During the mashing and malting, the highly active nucleases degrade the nucleic acid contained in the malt into nucleotides, which are further hydrolyzed to nucleosides and phosphates<sup>24</sup>. Then, a portion of the nucleosides is degraded into sugars and free bases<sup>24</sup>. The majority of free bases, sugars, and nucleosides remain in the wort<sup>24</sup>.

## 1.2. DNA and beer purines

### 1.2.1. Purines origin

As referred to in the previous chapter the purines presence into beer is due to nucleic acids from yeast and malt DNA<sup>16,17,26</sup>.

DNA is an important element of the living cell that contains genomic information<sup>27</sup>. The structure of the DNA is a double helix (Figure 3 (a)), consisting of two polynucleotide chains<sup>27,28</sup>. Each chain consists of a random repetition of nucleotides that are connected to each other through hydrogen bonds<sup>28</sup>. Each nucleotide contains a phosphate group, a sugar group and a nitrogen base (Figure 3 (b))<sup>28</sup>. The bases are the purines comprised of adenine (A) and guanine (G), and the pyrimidines comprised of thymine (T) and cytosine (C)<sup>28</sup>. The stability of the DNA molecule is governed by the hydrogen bonds between the purines and pyrimidines (two hydrogen bonds for A-T and three for G-C), the  $\pi$ -stacking of the bases, and the screening of the negative charges carried by the phosphate groups on its backbone<sup>27</sup>.

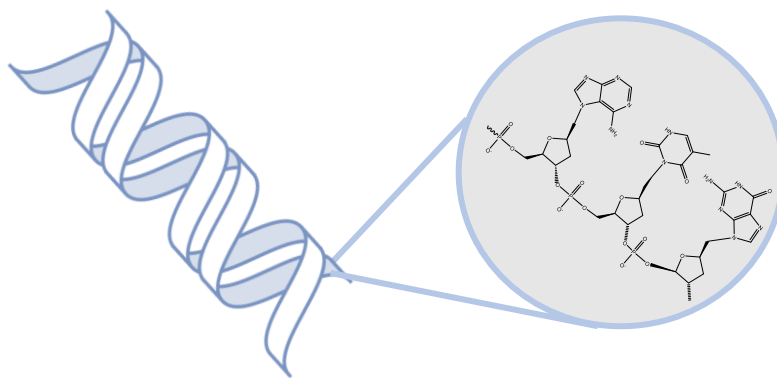


**Figure 3** – Helicoidal structure (a) and chemical structure of DNA (b).

The nitrogen bases present in DNA are pyrimidines and purines. However, in this work the target is purines.

### 1.2.2. Types of purines

Purines are known to play an important role in animals, bacteria, fungi, viruses, and plants, as well as in other organisms<sup>7</sup>. They are the most widely distributed aromatic nitrogen heterocycle in nature, which consists of a six-membered pyrimidine ring fused to a five-membered imidazole ring (Figure 4)<sup>29,30</sup>.

Purines structures have in total nine atoms, four of them are nitrogen atoms present at the 1, 3, 7, and 9 positions. The numbering of purine starts with the first nitrogen of the six-membered ring and then proceeds in an anticlockwise direction. The imidazole ring is numbered clockwise<sup>7,29,30</sup>.

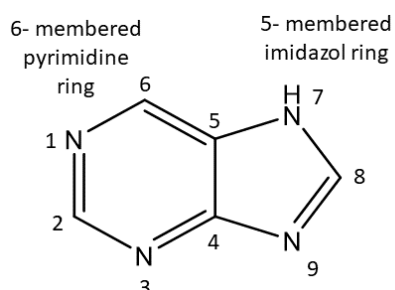


**Figure 4** – Base purine structure.

Purines compounds include bases, nucleosides, nucleotides and polymeric forms. In Figure 5 are represented the purine bases that comprise adenine (A), guanine (B), hypoxanthine (C), xanthine (D), uric acid (E), and isoguanine (F)<sup>29,30</sup>.

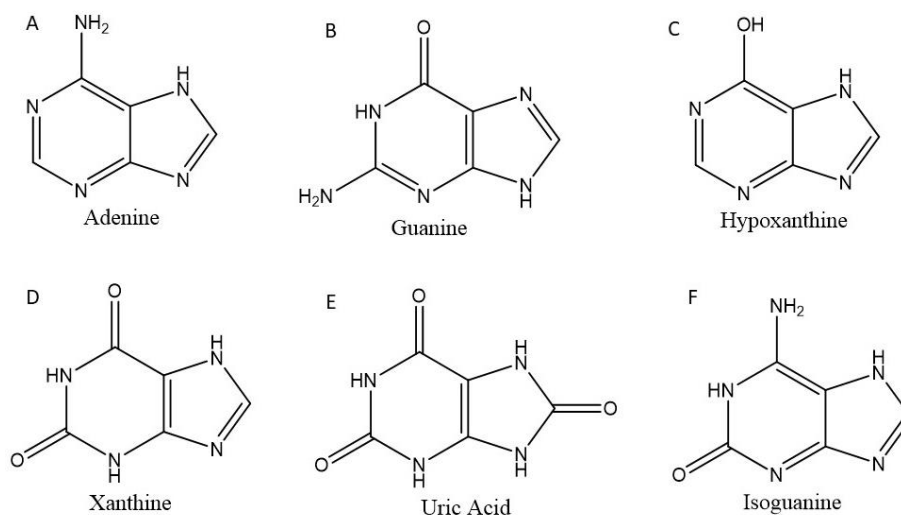


**Figure 5-** Several structures of purines. (A) adenine, (B) guanine, (C) hypoxanthine, (D) xanthine, (E) uric acid and (F) isoguanine

When a purine base connects through the ninth nitrogen atom with the carbon-1 'of a pentose (ribose or deoxyribose) results in a nucleoside<sup>29</sup>. The addition of one to three phosphate groups to nucleoside outcomes a nucleotide (Table 3)<sup>29</sup>.

**Table 3-** Structure of guanine and its nucleosides and nucleotides

Base	Nucleoside	Nucleotide
<p>Chemical structure of Guanine base, showing the fused bicyclic purine ring system with a carbonyl group at the 6-position and an amino group at the 2-position.</p>	<p>Chemical structure of Guanosine nucleoside, showing the guanine base attached to the N9 position of a ribose sugar at the C1 position.</p>	<p>Chemical structure of Guanosine monophosphate nucleotide, showing the guanosine nucleoside with a phosphate group attached to the C5' carbon of the ribose sugar.</p>

Table 4 summarizes the nomenclature of some association between purines and their nucleosides and nucleotides (with the addition of one group phosphate).

**Table 4** - Standard nomenclature of the major nucleic acid bases, nucleosides, and nucleotides.

Base	Nucleoside (Base+ Sugar)	Nucleotide (Base +sugar +1 phosphate)
Adenine	Adenosine	Adenosine monophosphate (AMP)
Guanine	Guanosine	Guanosine monophosphate (GMP)
Xanthine	Xanthosine	Xanthosine monophosphate (XMP)
Hypoxanthine	Inosine	Inosine monophosphate (IMP)
Adenine	Adenosine	Deoxyadenosine 5'-monophosphate (dAMP)
Guanine	Guanosine	Deoxyguanosine 5'-monophosphate (dGMP)

In humans, the most common expression of purines is found in the form of deoxyribonucleic acid (DNA) and ribonucleic acid (RNA) (containing the purines adenine and guanine bases), as well as single-molecule nucleotides (adenosine triphosphate [ATP] (for energy storage), nicotinamide adenine dinucleotide (NAD) (electron transporter in biochemical cell reactions), adenosine diphosphate [ADP], AMP, cyclic AMP (molecule responsible for signal transduction), and to a lesser extent, guanosine triphosphate [GTP] (energy transporter) and cyclic guanosine monophosphate [cGMP])<sup>31</sup>.

### 1.2.3. Beer as a strong source of purines

Foremost, it is important to understand the sources of purines in humans, and they are three main sources:

- ***De novo* synthesis from small molecules present in the body.**

This biochemical strategy occurs mainly in the liver and combines small molecules together step by step to form the purine ring<sup>29</sup>. This synthesis begins with the formation of 5-phosphoribosyl-1-pyrophosphate (PRPP) by condensation of pyrophosphate (PPi) and ribose 5'-phosphate<sup>29</sup>. This reaction is catalyzed by phosphoribosylpyrophosphate synthetase (PRPPS)<sup>29</sup>. Afterward, amidophosphoribosyl transferase (APRT) converts PRPP to 5-phosphoribosyl-1-amine, which consists of the addition of an amino group from the amino acid glutamine<sup>29</sup>. The 5-phosphoribosyl-1-amine is the precursor to synthesize the

first fully-formed nucleotide, IMP<sup>29</sup>. From this step, IMP can be converted into AMP or GMP. Each is formed through a different pathway that requires free energy from the hydrolysis of ATP or GTP respectively<sup>29</sup>. Figure 6 systematize this mechanism.

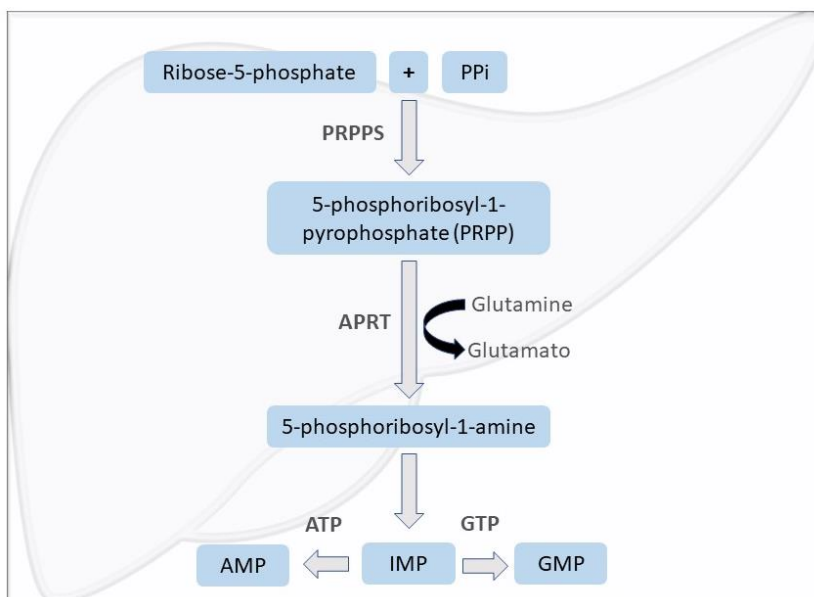
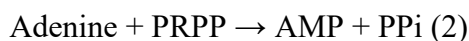


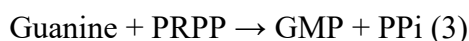
**Figure 6** - Outline of the *De novo* synthetic pathway for purines, adapted from Ahmed & James<sup>29</sup>.

- **Salvage pathway**

The main objective of this mechanism is the synthesis of nucleotides, through the recycling purine bases and nucleosides, expensing less metabolic energy<sup>29</sup>. In this biological system, free purine bases obtained in the diet or from the metabolic turnover of nucleotides can be reused or salvaged<sup>29</sup>. On one hand, this process uses the activity of adenine phosphoribosyltransferase (APPRT) to converts salvages free adenine into AMP (equation 2)<sup>29,32</sup>.



On another hand, it involves hypoxanthine-guanine phosphoribosyltransferase (HGPPRT) that converts not only guanine to GMP (equation 3) but can also catalyze the conversion of hypoxanthine to IMP (equation 4)<sup>29,32</sup>.





- **Dietary intake.**

Dietary purines through the ingestion of certain drinks and foods<sup>25,29,33</sup>. In these food products, the main source of purines is nucleic acids, which are degraded through the action of certain enzymes<sup>30,34</sup>. The resulting purines can be absorbed in the nucleoside or base form by the small intestine and then enter the purine metabolic pathway<sup>29</sup>.

Many studies on the determination of purine bases in alcoholic beverages and wort have been conducted. Until recently, high-performance liquid chromatography (HPLC), gas chromatography (GC) and capillary electrophoresis (CE) were the main tools in beer analysis<sup>7,17,25,34</sup>. Several authors concluded that beers contain high levels of purines, derived both from the mash and from yeast activity during fermentation being one the highest source of purines<sup>7,16,17</sup>. According to several reports, the nucleoside guanosine is the most abundant, in comparison with other types of purines<sup>7,34-36</sup>.

The pioneering work of Harris and Parsons<sup>26</sup> showed by means of paper chromatography the presence of certain nucleosides (adenosine and guanosine) and free bases (adenine and guanine) in the wort.

Latter another study demonstrated that British beer and Lager beer each contain many different types of purines, such as adenine, hypoxanthine, adenosine, and guanosine<sup>35</sup>. In this work, the average purine nitrogen content of seven British beers was 22.2 mg/L<sup>35</sup>. Of this, 61% was present as guanosine<sup>35</sup>. The total purine nitrogen and guanosine content of Lager was slightly lower (17.7 mg/L; of this 6.9 mg/L was guanosine; 3.5 mg/L was xanthine, 3.0 mg/L was hypoxanthine and 4.3 mg/L was adenine)<sup>35</sup>. Also, according to Charalambous and colleagues<sup>37</sup>, the average total purine nitrogen content of American beers was 22.3 mg/L, of which guanosine comprised 71%. In another work with Japanese beer was concluded that this beer contains greater amounts of purines, including purine nucleosides (inosine, guanosine, adenosine) and purine bases (hypoxanthine, xanthine, guanine, and adenine), with guanosine being the most abundant<sup>7</sup>.

In 2015, H. Li *et al*<sup>25</sup> measured purine contents of several drinks and conclude that it was much higher in fermented malt drinks (mean content 72.87 mg/L) than the others measured alcoholic beverages (mean content: 0.22 mg/L in Chinese spirits, 45.99 mg/L in rice wine, and 29.67 mg/L in wine)<sup>25</sup>.

#### 1.2.4. Purines catabolism

Uric acid (UA) is the end product of purines catabolism<sup>30,38,39</sup>. Such as described in topic 3.1., UA is a C<sub>5</sub>H<sub>4</sub>N<sub>4</sub>O<sub>3</sub> heterocyclic organic compound and has a molecular weight of 168 Da<sup>30,39,40</sup>. After consumption, nucleotides are decomposed in the intestinal tract<sup>29</sup>. There, they can be absorbed or converted into purine and pyrimidine bases<sup>29,40</sup>. Afterward, several enzymes are responsible for the transformation of adenine and guanine to UA<sup>29,30,40,41</sup>. Thus, UA is formed by the liver and mainly excreted by the kidneys (65-75%) and intestines (25-35%)<sup>38</sup>.

In the liver occurs the transformation of AMP in inosine<sup>29,39,40</sup>. This transformation can occur in two different ways. Either removing an amino group by deaminase to form IMP followed by dephosphorylation with nucleotidase to form inosine or by first removing a phosphate group with nucleotidase to form adenosine followed by deamination to form inosine<sup>39,40</sup>. At the same time, GMP is converted to guanosine also by nucleotidase<sup>39,40</sup>. The nucleosides, inosine, and guanosine are further converted to purine base hypoxanthine and guanine, respectively, by purine nucleoside phosphorylase (PNP)<sup>39,40</sup>. Hypoxanthine is then oxidized to form xanthine by xanthine oxidase (XO), and guanine is deaminated to form xanthine by guanine deaminase<sup>39,40</sup>. Xanthine is again oxidized by XO to form the final product, UA<sup>34,40</sup>. This compound has a very important function in humans<sup>38</sup>. Due to its structure with double bonds, this compound exhibits a good antioxidant activity, responsible for the majority of total plasma antioxidant capacity and protects blood vessels from being damaged<sup>38</sup>. Figure 7 systematizes the formation of uric acid.

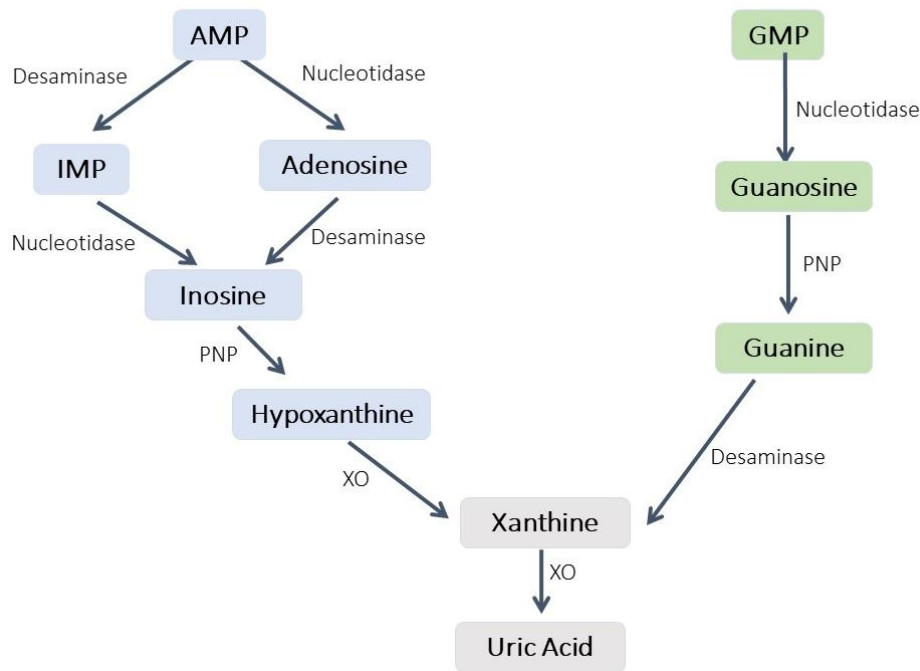


**Figure 7** - Overview of the breakdown of purines to uric acid.

At physiologic pH, UA is a weak acid with a pKa of 5.8 and circulates in plasma (pH 7.4) predominantly in the form of monovalent sodium salt (urate) (MSU)<sup>29,39,40</sup>. The solubility of UA in water is low and consequently in blood plasma too<sup>29,39,40</sup>. In humans, the UA average concentration in the blood is close to the solubility limit (6.8 mg/dL)<sup>29,40</sup>. When the level of UA is higher than this value, MSU crystals can be formed<sup>29,40</sup>. As urate concentration increases in the blood, uric acid crystal formation increases<sup>29,40</sup>.

### 1.2.5. Hyperuricemia: a problem of purines consumption

Hyperuricemia is an elevated UA level in the blood and is defined as  $\geq 7$  mg/dL for men and  $\geq 6.0$  mg/dL for women<sup>42</sup>. This elevated level of UA is the result of increased production (liver), decreased excretion of UA (kidneys and intestines), or a combination of both processes<sup>29</sup>. The reduction in excretion is the main cause of hyperuricemia in patients with gout<sup>29</sup>.

There are many factors that contribute to hyperuricemia, including obesity, insulin resistance, alcohol consumption, hypertension, renal insufficiency, among other causes<sup>43</sup>.

Alcohol (ethanol) is the most harmful, being not only relevant ingested ethanol volume, but also the type of alcoholic beverage, daily drinking habits, and genetic makeup<sup>43</sup>.

Lieber *et al.*<sup>44</sup> demonstrated a direct relationship between increased serum UA levels and alcohol consumption, proposing that lactic acid formed during the metabolism of alcohol interfered with the urinary excretion of uric acid<sup>44</sup>. Thus leading to increased plasma concentration<sup>44</sup>. It is also known that during the metabolism of alcohol, ATP is abruptly consumed, followed by its degradation into UA, as demonstrated in Figure 7<sup>43</sup>.

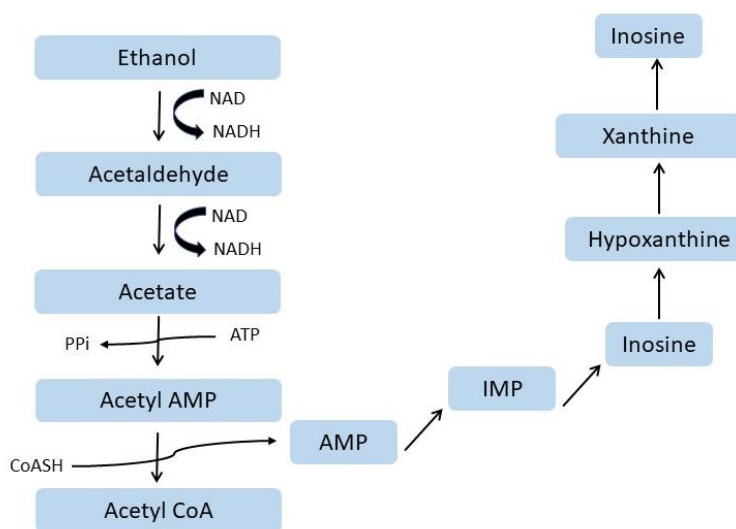


**Figure 8** - Proposed mechanism for adenine nucleotide degradation during ethanol metabolism, adapted from Yamamoto *et al.*<sup>43</sup>.

Focusing on beer, in addition to containing ethanol, this beverage also contains greater amounts of purines including nucleosides and bases, with guanosine being the most abundant<sup>45</sup>. Thus, guanosine is more quickly absorbed and converted to uric acid via guanine and xanthine and it may increase the serum concentration of uric acid<sup>45</sup>. Figure 9 summarizes the information described in Chapter 3: the source of purines in humans, the metabolism of purines and the quick catabolism of guanosine in beer (grey).

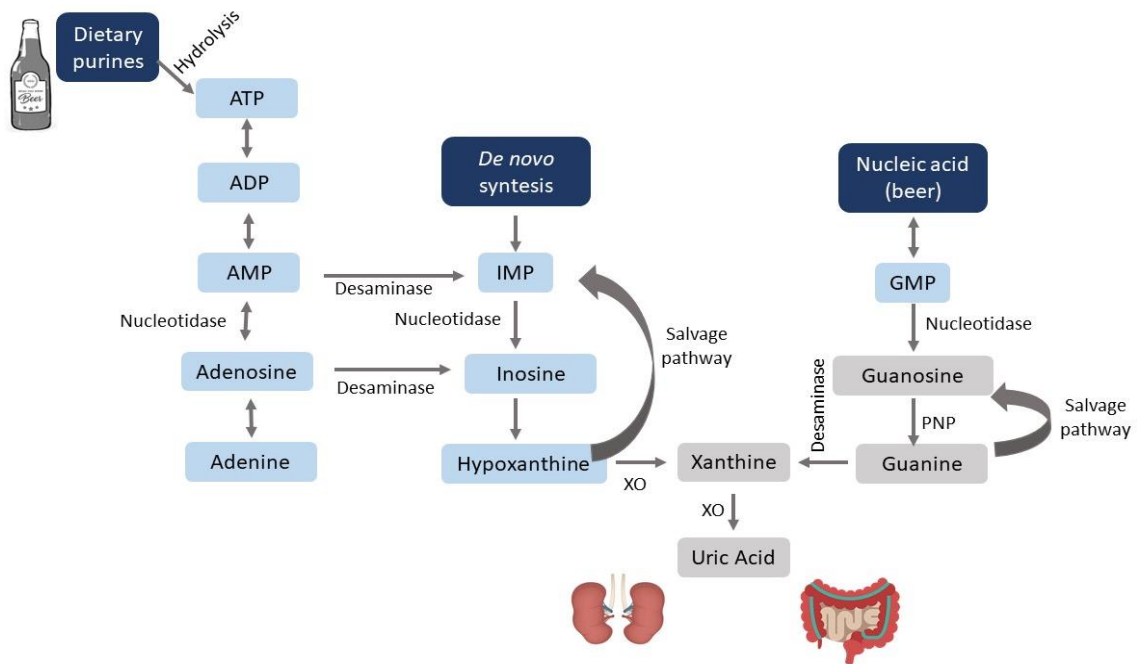


**Figure 9** – Purines metabolism (summary of chapter 3), adapted from Moriwaki & Yamamoto<sup>45</sup>.

### 1.3. Gout disease

#### 1.3.1. Pathogenesis

Although gout is usually associated with hyperuricemia, it is important to emphasize that not all individuals with hyperuricemia develop gout, but almost always patients diagnosed with gout had asymptomatic hyperuricemia for several years<sup>46</sup>.

Gout is defined as inflammatory arthritis caused by the crystallization of UA, which deposits inside the joint<sup>29,33</sup>. It is considered one of the most painful forms of arthritis, characterized by the abrupt onset of severe joint pain<sup>33</sup>. Patients often have symptoms swellings around the joints that are drastically painful<sup>29</sup>.

This disease could be categorized into four stages: **asymptomatic hyperuricemia** (stage 1); **acute gouty arthritis** (stage 2) (the MSU crystals present in the joint are phagocytosed by leukocytes, leading to the most frequent initial manifestation of gout); **intercortical gout** (stage 3) (period between acute attacks of gout with total absence of symptoms), and **chronic tophaceous gout** (stage 4) (accumulation of crystals at various

locations, revealing a prolonged and evolved state of the disease)<sup>29,46</sup>. Figure 10 shows the progression of gout.

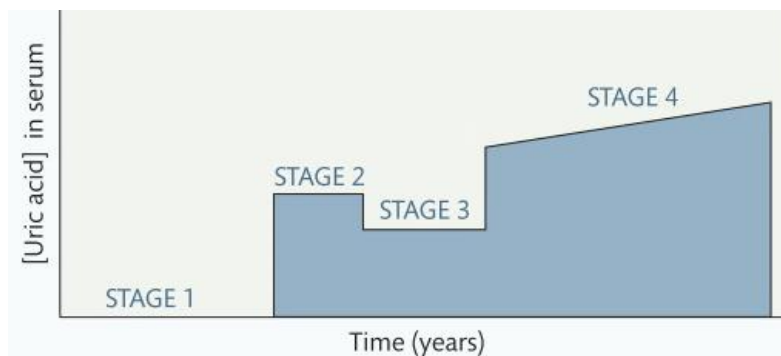


**Figure 10** - Schematic diagram showing the progression of gout from stage 1 (asymptomatic hyperuricaemia), 2 (acute), 3 (intercritical), to 4 (chronic tophaceous) from Ahmed & James<sup>4</sup>.

It is still not well clarified the factors that control crystal formation, but those affecting urate solubility, such as temperature, pH, salt concentration, and cartilage matrix components, might contribute to the process<sup>47</sup>. In peripheral joints with lower tissue pH and temperature, monosodium urate crystallization can occur at urate concentrations lower than 408  $\mu\text{mol/L}$ <sup>47</sup>. Nucleation occurs when monosodium urate molecules have clustered and reached a critical stable mass and are no longer susceptible to dissolution within the solvent<sup>47</sup>.

### 1.3.2. Epidemiology

Epidemiological evidence suggests that the prevalence of gout has increased in recent decades<sup>38,46,47</sup>. Also, the occurrence of this disease can be influenced by a variety of factors: age, gender, genetic predisposition, and diet, due to their contributions to hyperuricemia development<sup>38,46,47</sup>.

In UK and US studies, the incidence of gout varies from 0,30 per 1000 person-years in the 1970s to 2,68 per 1000 person-years in the 2000s<sup>48</sup>. In western developed countries, the prevalence of gout is 3–6% in men and 1–2% in women<sup>47</sup>.

Also, according to The National Health and Nutrition Examination data, in the United States of American, the prevalence of gout in 2007-2008 was 3.9% (8,3 million adults), corresponding to 5.9% in men and 2.0% in women<sup>46</sup>.

In Portugal, an epidemiologic study performed with a representative sample in Oporto concluded that the values of hyperuricemia are lower relatedly in the USA but have been increasing in the last years<sup>46,47</sup>. The prevalence of hyperuricemia was 12,8%, being higher in men<sup>46,47</sup>.

It was also identified the peak incidence of acute gout that occurs between 30 to 50 years of age<sup>47</sup>.

### **1.3.3. Treatment and diet**

Nowadays, there is still no cure for gout. However, exists treatment that consists of medication or a restrictive diet<sup>46</sup>. The choice of treatment depends on the clinical phase of the disease and the patient's specific risk factors, such as high serum urate, body weight, and alcohol consumption<sup>46</sup>.

Generally, the pharmacological treatment for hyperuricemia is to use allopurinol, which acts for example as an inhibitor of the xanthine oxidase enzyme (responsible for converting hypoxanthine to xanthine and into uric acid)<sup>49</sup>.

In cases of gouty arthritis, it is recommended colchicine, a drug used primarily in the first 24 hours after the crisis<sup>46,49</sup>. In this situation, it also recommended non-steroidal anti-inflammatory drugs<sup>46,49</sup>. The goal of the treatment at this stage is pain relief and elimination of inflammation in the joints<sup>46,49</sup>. During the second stage (between the attacks) it is given to the patient drugs that lower urate concentration which helps to prevent future attacks<sup>46,49</sup>.

Notwithstanding various pharmaceutical options, it is also advised weight control, reduction on the intake of alcohol, and lifestyle changes such as limiting consumption of foods rich in purines, restrictions in the consumption of meat, seafood, vegetables, and others high-purine-content foods<sup>29,46,47</sup>.

Alcoholic beverages are not recommended, mainly beer, due to their content of alcohol and purines, which further hyperuricemia and the risk of gout<sup>41,46</sup>. These dietary changes are essential and enhance the effectiveness of every pharmaceutical treatment<sup>29,46</sup>.

#### 1.4. Purines removal

In order to contradict the close relation of beer with hyperuricemia and gout, some efforts have been carried out to reduce the total purine content in the food industry either via enzymatic degradation processes or using adsorbent materials.

Regarding enzymatic methods, Shibano *et al.* disclose a brewing process wherein nucleoside phosphorylase is activated in beer to degrade nucleoside in the wort. In this process, purine nucleosides are degraded to purine bases using an enzyme. These purine bases are assimilated to yeast in the fermentation step. Then, is obtained beer with a reduced content of purine compounds. This method has disadvantages since it depends on the degradation rate of purine nucleosides, the purine bases that were originally present in the wort and the assimilation rate by yeast<sup>50</sup>. In other words, the removal cannot be accomplished in totality.

Jankowska *et al.*<sup>49</sup> developed a novel enzyme system that decreases the purine concentration of food products<sup>49</sup>. This system consists of an enzyme mixture that contains 4 purine-degrading enzymes: adenine deaminase, guanine deaminase, xanthine oxidoreductase, and urate oxidase, which simultaneously break down purines to a water-soluble 5-hydroxyisourate<sup>49</sup>. Urate oxidase is an enzyme that is not synthesized by humans, however, it is possessed by yeast *Arxula adenivorans*<sup>49</sup>. The urate oxidase converts uric acid to 5-hydroxyisourate, thus preventing uric acid accumulation<sup>49</sup>. This cocktail was studied in a rolled fillet of ham<sup>49</sup> but hereafter could be applied in other products, namely in fermented malt beverages.

In short, the enzymatic method can reduce purines content but doesn't remove it completely<sup>49</sup>. In addition, the use of enzymes in the food industry has major problems, namely finding urate oxidases that preserve their activity in a manner compatible with food storage conditions for long periods<sup>49</sup>. Beyond this, the production of enzymes has high costs and further research must be done before being used commercially<sup>49</sup>. Given this, several studies were conducted in order to remove, by adsorption methods, purine compounds from solutions for instance with some novel materials.



### 1.4.1. Solid-phase extraction

During the last years, significant efforts have been devoted to developing and characterize new advanced sorbent materials for solid-phase extraction (SPE) in order to improve selectivity or specificity towards target analytes<sup>51</sup>. Sorbent materials use the adsorption phenomenon, in other words, they lead to the adhesion of a molecule of one fluid volume to a solid surface<sup>52,53</sup>. Solids that are used to adsorb dissolved substances are called adsorbents; the adsorbed molecules are usually referred to as the adsorbate<sup>52,53</sup>. This can occur because of physical forces or chemical bonds<sup>52,53</sup>. Usually, it is reversible, that is, the drop of a molecule from a solid surface is called desorption<sup>52,53</sup>. This process has many industrial applications, include food industries<sup>52</sup>.

In this way and involving the problem of gout, some researchers developed several materials that have the capacity for removal of purines compounds. Until now, some adsorbents such as activated carbon, macroporous polymer granule, zinc oxide/activated carbon and polyethyleneimine/SiO<sub>2</sub> have been tested for their potential application to remove purines and DNA (Table 4)<sup>54</sup>.

**Table 5** - Review of literature on purine removal materials.

Type of adsorbent	Material	Adsorbate and source	References
Activated carbon	Pitch-based spherical activated carbon (PSAC) by vapor deposition of NH <sub>3</sub>	UA in blood samples	55
Activated carbon	Zinc oxide nanoparticles loaded on activated carbon	UA in blood samples	56
Carbon nanotubes	Metallic and semiconducting single-wall carbon nanotubes	Adenine, thymine, and their radicals in DNA samples	27
Carbon nanotubes	Choline monolayer supported multiwalled carbon nanotubes film	Guanine, adenine, thymine, and cytosine from aqueous solutions	57
Carbon nanotubes	Electrodes Modified with Carbon Nanotubes	Nitrogen bases and their derivatives r	58

Carbon nanotubes	Glassy carbon electrode modified with “as commercially received” multiwalled carbon nanotubes	UA, xanthine, and hypoxanthine	59
Chromatography	Hydrophilic interaction chromatography	Purine and pyrimidine bases and nucleosides	60
Clay Minerals	Co <sup>2+</sup> , Ni <sup>2+</sup> , Cu <sup>2+</sup> , and Fe (III) montmorillonite	Nucleic Acid Bases, Ribose, and Phosphate	61
Graphene	Pristine and Ni-decorated graphene's	Adenine aqueous solutions	62
Graphene	Graphene	Single-stranded DNA from aqueous solutions	63
Graphite	Aqueous Graphite and Au (111)	DNA fragments	64
Macroporous polymer granule	2-hydroxyethyl methacrylate and ethylene glycol dimethacrylate in the shape of granules	UA in blood samples	65
Phyllosilicates	Pyrophyllite, chlorite, lizardite, and chrysotile suspended in an aqueous saline solution	RNA and DNA monomers	66
Silica	Polyethyleneimine was grafted onto the surface of silica gel, coupling effect of $\gamma$ -chloropropyl trimethoxysilane	UA in blood samples	67

Focusing on fermented drinks, some studies reported the use of adsorbent materials in beer. In 1974, Buday & Belleau<sup>68</sup> reveals the use of activated carbon for recovery and concentration of nucleic acid derivatives, guanine or guanosine, from biological samples, such as wort and beer<sup>68</sup>. Nevertheless, the use of finely powdered activated carbon involves several difficulties and inconveniences, namely: the difficulty to package finely powdered activated carbon because of the dust; when finely powdered activated carbon is added to the liquid to be treated, sedimentation will take a long time<sup>68</sup>. Besides, the resulting sediment is very loose and tends to be whirled up as the supernatant clarified liquid is siphoned off, resulting in losses<sup>68</sup>.

To increase the performance in the treatment of beer, the activated carbon was mixed with silicic acid, preferably fine powder (with a particle size <45  $\mu\text{m}$ )<sup>69</sup>. Later, was develop

an adsorbent which selectively adsorbs purine compounds, activated charcoal with an average pore diameter of 1 - 3.5 nm<sup>70</sup>.

In 2009, Shibata, Murayama, & Tateyama<sup>71</sup> researched the effect of the physical properties of activated carbon derived from beer lees on the adsorption behavior of purine compounds. It was concluded that the beer lees activated carbon can remove purine compounds and that the removal performance of beer lees activated carbon almost equals to the commercial activated carbon<sup>71</sup>. However, this material has the behavior like a molecular sieve in the sense that the adsorption ability decreases for relatively small purine compounds such as adenine while the adsorption ability increases for relatively large purine compounds such as AMP<sup>71</sup>. In short, adsorption/removal of purine compounds using activated charcoal yet displaying low selectivity, cause also amino acids, flavors, and essential nutrients are removed or purines with high molecular weight aren't removed, limiting thus their widespread application<sup>71</sup>.

In this context, it is crucial to develop efficient techniques for the removal of purine compounds from alcoholic beverages. In addition, it is essential that the new material synthesized is selective in order to keep the flavors and the aroma profile of beers.

#### **1.4.2. Supported ionic liquids as alternative adsorbent materials**

Ionic liquids (ILs) are salts with a melting temperature below the boiling point of water (100°C), usually close to room-temperature<sup>72,73</sup>. They are typically composed of large organic cations (e.g., imidazolium, pyrrolidinium, pyridinium, tetraalkylammonium, tetraalkylphosphonium) and by an organic or inorganic anion (e.g., tetrafluoroborate, hexafluorophosphate, bromide)<sup>74,75</sup>. This allows that ILs possess an array of properties that make them attractive for academy and industry: extremely low vapor pressure, high thermal and chemical stabilities, non-flammability, high solvent capacity and is considered as a green solvent<sup>76,77</sup>. Moreover, ILs have been recognized as tunable designer solvents, a result of a large number of cation-anion combinations and the possibility of designing task-specific fluids<sup>74</sup>. Figure 11 shows the structure of some of the most common cations and anions that form ILs.

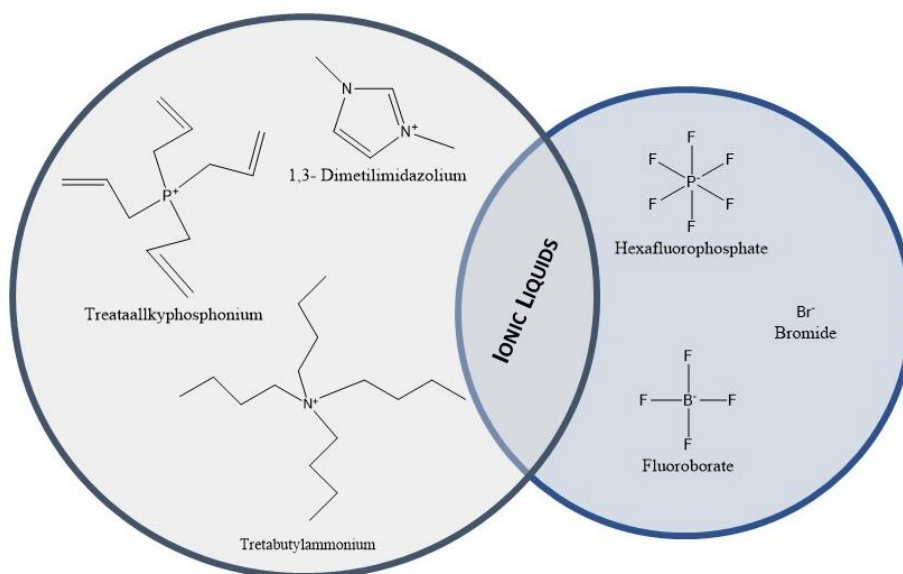


**Figure 11** - Structure of some cations and anions that could be used to form ILs<sup>74</sup>.

ILs are attractive compounds that are applied in several fields such as organic synthesis, electrochemistry, liquid-phase extraction, catalysis for clean technology and polymerization processes<sup>78</sup>.

The literature on food science and technology involving ILs is still scarce<sup>79</sup>. Until now, their use is not regulated by the Food and Drug Administration (FDA), International Food Standards (Codex Alimentarius) and the European Union legislation<sup>80</sup>. This is because toxicological studies still present large gaps, especially those concerning toxicity toward mammals or human cells<sup>79</sup>. To deal with such a problem, ILs based on ions obtained from natural sources, such as cholinium, amino acids, organic acids derivatives have emerged<sup>79</sup>.

In this context, there are several studies related to food industry process that promises to be commercially applied in the future due to the many advantages of ILs<sup>80</sup>. The prospects of IL uses are food analysis, treatment of food waste, extraction of some compounds, surfactant and solubility agent and enzymatic activity inductor<sup>79</sup>. To the best of our knowledge, ILs have not yet been applied in research related to the alcoholic beverage industry. In Table 6 are summarized studies where ILs have been applied.

**Table 6 - ILs in the food industry**

IL	Process	Objective	Reference
1-butyl-3-methylimidazolium chloride	Catalyst and solvent	Conversion of xylose into furfural	81
1-butyl-1-methylpyrrolidinium bis(trifluoromethylsulfonyl) imide	Solvent extractor	Separation of vitamin D	82
tetrabutylphosphonium chloride	Solvent extractor	Extraction and stability of bovine serum albumin	83
1-hexyl-3-methyl-imidazolium bromide	Solvent extractor	Determinate isoflavones in soy food	84
1-butyl-3-methyl-imidazolium bromide	Solvent extractor	Determination of acrylamide content in coffee and milk	85

Although the advantages are the same, sometimes ILs are more efficient when immobilized in materials<sup>86</sup>. Supported ionic liquids (SIL) refer to ILs that are immobilized on solid, polymer or aerogel supports by either covalent or noncovalent bonding, using different methods<sup>73</sup>. ILs can be immobilized on solid supports by physical and chemical techniques<sup>87</sup>. The physical immobilization of an IL can be performed through several techniques, such as simple impregnation, sol-gel method or encapsulation<sup>87</sup>. The chemical immobilization happens when ILs moieties are supported on solids via a covalent bond, resulting in functionalized materials<sup>87</sup>. The solid supports used for immobilization include inorganic porous materials and polymer, such as activated carbon, silica gel, polystyrene resin, and polymer membranes<sup>87</sup>. One of the most used support materials is silica because is a low cost and it is biocompatible material<sup>88</sup>.

When ILs are immobilized on the silica surface, they lost the liquid state<sup>75</sup>. However, the other properties, such as polarity and be a tunable designer are maintained. The power of these materials consists of their dual nature: they could act as low-polarity phases for non-polar compounds and in the opposite manner for compounds bearing strong proton-donor groups<sup>75</sup>. This behavior depends on the separation mechanism, which involves multiple interactions (electrostatic, hydrophobic,  $\pi$ )<sup>75</sup>.

SILs are among the most important branches in the IL community and has been applied in both fundamental research and practical applications<sup>73,74</sup>. Over the last years, SILs have been used as functional materials for supports of catalysts, the surface modifying agents, stationary phases in separation technologies, and electrodes in electrochemistry<sup>73</sup>.

The first application of SILs was done in 2005 on the extraction of aromatic compounds (benzene, toluene, ethylbenzene, and xylene) from paints using a Solid Phase Micro Extraction technique<sup>89</sup>.

Relatively to the food industry, in recent years, several works have been carried out with the objective of extracting and separating bioactive compounds, amino acids and proteins using silica or polymers as solid phases<sup>74</sup>.

An overview of the application of IL- modified silica or polymers in the extraction and separation of small organic extractable compounds is provided in Table 7.

**Table 7** - Extraction and Separation of Small and Extractable Organic Compounds Using IL-Modified Materials in SPE.

Target	Source	SIL	Remark
Alkaloid oxymatrine (Bioactive compound)	<i>Sophora flavescens</i> Ait	Imidazolium [BF <sub>4</sub> <sup>-</sup> ] [PF <sub>6</sub> <sup>-</sup> ] and [NTf <sub>2</sub> <sup>-</sup> ] based silica	Short-chain imidazolium ILs showed to be the most effective <sup>90</sup>
Protocatechuic, ferulic, and caffeic acids (Bioactive compound)	<i>Salicornia herbacea</i> L	Imidazolium chloride-based silica	Recovery yields of 94.69%, 79.09%, and 87.32% <sup>91</sup>
Phenolic acids and flavonoids (Bioactive compound)	Raw propolis	1-Butyl-3-methylimidazolium chloride ([C <sub>4</sub> MIm]Cl), 1-hexyl-3-methylimidazolium chloride ([C <sub>6</sub> MIm]Cl) 1-octyl-3-methylimidazolium chloride ([C <sub>8</sub> MIm]Cl) based silica.	Performances of this method were satisfactory <sup>92</sup>
Lactic acid	Fermentation broth	Imidazole- based silica (SilprIm)	Recovery yield of 91.9% <sup>93</sup>
D-Phe (Amino acids)	Aqueous media	[C <sub>2</sub> (L-Phe)][NTf <sub>2</sub> <sup>-</sup> ]-based silica	Recovery yields of 97.35% at pH 3.0 <sup>94</sup>

Imidazolium-based ILs have been the preferred choice for the modification of silica. Most of the mentioned compounds have many hydroxyl groups. Thus, it is possible that the aromatic imidazolium/pyridinium rings may be responsible for some specific interactions, including  $\pi \cdots \pi$  interactions and additional hydrogen-bonding interactions, with the target compounds, resulting therefore in higher selectivity and extraction efficiencies<sup>74</sup>. Also, due to the anion that is not covalently attached to the solid material, it is very important to guarantee the lack of ionic exchange during the separation of the target biocompounds<sup>74</sup>. Furthermore, it is important to emphasize that the optimization of the performance of these processes should be carried out case-by-case, taking into account the specific chemical characteristics of the target molecules being extracted and of the main contaminants present, so that IL-modified materials can be properly designed<sup>74</sup>.

Once the selective ability of SILs has been proven, it is important to focus on the aim of this MSc dissertation. In bibliography research, only one study was found relating purines and SILs and another relating DNA and IL-modified materials.

About purines, Tian and co-workers<sup>95</sup> further prepared a methylimidazolium-modified polymer for the extraction of caffeine and theophylline from green tea extracts<sup>95</sup>. The modified stationary phase synthesis was performed with 1-methylimidazole and the chemical reaction is represented in Figure 11. The IL-modified polymer sorbents showed a high affinity to the analytes and were applied successfully as a special adsorbent of SPE to extract the two compounds from extracts of green tea<sup>95</sup>.

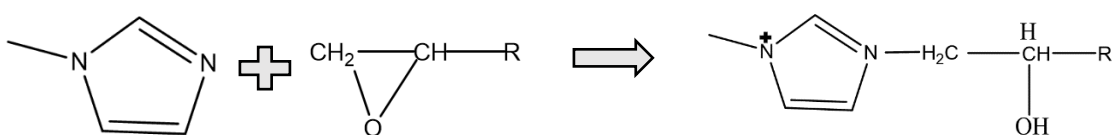


**Figure 12** - Schematic illustration of synthesise of ionic liquid-modified polymer, adapted from Tian *et al.*<sup>95</sup>.

Regarding the structures of caffeine and theophylline (Figure 12), there is one more methyl linked with a nitrogen atom in caffeine than in theophylline<sup>95</sup>. This methyl group decreases the interaction of the nitrogen atom between caffeine and ionic liquid-modified polymer<sup>95</sup>. This fact indicated that the ionic liquid-modified polymer had a higher interaction with theophylline<sup>95</sup>. The extracted amounts of caffeine and theophylline, taken from green teen (20 mg/mL), were 0.025 mg/mL and 0.58 mg/mL, respectively<sup>95</sup>.

Caffeine and theophylline are purines<sup>29</sup>, that are not present in fermented drinks. Nevertheless, the positive results of this work give good perspectives for the use of SILs as an adsorbent to reduce purines content from beer.

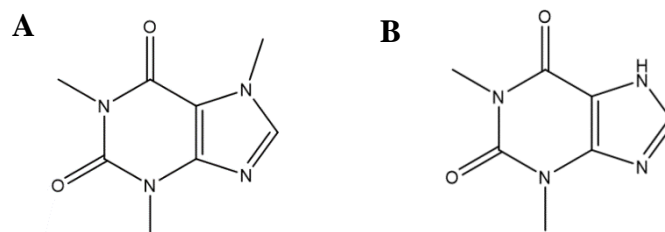


**Figure 13** - Molecular structures of caffeine (a) and theophylline (b).

A single entry in the literature is dedicated to the development of IL-modified materials for the SPE of nucleic acids, in which polymeric ILs were used. Wang *et al.*<sup>96</sup> prepared a novel polymeric ionic liquid (PIL) microsphere, poly(1-vinyl-3-(2-methoxy-2-oxyethyl)imidazolium) hexafluorophosphate, via cross-linking emulsion polymerization<sup>96</sup>. The main objective of this research was the adsorption of DNA from *Escherichia coli* cultures<sup>96</sup>. In this work, was observed a rapid ion exchange between the anionic portions of PIL and DNA fragments, with the exchange equilibrium to be reached after 1 minute<sup>96</sup>. In addition, the amount of binding DNA in the PIL microspheres was increased rapidly with DNA concentration, and a maximum binding capacity of 190.7  $\mu\text{g/L}$  was demonstrated<sup>96</sup>. Also, was proved that PIL microspheres performed better than the commercial kit while both DNA purity and integrity were maintained<sup>96</sup>.



## 1.5. Scope and objectives

Beer is the most preferred alcoholic beverage in the world<sup>11</sup>. This is also a fermented alcoholic beverage composed of a range of several components which includes purine compounds, it came from DNA and metabolism of yeast and DNA malt<sup>11,24</sup>. Purines are compounds found in all cells and are present virtually in all foods<sup>7</sup>. Approximately, 20-75 mg/L of total purine compounds are present in beer<sup>7,25</sup>. Purine compounds, such as purine bases (adenine, guanine, xanthine, etc.), purine nucleosides (adenosine, guanosine, inosine, etc.), purine nucleotides, and their polymer-nucleic acids are degraded into uric acids when ingested as diet<sup>29</sup>. When there is an excess of uric acid in the bloodstream, hyperuricemia, its accumulation occurs in the synovial fluid, giving rise to "gout"<sup>29</sup>. This disease causes inflammation and intense pain and can present as acute or chronic<sup>29</sup>. The choice of treatment depends on the clinical phase of the disease and the patient's specific risk factors<sup>29</sup>. This treatment is recommended for some medications. At the same time, it is crucial a dietary restriction for hyperuricemia, and beer is a target of this diet<sup>7,29,30</sup>.

There are several studies that trying solves the problem of the high content of purines in beer and contradict the close relation of beer at hyperuricemia and gout. These methods consist of beer treatment with enzymatic cocktails or in the use of removal purines materials (adsorbent), such as activated carbon<sup>50,68,70,71</sup>. These procedures don't remove totally purines. So, it is crucial to develop efficient techniques for the selective removal of purine compounds from alcoholic beverages.

In conclusion, in this master's project, the main objective is the development of a technique to remove selectively purines or its precursor from aqueous solutions for future application in industrial beer production. The use of SILs is promisor, opening new opportunities in different areas of separation science, with new many applications. Given the several structures, we can obtain with SILs, unique properties and their applicability in a variety of scientific fields, including food studies, SILs exhibit a huge capacity of being used for that purpose. Therefore, with selective removal of purine and acid nucleic compounds from beer, the former cannot be catabolized into its final degradation product uric acid and further its content on serum cannot be augmented after beer ingestion, helping in maintaining serum uric acid levels in the normal range, preventing against such related conditions as hyperuricemia and consequently gout.



## **II- Experimental section**



For the purpose of this master thesis, the experimental practice was divided into three parts: SILs synthesis and characterization; DNA extraction from *Saccharomyces Cerevisiae* and purines/DNA adsorption assays in aqueous solutions.

## 2.1. Materials

The reagents used for the purpose of this master thesis are described in Table 8.

**Table 8** – Reagents used in the synthesis of the materials and preparation of solutions and their respective purity and providers.

Reagent	Purity	Supplier
1-Methylimidazole	99 %	Acros organics / Iolitec
(3-Chloropropyl)trimethoxysilane	98%	Acros Organics
Adenine	99%	Sigma
Adenosine	99%	Alfa Aesar
Baker yeast	--	Commercial yeast
Caffeine	99 %	Sigma
Ethanol	99.9 %	Fisher Scientific
Guanine	98%	Aldrich
Guanosine	98%	Alfa Aesar
Isopropanol	99%	Fisher Scientific
Methanol	99.9 %	CHEM-LAB
N,N-dimethylbutylamine	99 %	Aldrich
Silica Gel (90A)	99%	Fisher Scientific
Sodium chloride	99.5%	Panreac
PK-proteinase	99%	Fisher Scientific
RNAse	99%	Fisher Scientific
Toluene	99%	Alfa Aesar
Tributylamine	99%	Acros Organics
Triethylamine	99%	Fisher Chemical

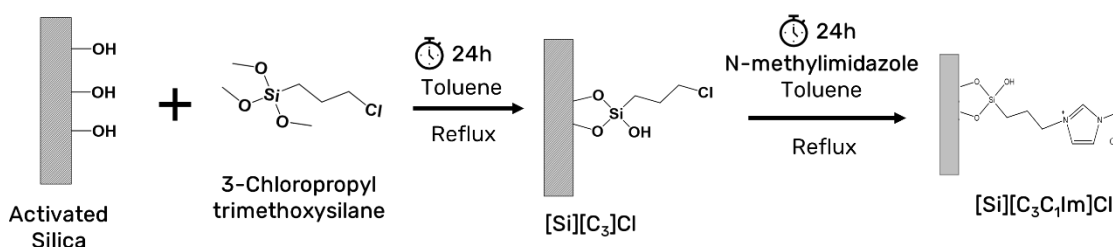
Trioctylamine	<98.0 %	Fluka
Tris(hidroximetil)aminometano	99%	Acros Organics
Tryptone	99%	Oxoid
Xanthine	99 %	Sigma-Aldrich
Yeast extract	99%	Oxoid

## 2.2. SILs synthesis

SILs were synthesized from commercial silica gel, with a pore size of 60Å and size 0.2-0.5 nm. Initially, silica was activated with chloride acid solution (37%, w/w) for 24 hours. After, it was washed with distilled water and dried at 55°C, also for 24 hours.

Then, 5 g of activated silica was added to 60 mL de toluene and 5 ml of (3-chloropropyl)trimethoxysilane in a round bottom flask. The reaction was kept in reflux with stirring for 24 hours, using a heating plate and a condenser. This material was filtered and washed with toluene (100 mL), ethanol: H<sub>2</sub>O 1:1 (200mL), distilled water (500 mL) and methanol (100 mL) and dried at 55°C for 24 hours. Silica functionalized with 3-chloropropylsilane is referred as [Si][C<sub>3</sub>]Cl.

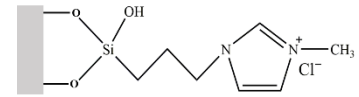
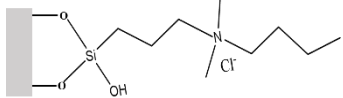
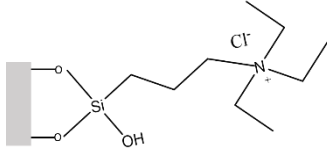
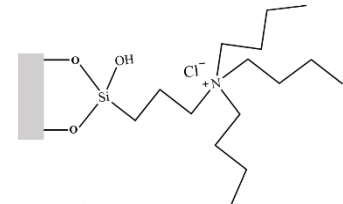
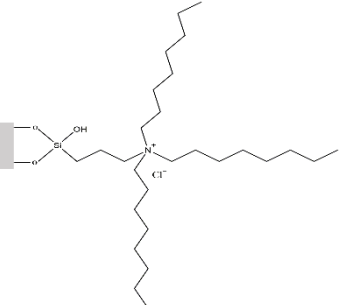
Afterward, to 5g of this material was added 50 mL of toluene and 5 mL of the cation source, for example, N-methylimidazole. This suspension stayed during 24 hours in reflux and under magnetic stirring. After this period, this material was filtered and washed with toluene (100 mL), methanol (350 mL), distilled water (300 mL) and methanol (150 mL) and dried at 55°C for 24 hours. The obtained material is silica functionalized with the ionic liquid propylmethylimidazolium chloride ([Si][C<sub>3</sub>C<sub>1</sub>Im]Cl). Figure 14 schematizes this synthesis.



**Figure 14** - Preparation of the functionalized silica with propylmethylimidazolium chloride.

In the synthesis of the other SILs, the 1-methylimidazole was replaced by other reagents. As the same volume of cation source was used in all syntheses and once that each has a different molar mass (Tab.1 - Annex), consequently distinct amounts of cation source were applied in each synthesis. Table 9 shows the SIL synthesized, their molecular structure, the cation source and the respective amount used in the syntheses.

**Table 9** - Source of the cation and representation of the corresponding SIL.

Name	Molecular structure	Cation source	Amount of cation source (moles)
[Si][C <sub>3</sub> C <sub>1</sub> Im]Cl		1-Methylimidazole	0.026
[Si][N <sub>3114</sub> ]Cl		Dimethylbutylamine	0.061
[Si][N <sub>3222</sub> ]Cl		Triethylamine	0.035
[Si][N <sub>3444</sub> ]Cl		Tributylamine	0.036
[Si][N <sub>3888</sub> ]Cl		Trioctylamine	0.021

## **2.3. Supported Ionic liquids characterization**

### **2.3.1. Elemental analysis**

The content (%) of carbon, hydrogen and nitrogen of [Si][C<sub>3</sub>]Cl and of the synthesized SILs ([Si][C<sub>3</sub>C<sub>1</sub>Im]Cl, [Si][N<sub>3114</sub>]Cl, [Si][N<sub>3222</sub>]Cl, [Si][N<sub>3444</sub>]Cl and [Si][N<sub>3888</sub>]Cl) were determined by elemental analysis equipment TruSpec 630-200-200, using approximately 2 mg of each material. The combustion temperature was at 1075 °C, and a post-combustion furnace temperature was at 850 °C. The method of quantification of carbon and hydrogen corresponds to infrared absorption, and that of nitrogen was the thermal conductivity.

### **2.3.2. Fourier-transform infrared spectroscopy (FTIR) with Attenuated total reflectance**

To obtain the Fourier transform infrared (FTIR) spectra, approximately 2 mg of each material was placed in the Perkin Elmer BX Spectrometer, with a resolution of 5 cm<sup>-1</sup> and equipped with a horizontal Golden Gate ATR cell, in the range of 4000-500 cm<sup>-1</sup>. A resolution of 8 cm<sup>-1</sup> and 128 scans were specified, the results being in transmittance mode.

### **2.3.3. Solid state <sup>13</sup>C nuclear magnetic resonance (Solid state <sup>13</sup>C NMR)**

Solid-state <sup>13</sup>C NMR spectra were recorded at 9.7 T on a Bruker Avance III – 400 MHz spectrometers (DSX model) using a 4 mm BL cross-polarization magic angle spinning (CPMAS) VTN probes at 100.6 MHz, at room temperature. In order to increase the signal-to-noise ratio of the solid-state spectra, the CPMAS NMR <sup>13</sup>C settings used were the following:  $\nu^{13}\text{C} = 55\text{ kHz}$ ; recycle delay, 4 s; contact time, 1-2 ms; NS = 1k;  $\nu\text{R} = 12\text{ kHz}$ . SPINAL-64 decoupling was used during data acquisition.



#### **2.3.4. Point zero charge**

The point of zero charges (PZC) of the materials was performed from measurements of zeta potential obtained with the Malvern Zetasizer Nano ZS equipment (Malvern Instruments Ltd. Malvern). Zeta potential values were recorded for suspensions of materials in the water at different pH values. To adjust the pH values of the suspensions NaOH and HCl aqueous solutions (0.01 M) were added. Measures were taken at 25 °C using a cell suitable for this purpose.

#### **2.3.5. Surface area and pore structure characterization**

The specific surface area and pore structure characterization of SILs were obtained by nitrogen adsorption at 77 K using a surface area analyzer Micromeritics Gemini V-2380. The samples were degassed overnight at 373 K before these measurements. The surface area ( $S_{\text{BET}}$ ) of silica, of  $[\text{Si}][\text{C}_3]\text{Cl}$  and of the prepared SILs was estimated by the BET (Brunauer-Emmett-Teller) method, the pore surface area (A) and pore volume (V) were obtained by the BJH (Barrett-Joyner-Halenda) model, and the mean pore diameter (Dp) was calculated from  $D_p = (4V)/A$ .

#### **2.3.6. Scanning electron microscope (SEM)**

Scanning electron microscopy (SEM) was performed using a Hitashi SU-70 microscope. A suspension of the materials in water was deposited on a glass substrate. After evaporation of the solvent, a thin carbon film was deposited in the sample to increase the conductivity.

### **2.4. *Saccharomyces cerevisiae* DNA extraction**

To obtain *Saccharomyces cerevisiae* DNA, all materials and growth media were autoclaved (Autoclave 88). First, it was prepared 100 mL of culture medium composed with 1 g of tryptone, 0.5 g of yeast extract and 1 g of NaCl in an Erlenmeyer. Then, 5 g of baker's yeast was added to this medium, this step was performed in the laminar chamber

class II. The Erlenmeyer was placed in an orbital shaker (IKA incubator shaker KS 4000 ic control equipment) at 37 °C with 250 rpm, for at least 46 hours and after the suspension became turbid, it was centrifuged (Eppendorf 5810R Refrigerated Centrifuge) with 5000 g, for 5 minutes. In the end, the supernatant was discarded, and it was obtained a pellet of cells. This pellet was resuspended in 10 mL of TRIS-HCL 10 mM pH 8 and mixed with 5g of glass beads. With the aim of lysis cell, this suspension was subjected to 4 cycles of 1-minute vortex 1 minute on ice. Then the glass beads were discarded, and the suspension separated in Eppendorf's with 1 mL, centrifugated at 4°C with 16000 g for 30 minutes. The supernatant was recuperated and was added 2.5 µL of pK-protease for 1 hour at 50 °C. Posteriorly, was added 0.7 mL of isopropanol and the suspension was incubated for 30 minutes on ice, centrifugated at 4°C with 16 000 g for 20 minutes. The supernatant was discarded, and the pellet was solubilized in 100 µL of TRIS-HCL 10 mM pH 8. To this solution was added 1 µL of RNAase for 1 hour at 37 °C. In the end, the purity of DNA was measured with equation 5, by a microplate reader with an integrated UV / VIS spectrophotometer (Synergy HT- micro plaque reader).

$$\text{DNA purity} = \frac{\text{Abs } 260 \text{ nm}}{\text{Abs } 280 \text{ nm}} \quad (5)$$

When the ratio is approximated at 1.8, means that the DNA is pure, below this value, the solution is contaminated by proteins. In addition, if the value is above 1.8, the sample could be contaminated by RNA.

## 2.5. Adsorption assays

In this work, the synthesized SILs were the adsorbents investigated and it aims to remove purines and/or purine precursors (DNA) from beer.

Previously adsorption assays, it is important to mark two equations. One is the equation 6 that calculate the quantity of the purines or DNA adsorbed per unit mass of modified silica gel ( $\mu\text{g}/\text{mg}$ )<sup>97</sup>:

$$q_t = \frac{(C_i - C_t) \times V}{w} \quad (6)$$

Where  $C_i$  are the initial concentrations ( $\mu\text{g}/\text{mL}$ ),  $C_t$  are the concentration at  $t$ , while  $w$  and  $V$  represent the weight of the adsorbent (SIL) (mg) and the volume of the solution (mL), respectively.

The other is the adsorption efficiency (% AE), that is represented in equation 7:

$$\%AE = \frac{C_i - C_t}{C_i} \times 100 \quad (7)$$

### 2.5.1. Purines adsorption assays

To evaluate purine removal capacity, 10 mL of adenine, guanosine, inosine, xanthine and adenosine aqueous solutions with a concentration appr. 25 mg/L was contacted with 100 mg of each SIL for 24 hours, in a shaker at 150 rpm and at room temperature. Then, 4 mL of the sample was collected, centrifuged in Eppendorfs at 12,000 rpm for 10 minutes. The purine content in the solution was determined by UV-vis at different wavelengths. Previously, it was done calibration curves for concentration determination (Fig. 1 -4- Anexo).

### 2.5.2. DNA adsorptions assays

In order to evaluate the purines precursor (DNA) removal efficiency, 100 mg of each SIL were contacted with 0.250 mL of the DNA solution, at different concentration ( $\mu\text{g}/\text{mL}$ ). These suspensions were placed in Eppendorf's on an orbital mixer at 50 rpm, 3 vibrations and at  $(25 \pm 0.5)^\circ\text{C}$ , for one hour. Later, the sample was centrifuged at 16,000 g for 5 minutes. The DNA content in the solution was determined by UV-vis at 260 nm. The solution concentration was determined by equation 8.

$$[DNA](\mu\text{g}/\text{mL}) = Abs * 50 * FD \quad (8)$$

Where Abs is the absorbance read from the microplate reader and FD the dilution factor.

The materials that demonstrated higher DNA efficiency removal were used for Kinetics and Isotherms assays

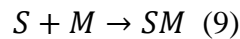
### 2.5.2.1. DNA Kinetics

Adsorption kinetics for the best removal materials of DNA was determined using the same DNA solution volume of and SILs weight, and these suspensions were mixed using the conditions mentioned above.

For the adsorption kinetic analysis, samples of the aqueous solution were recovered between 0 and 60 min. Each Eppendorf was collected at different times, and centrifuged at 16 000 g at 4°C, for 5 minutes. The DNA content in the solution was determined by UV-vis at 260 nm.

After that, two kinetic models were applied to the experimental results: the pseudo-first-order (PFO) from Lagergren and the pseudo-second-order (PSO) from Ho.

On the one hand, the Lagergren model is described by the non-reversible equation (9)<sup>98</sup>. This model is used to describe the adsorption of adsorbate from an aqueous solution, and it is based on the adsorption capacity of the solid.



Where  $S$  represent adsorption sites,  $M$  is the adsorbate and  $SM$  is the concentration of adsorbate bound to the sorbent <sup>98</sup>.

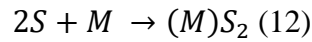
This model is expressed by the equation 10 and equation 11 shows the linear integration.

$$\frac{dq_t}{dt} = K_1(q_e - q_t) \quad (10)$$

$$\ln(q_e - q_t) = \ln(q_e) - k_1 t \quad (11)$$

Here  $t$  represents the time (min),  $q_e$  is the amount of adsorbate adsorbed by the adsorbent in equilibrium ( $\mu\text{g}/\text{mg}$ ),  $q_t$  symbolizes the amount of adsorbate adsorbed by an adsorbent at different times ( $\mu\text{g}/\text{mg}$ ) and  $k_l$  ( $\text{g mg}^{-1} \text{min}^{-1}$ ) signifies pseudo adsorption rate constant<sup>98</sup>.

On the other, Ho proposes the following equation (12) to explain the adsorption phenomena.



This model is similar to pseudo-first-order, except that adsorption of adsorbate on adsorbent is governed by a second-order equation, where kinetics is described by Equation 13 and equation 14 shows the linear integration:

$$\frac{dq_t}{dt} = K_2(q_e - q_t)^2 \quad (13)$$

$$\frac{t}{q_t} = \frac{1}{k_2 q_e^2} + \frac{t}{q_e} \quad (14)$$

where  $k_2$  ( $\text{ug mg}^{-1} \text{min}^{-1}$ ) is the pseudo-second-order constant.

#### 2.5.2.2. DNA Isotherm

To determine the adsorption isotherms of DNA in the best removal materials, a procedure described above was used. Aqueous solutions of different concentrations of DNA, ranging from 10.15 to 762.0  $\mu\text{g.mL}^{-1}$ , were utilized. The amount of SIL weighted was 100.0 mg and the equilibration time was defined depends on the material. The agitation and centrifugation conditions were the same applied to the kinetic study. After that, the most common adsorption equilibrium models were applied (Langmuir and Freundlich)<sup>52,97</sup> and SIPs<sup>97</sup>.

Langmuir adsorption isotherm was developed at first to describe gas–solid-phase adsorption onto activated carbon<sup>99</sup>. Nowadays has been used to quantify and contrast the performance of different bio-sorbents<sup>97</sup>.

The assumptions of the Langmuir model<sup>97,99,100</sup> are:

- adsorption can only occur at a fixed number of definite localized sites;
- monolayer and homogenous adsorption, in other words, the adsorbed layer is one molecule in thickness and each all sites possess an equal affinity for the adsorbate;
- no lateral interaction between the adsorbed molecules;
- graphically, it is illustrated by a plateau ( $q_{m\acute{a}x}$ ), this means an equilibrium saturation point where once a molecule occupies a site, no further adsorption can take place<sup>100</sup>.

This model is described by the below equation<sup>99</sup>:

$$q_e = \frac{q_{m\acute{a}x} \times K_L \times C_e}{1 + K_L \times C_e} \quad (15)$$

Where  $C_e$  is the equilibrium concentrations ( $\mu\text{g/mL}$ ), while  $K_L$  is the Langmuir constant associated the bonding energy of sorption ( $\text{mL}/\mu\text{g}$ ) and  $q_{m\acute{a}x}$  represents the maximum monolayer coverage capacity ( $\text{mg/g}$ ).

About Freundlich isotherm, historically it was developed for the adsorption of animal charcoal, demonstrating that the ratio of the adsorbate onto a given mass of adsorbent to the solute was not a constant at different solution concentrations<sup>97</sup>. In this way, Freundlich isotherm appears as the first model that describes the reversible adsorption, not restricted to the formation of monolayer<sup>97</sup>.

This empirical model can be applied to multilayer adsorption, with non-uniform distribution of adsorption heat and affinities over the heterogeneous surface<sup>97</sup>. The equation 14 describes the model:

$$q_e = K_F \times C_e^{1/n_f} \quad (16)$$

Where  $C_e$  is the equilibrium concentrations ( $\mu\text{g/mL}$ ), while  $K_F$  ( $\mu\text{g mg}^{-1}\text{mL}^{-1}$ ) and  $n_f$  (dimensionless) are the Freundlich isotherm constant related to adsorption intensity constant and the surface heterogeneity.

The last isotherm is Sips. This isotherm is a combined form of Langmuir and Freundlich expressions deduced for circumventing the limitation of the rising adsorbate concentration associated with the Freundlich isotherm model and predicting the heterogeneous adsorption systems<sup>97</sup>. At low adsorbate concentrations, it reduces to Freundlich isotherm; while at high concentrations, it predicts a monolayer adsorption capacity characteristic of the Langmuir isotherm<sup>97</sup>. This model assumes that the surface is homogeneous, but that the sorption is a cooperative process owing to the sorbate- sorbate interactions<sup>101</sup>. The equation is:

$$q_e = \frac{qmáx_s(K_s \times C_e^{n_s})}{1 + K_s \times C_e^{n_s}} \quad (17)$$

Where  $C_e$  is the equilibrium concentrations ( $\mu\text{g/mL}$ ), while  $K_s$  is its equilibrium constant, related to the bonding energy of sorption or binding affinity ( $\text{mL}/\mu\text{g}$ ),  $qmáx_s$  is Sips sorption capacity at monolayer coverage ( $\mu\text{g}/\text{mg}$ ),  $n_s$  is a heterogeneity index. When  $1=n_s$  the model reduces to the Langmuir isotherm. On the other hand, the deviation of  $1=n_s$  from unity indicates a heterogeneous surface<sup>97,101</sup>.

### 2.5.3. Error analysis of the data

The parameters of the equilibrium and kinetic models were obtained by nonlinear regression analysis using GraphPad Prism 5 program (trial version), which uses least-squares and the Marquardt and Levenberg method for adjusting the variables. Although linear regression analysis is simple to implement (Eqs 11 and 14) and is applicable to a broad array of kinetic adsorption systems, the PSO and PFO models provide sometimes-widely different parameter values<sup>102</sup>. For this reason, nonlinear regression is used in this work to circumvent this problem. This regression has more realistic values of  $q_e$  and  $k$  values, and often a higher correlation coefficient ( $R^2$ ) value is obtained. The coefficient of determination is restricted to  $0 < R^2 \leq 1$ . An  $R^2$  value closer to unity indicates a better fit<sup>102</sup>

The results are showed and discussed in chapter III.



## **III - Results and discussion**



### 3.1. Materials synthesis and characterization

First, before study the removing of purines and DNA from aqueous solutions with SILs it was needed to verify if the SIL synthesis was successfully by characterizing them. With this purpose, several techniques were used, and results are presented below.

#### 3.1.1. Elemental analysis

As referred to in the previous chapter, the % of carbon, hydrogen, and nitrogen of synthesized SILs (w/w) were obtained for elemental analysis and the results are in Table 10.

**Table 10** –SILs elemental analysis.

SIL	% Carbon	% Hydrogen	% Nitrogen
[Si][C <sub>3</sub> ]Cl	4.637	1.394	0.0000
[Si][C <sub>3</sub> C <sub>1</sub> Im]Cl	8.382	2.120	2.841
[Si][N <sub>3114</sub> ]Cl	7.719	1.840	0.7670
[Si][N <sub>3222</sub> ]Cl	7.289	1.509	0.2630
[Si][N <sub>3444</sub> ]Cl	5.741	1.336	0.1480
[Si][N <sub>3888</sub> ]Cl	6.899	1.335	0.07100

Analyzing the results, the intermediary material ([Si][C<sub>3</sub>]Cl) contains, as expectably, C (4.637%) and H (1.394%) which corresponds to the theoretical structure of the material and don't show content in nitrogen.

Regarding the supported ionic liquid materials, the carbon content ranges from 6.899 to 8.382 % depending on the carbon content of the cation precursor. In relation to nitrogen content, it ranges from 0.07100 to 2.841 %. The increase of % C atoms and the presence of N content proves that the synthesized ILs were immobilized on the silica surface.

Nevertheless, [Si][N<sub>3888</sub>]Cl presents a small percentage of N when compared for example with [Si][C<sub>3</sub>C<sub>1</sub>Im]Cl.

Consequently, in order to get the bonding amount (*BA*) ( $\mu\text{mol}/\text{m}^2$ ) of [Si][C<sub>3</sub>]Cl the equations are shown below were used. This value gives the amount of 3-(chloropropyl)triethoxysilane immobilized per unit area of silica surface ( $\text{m}^2$ ), which in this case was  $434.545 \text{ m}^2/\text{g}$ , obtained using the BET method.

$$BA_{[Si][C_3]Cl} = \frac{\% C / (3M_C)}{S_{BET_{silica}}} \quad (18)$$

Where % *C* (w/w) is obtained by elemental analysis,  $3 M_C$  corresponds to the molar mass of 3 atoms of carbon existed in [Si][C<sub>3</sub>]Cl and  $S_{BET_{silica}}$  ( $\text{m}^2/\text{g}$ ) is the area of silica surface ( $\text{m}^2$ ).

The BA of [Si][C<sub>3</sub>C<sub>1</sub>Im]Cl also was calculated. The equation 19 informs about the 1-Methylimidazole amount immobilized per unit area of silica surface ( $\text{m}^2$ ).

$$BA_{[Si][C_3C_1Im]Cl} = \frac{\% N / (2M_N)}{S_{BET_{silica}}} \quad (19)$$

Where % *N* (w/w) is obtained by elemental analysis,  $2M_N$  corresponds to the molar mass of 2 atoms of carbon presented in [Si][C<sub>3</sub>C<sub>1</sub>Im]Cl and  $S_{BET_{silica}}$  ( $\text{m}^2/\text{g}$ ) is the area of silica surface ( $\text{m}^2$ ).

The BA of each quaternary ammonium synthesized is given by equation 20.

$$BA_{quaternary\ ammonium} = \frac{\% N / (M_N)}{S_{BET_{silica}}} \quad (20)$$

Where % *N* (w/w) is obtained by elemental analysis,  $M_N$  corresponds to the molar mass of the only nitrogen present in cation source of amines and  $S_{BET_{silica}}$  ( $\text{m}^2/\text{g}$ ) is the area of silica surface ( $\text{m}^2$ ).

**Table 11** – SILs Bounding amount.

SIL	BA ( $\mu\text{mol}/\text{m}^2$ )
[Si][C <sub>3</sub> ]Cl	2.964
[Si][C <sub>3</sub> C <sub>1</sub> Im]Cl	2.335
[Si][N <sub>3114</sub> ]Cl	1.261
[Si][N <sub>3222</sub> ]Cl	0.4320
[Si][N <sub>3444</sub> ]Cl	0.2430
[Si][N <sub>3888</sub> ]Cl	0.1170

The results of the previous table corroborate the fact of [Si][N<sub>3888</sub>]Cl was less functionalized than the other SILs. For example, the BA of [Si][C<sub>3</sub>]Cl and [Si][C<sub>3</sub>C<sub>1</sub>Im]Cl are similar, meaning that this synthesized SIL was almost all functionalized on [Si][C<sub>3</sub>]Cl. On the other hand, [Si][N<sub>3888</sub>]Cl was less functionalized. Consequently, in the future, a higher volume of dimethylbutylamine, tributylamine, triethylamine, and trioctylamine must be used to equal the number of moles used in [Si][C<sub>3</sub>C<sub>1</sub>Im]Cl synthesis.

### 3.1.2. FTIR-ATR

In order to confirm the silica functionalization with ILs, the FTIR-ATR spectra of SILs were acquired. FTIR-ATR spectroscopy is a powerful tool for providing conformational and structural information in the form of infrared spectrum<sup>103,104</sup>.

The results of this technique are given in Figure 15, where it was detected in all materials the appearance of a band at 1073  $\text{cm}^{-1}$ , which corresponds to Si-O bonds<sup>105</sup>. In addition, it was observed one band at 2351  $\text{cm}^{-1}$ , due to CO<sub>2</sub> present in the room<sup>106</sup>.

Furthermore, in these spectra is noted a few differences between the activated silica and the IL-functionalized silica. One is the disappearance of the band at 960  $\text{cm}^{-1}$  related to the bending vibration mode of Si-OH, thus indicating the silica functionalization<sup>107,108</sup>.

Another evidence of [Si][C<sub>3</sub>]Cl synthesis success is the appearance of a band at the wavelength of 700  $\text{cm}^{-1}$  when 3-(chloropropyl)triethoxysilane was added. This band is the fingerprint region of the C-Cl group<sup>104</sup>. It was also observed a band at 1575  $\text{cm}^{-1}$  in [Si][C<sub>3</sub>C<sub>1</sub>Im]Cl, corresponding to the characteristic frequency of the imidazole ring<sup>109</sup>. Thus, this technique proved SILs synthesis success.

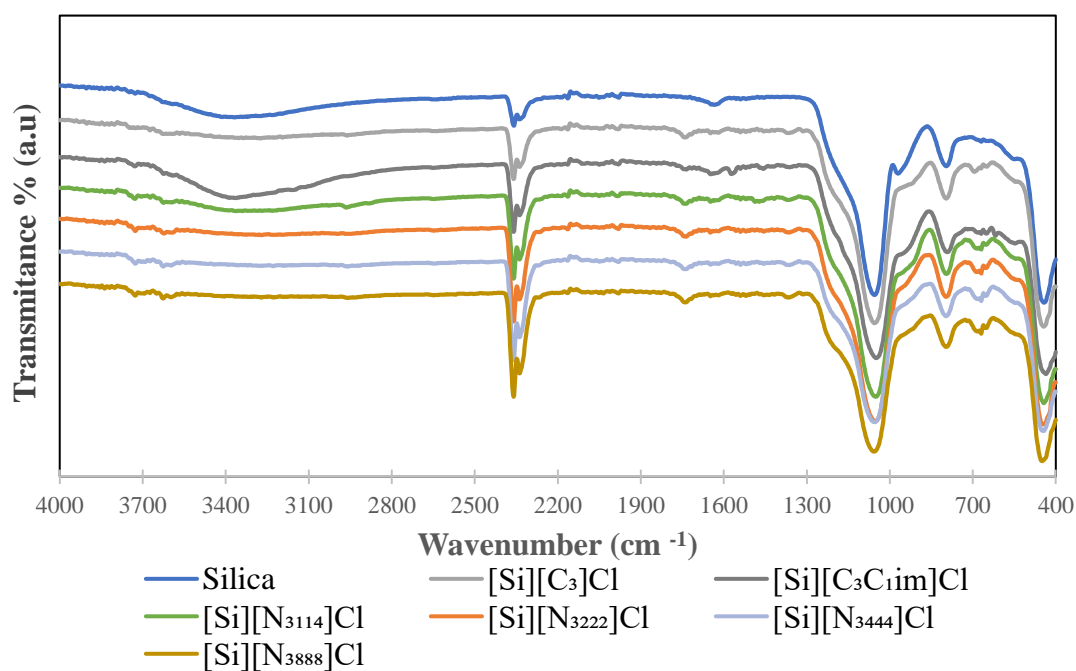


**Figure 15** – FTIR-ATR spectra of silica, [Si][C3]Cl and SILs.

### 3.1.3. Solid-state $^{13}\text{C}$ NMR

The successful preparation of SILs was further confirmed through solid-state  $^{13}\text{C}$  nuclear magnetic resonance (NMR). Solid-state NMR spectroscopy has emerged as an exceptionally powerful analytical technique for the characterization of chemical molecules<sup>110</sup>. NMR data is mostly used to confirm the precise arrangement of atoms that make up a molecule either by showing how they are bonded or how close they are to each other in space<sup>110</sup>. Theoretically, in the solid-state  $^{13}\text{C}$  NMR spectra, contributions due to aromatic and aliphatic groups are readily separated based on the  $^{13}\text{C}$  isotropic chemical shifts<sup>110</sup>. Freitas *et al.* declare that aliphatic groups are typically between 0 and 90 ppm and aromatic groups in the range 110–160 ppm. Thus, NMR helps to understand the SILs chemical structure.

The spectrum of [Si][C<sub>3</sub>]Cl (Figure 16) shows signals at 10, 27 and 47 ppm, corresponding to the three carbon atoms (C2, C1, and C3).

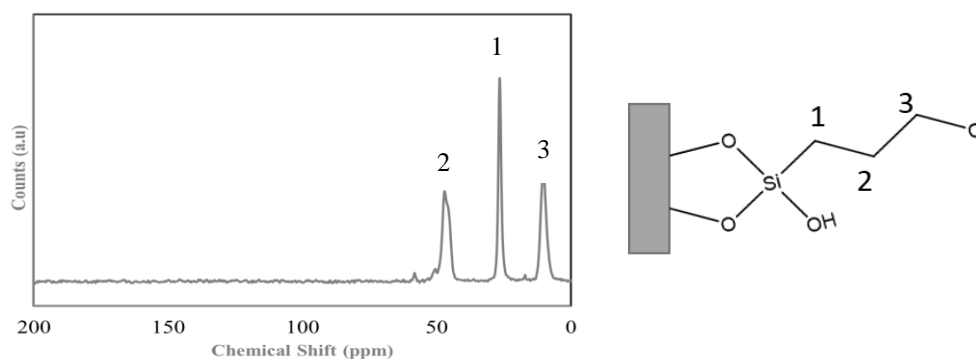


**Figure 16** - Solid-state <sup>13</sup>C NMR spectrum of [Si][C<sub>3</sub>]Cl.

In addition, the spectrum of Figure 17 reveals the successful preparation of [Si][C<sub>3</sub>C<sub>1</sub>Im]Cl. The signals at 51, 24 and 10 ppm correspond to the three carbon atoms of the imidazolium alkyl chain length (C3, C2, and C1), the peaks ranging from 120-140 ppm correspond to the aromatic carbons of imidazolium (C4 and C5), and the signal at 37 ppm corresponds to the carbon of the methyl chain (C6).

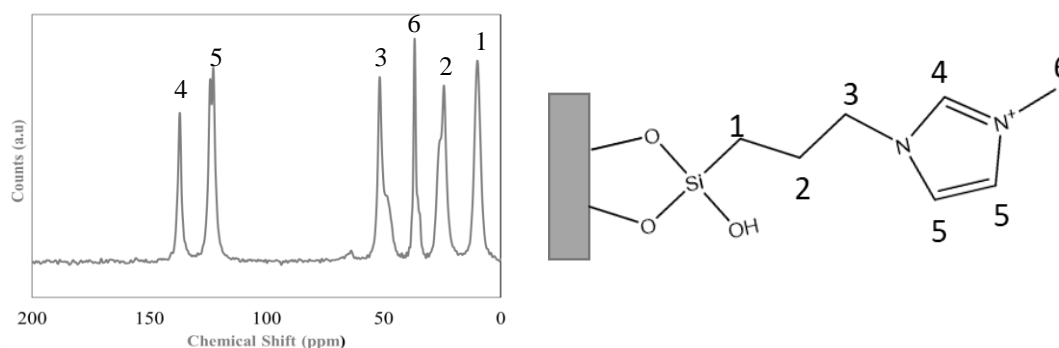


**Figure 17** - Solid-state <sup>13</sup>C NMR spectrum of [Si][C<sub>3</sub>C<sub>1</sub>Im]Cl

The [Si][N<sub>3114</sub>]Cl preparation also confirmed by <sup>13</sup>C NMR (Figure 18), where signals at 14, 15 and 64 ppm correspond to the three carbon atoms of the [Si][C<sub>3</sub>]Cl main chain (C2, C1, and C3). The signals at 17, 64, 20 and 30 ppm coincide with the carbon of dimethylbutyl chain (C8, C5, C7, and C6). At the peak at 50 ppm is related to carbon C4, which proves the existence of alkyl chains in quaternary ammonium.

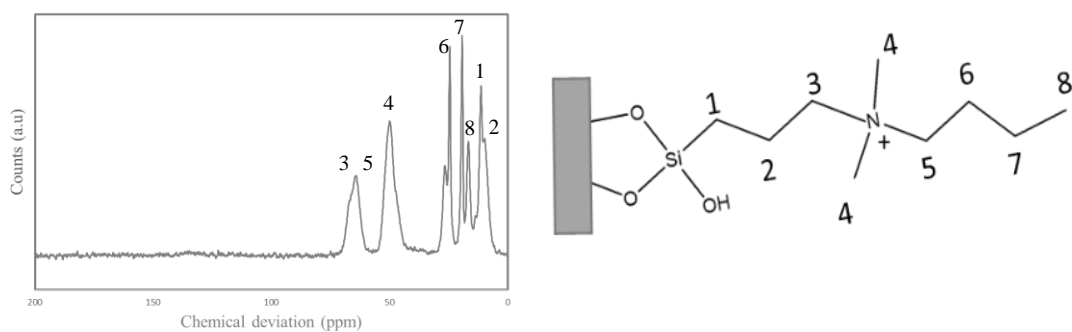


**Figure 18** - Solid-state  $^{13}\text{C}$  NMR spectrum of  $[\text{Si}][\text{N}_{3114}]\text{Cl}$ .

This technique also shows the efficacy of  $[\text{Si}][\text{N}_{3222}]\text{Cl}$  synthesis, it was observed in Figure 19. There was observed 3 peaks at 51, 25, 14 ppm that corresponds to three carbons  $[\text{Si}][\text{C}_3]\text{Cl}$  and the peaks at 50 and 10 ppm are related with C4 and C5, belong to alkyl chains ammonium.

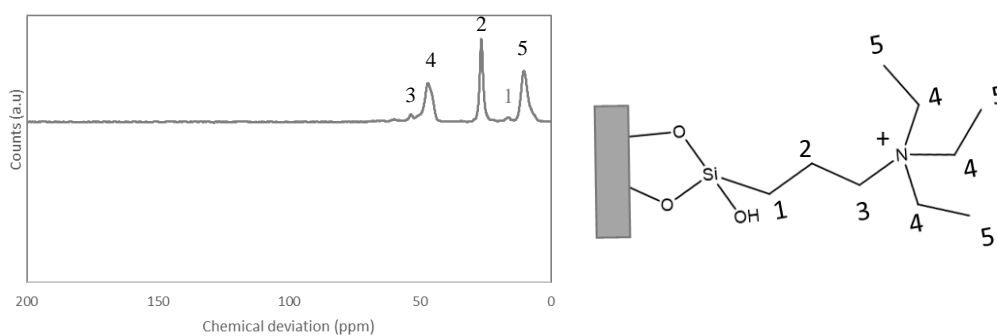


**Figure 19** - Solid-state  $^{13}\text{C}$  NMR spectrum of  $[\text{Si}][\text{N}_{3222}]\text{Cl}$ .

Analyzing the CPMAS  $^{13}\text{C}$  spectra  $[\text{Si}][\text{N}_{3444}]\text{Cl}$  and  $[\text{Si}][\text{N}_{3888}]\text{Cl}$  (Figure 20), it cannot be concluded whether or not they are functionalized, this is due to the low extent of functionalization of the materials with the respective ionic liquids, as explained in the elemental analysis subchapter. However, other techniques prove the functionalization of these materials namely elemental analysis and FTIR-ATR.



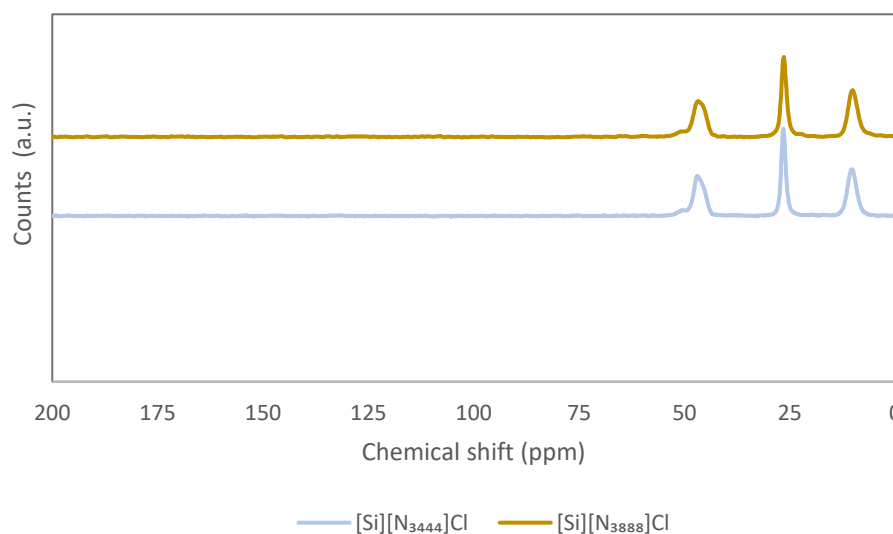


**Figure 20** - Solid-state $^{13}\text{C}$  NMR spectrum of  $[\text{Si}][\text{N}_{3444}]\text{Cl}$  and  $[\text{Si}][\text{N}_{3888}]\text{Cl}$  .

### 3.1.4. Zeta Potential (ZP)

The point of zero charge (PZC) was also studied for SILs characterization. ZP is defined by the electric potential at the shear plane of a particle and it is a very important property to a huge number of natural phenomena, such as adsorption<sup>111</sup>. Each particle is surrounded by oppositely charged ions in what is called a stern layer<sup>111</sup>. Beyond the stern layer, there are both positive and negative ions in what can be considered a charge “cloud”<sup>111</sup>. These along with the ions in the stern layer form the electrical double layer at the particle-liquid interface<sup>111</sup>. The ions within the charge cloud region move about freely becoming less and less further away from the particle and eventually decay to zero<sup>111</sup>. The potential at the boundary of the stern plane and the diffuse (shear) plane is known as the zeta potential<sup>111</sup>. One of the factors that have the greatest influence on zeta potential is the pH of the medium<sup>111</sup>. The pH at which the solid surface has a neutral charge is called PZC<sup>111</sup>. This means that on average the particles have zero mobility when subjected to an electric field<sup>111</sup>.

Figure 21 represents the potential zeta as a function of pH for the different materials, and PZC values are represented in Table 12.

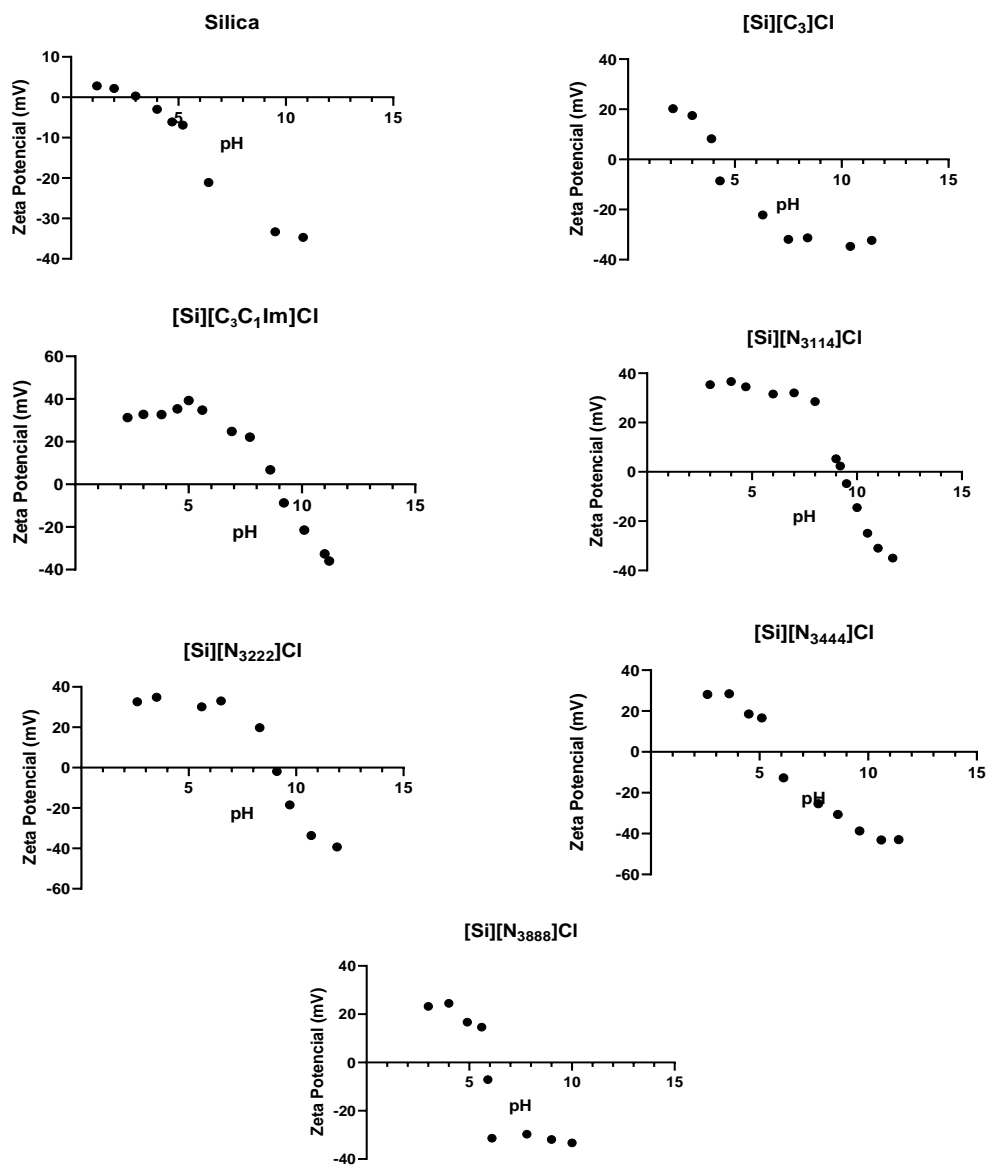


**Figure 21** - Potential zeta as a function of pH values for all synthesized SIL.

**Table 12** - Table with PZC values for silica, [Si][C<sub>3</sub>]Cl and each SIL

Material	PZC
Silica	3.4
[Si][C <sub>3</sub> ]Cl	4.2
[Si][C <sub>3</sub> C <sub>1</sub> Im]Cl	8.9
[Si][N <sub>3114</sub> ]Cl	9.3
[Si][N <sub>3222</sub> ]Cl	9.0
[Si][N <sub>3444</sub> ]Cl	6.0
[Si][N <sub>3888</sub> ]Cl	5.5

Silica has the lowest PZC value. The PZC increases to 4.2, after the reaction with (3-Chloropropyl)trimethoxysilane. The [Si][C<sub>3</sub>C<sub>1</sub>Im]Cl present a higher PZC value when compared with silica and the precursor material ([Si][C<sub>3</sub>]Cl). The same as before is heeded with the four SILs synthesized with tertiary amines ranging from 5.5 ([Si][N<sub>3888</sub>]Cl) to 9.3 ([Si][N<sub>3114</sub>]Cl). These results indicate that the SILs surface is more positively charged when compared to the silica and the [Si][C<sub>3</sub>]Cl material. It is also noted that the less functionalized the material is, the closer its PZC value is to the PZC of [Si][C<sub>3</sub>]Cl. Thus, in the structure point of view, these results proved the success of SILs syntheses, once SILs have the cations present on the silica surface.

### 3.1.5. Brunaver-Emmett-Teller

The specific surface area of silica, of [Si][C<sub>3</sub>]Cl and of the synthesized SILs were determined by nitrogen adsorption using the BET method and the pore surface area (A) and pore volume (V) were obtained by the BJH (results are given in Table 13).

**Table 13** - BET surface area ( $S_{BET}$ ), pore surface area (A), pore volume (V) and pore size diameter (Dp) of silica, [Si][C<sub>3</sub>]Cl and SILs.

Material	$S_{BET}$ (m <sup>2</sup> /g)	A (m <sup>2</sup> /g)	V (cm <sup>3</sup> /g)	Dp (Å)
Silica	434.6	569.5	0.7050	49.49
[Si][C <sub>3</sub> ]Cl	322.9	326.9	0.3170	38.75
[Si][C <sub>3</sub> C <sub>1</sub> Im]Cl	185.3	256.1	0.2890	45.21
[Si][N <sub>3114</sub> ]Cl	187.1	175.3	0.2650	46.74
[Si][N <sub>3222</sub> ]Cl	317.2	297.7	0.4990	46.74
[Si][N <sub>3444</sub> ]Cl	323.4	302.7	0.3290	42.20
[Si][N <sub>3888</sub> ]Cl	299.2	319.3	0.3290	43.62

A decrease of the specific surface area of [Si][C<sub>3</sub>]Cl is observed when compared to the original silica and the same is detected when SILs are compared with the respective precursor material ([Si][C<sub>3</sub>]Cl). Silica has the highest value of pore diameter (49.485 Å), whereas [Si][C<sub>3</sub>]Cl has the lowest value (38.746 Å). The synthesized SILs show a pore diameter in the range between 42.198 and 46.740 Å. The differences in surface area and

pore diameter observed between the materials are not relevant to influence the adsorption efficiency.

### 3.1.6. Scanning electron microscope (SEM)

Scanning electron microscope (SEM) images were also acquired for SILs, Figures 22-27, with two distinct magnifications. SEM creates an image scanning a focused electron beam over a surface<sup>112</sup>. The interaction between electrons in the beam and the sample produces various signals that can be used to obtain information about the surface composition and topography<sup>112</sup>. With this technique, no significant differences in morphology were observed between the Silica and each SILs prepared.

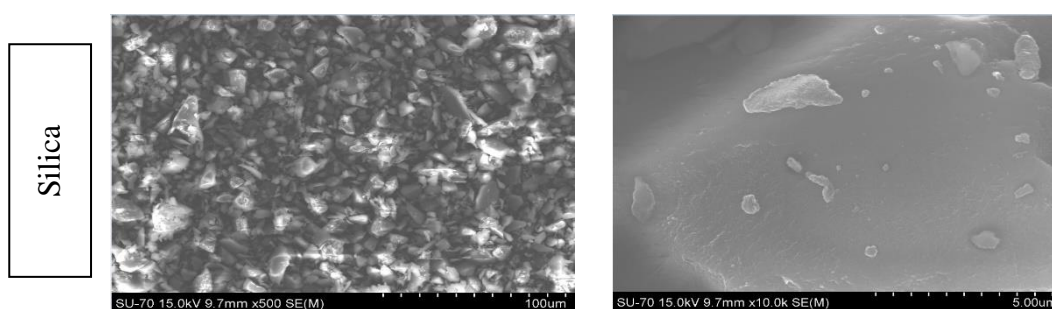


Figure 22 - SEM images of Silica

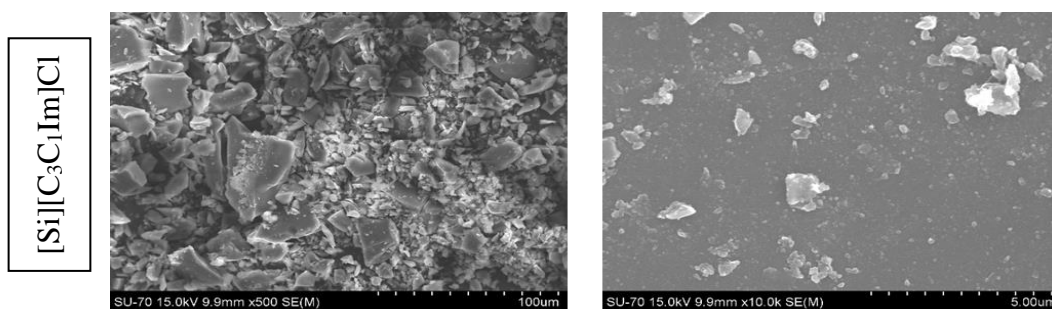


Figure 23 - SEM images of [Si][C<sub>3</sub>C<sub>1</sub>Im]Cl

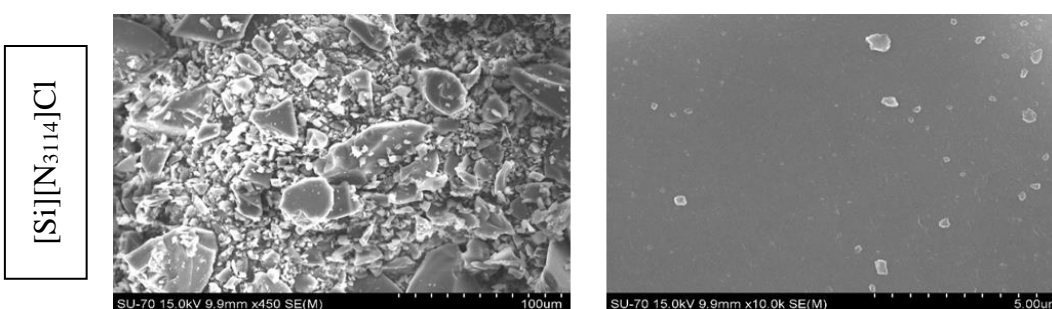
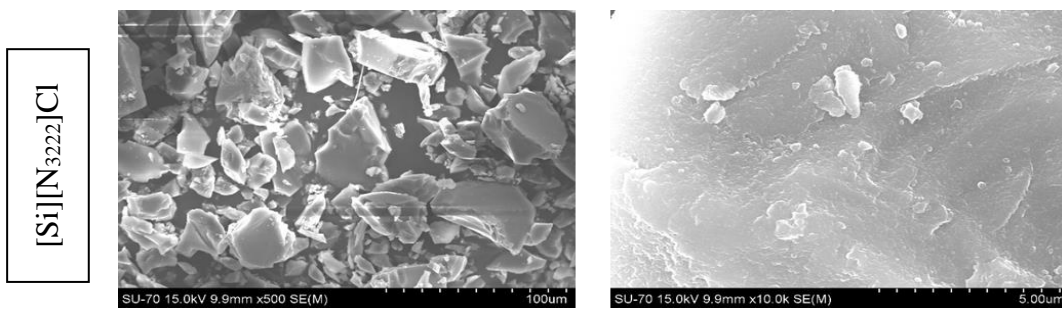
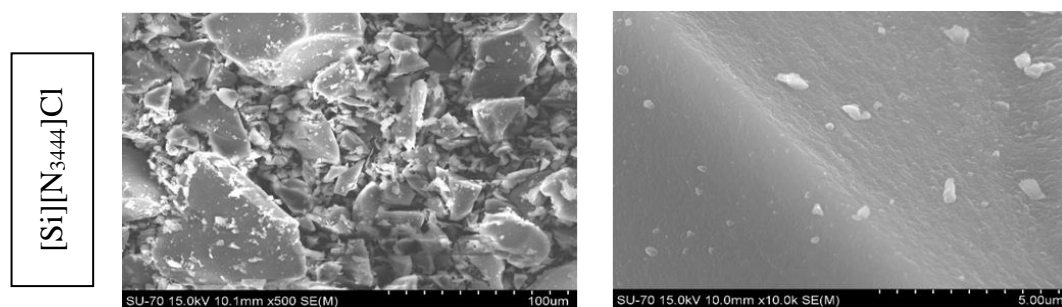


Figure 24 - SEM images of [Si][N<sub>3114</sub>]Cl.



**Figure 25** - SEM images of [Si][N<sub>3222</sub>]Cl.



**Figure 26** - SEM images of [Si][N<sub>3444</sub>]Cl.

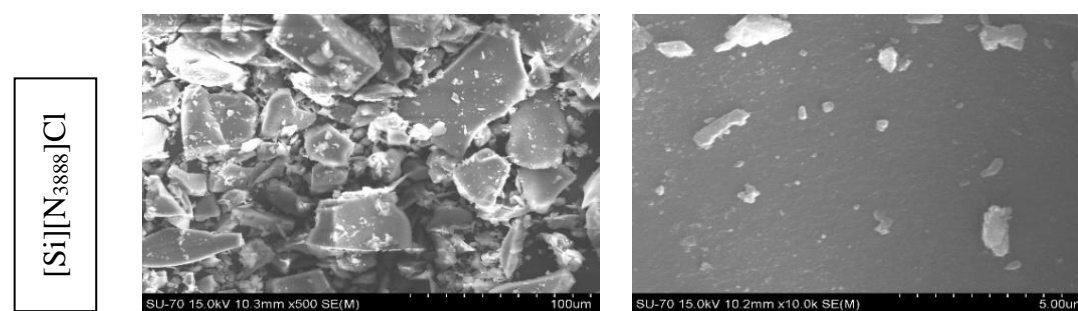


**Figure 27** - SEM images of [Si][N<sub>3888</sub>]Cl.

After the materials characterization that proved the success of SILs syntheses, these materials were used for adsorption of purines and DNA from water.

### 3.1.7. Purines adsorption

As referred in chapter 2.6, to evaluate the efficiency of SILs as adsorbents for purines present in beer, 100 mg of silica and each synthesized material was contacted with 10 mL of purines solutions with similar concentration (~25 mg/L), for 24 hours.

The purines tested were adenine (24.70 mg/L), adenosine (23.10 mg/L), guanosine (22.93 mg/L) and inosine (27.10 mg/L), all present in beer<sup>35</sup>. The method of measurement of purine concentration obeys Lambert-Beer law, therefore it was used UV-VIS spectrometry. Spectra results of purines solutions absorbance at the initial time and then 24h of contact with SILs are in Figures 28 to adenine, Figure 29 to adenosine, Figure 30 to inosine and, finally Figure 31 to guanosine.

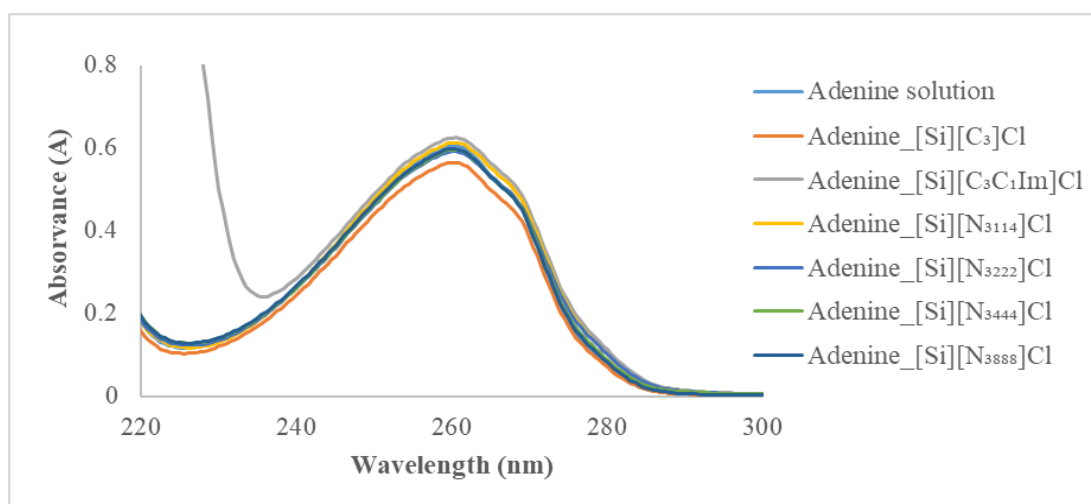


**Figure 28** - Adenine adsorption assays, after 24 hours in contact with SILs synthesized. This absorbance corresponds 2 times of dilution concentration.

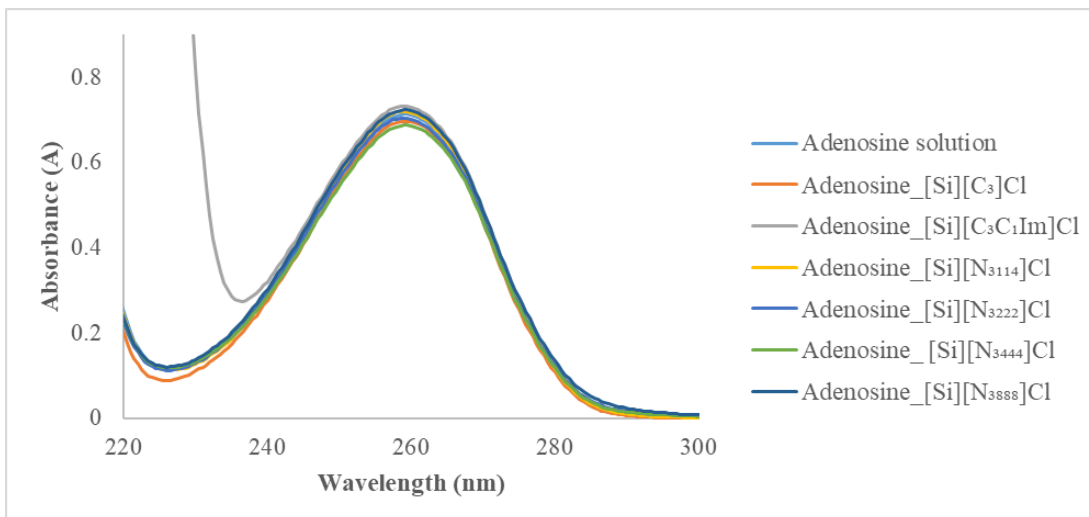


**Figure 29** - Adenosine adsorption assays, after 24 hours in contact with SILs synthesized. This absorbance corresponds to 2 times of dilution concentration.

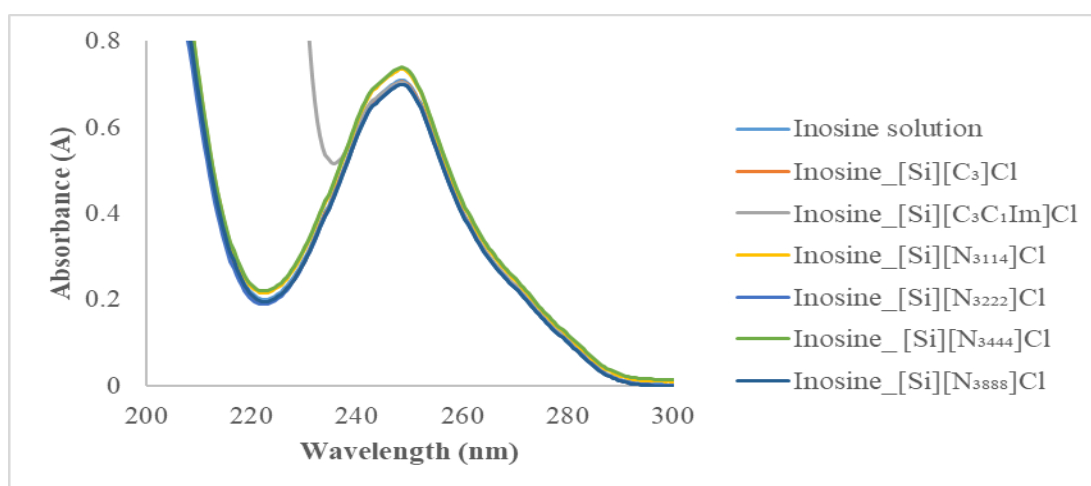


**Figure 30** - Inosine adsorption assays, after 24 hours in contact with SILs synthesized. This absorbance corresponds to 2 times of dilution concentration.

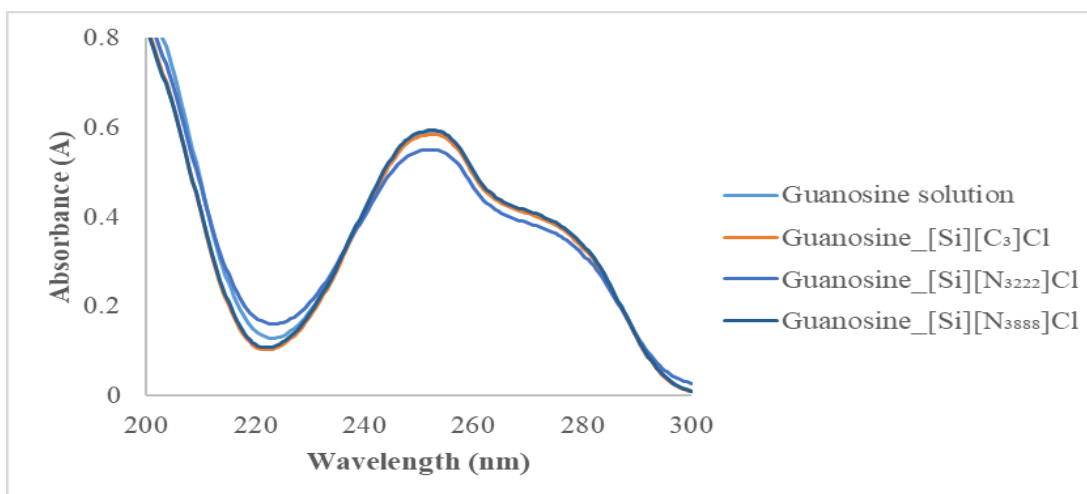


**Figure 31** - Guanosine adsorption assays, after 24 hours in contact with SILs synthesized. This absorbance corresponds 2 times of dilution concentration.

Analyzing the results (Figures 28-31), it was observed that the absorbance didn't decrease after contact with the SILs, which means the concentration of initial solutions was the same as purine solution after 24 hours in contact with SILs. Thus, all the synthesized materials have not a capacity for purine removal at conditions that were performed the assays.

According to the bibliography, the purines removal with modified graphene and carbon nanotubes happened due to physical process adsorption, where the removal of nitrogen bases and their radical from aqueous solutions is due to non-covalent interactions occurring between the delocalized  $\pi$ -orbitals from the molecules and the graphene or nanotubes<sup>27</sup>.

Theoretically, regarding the chemical structure of purines and  $[\text{Si}][\text{C}_3\text{C}_1\text{Im}]\text{Cl}$ , it was expected the interaction  $\pi$ - stacking between  $[\text{Si}][\text{C}_3\text{C}_1\text{Im}]\text{Cl}$  and purines aromatic ring, as it occurred in diclofenac sodium removal with  $[\text{Si}][\text{C}_3\text{C}_1\text{Im}]\text{Cl}$ <sup>108</sup>. In the results presented in Figures 28-31, it was not observed a decrease in absorbance after contact with the  $[\text{Si}][\text{C}_3\text{C}_1\text{Im}]\text{Cl}$  (grey line). Consequently, this suggests that there was no interaction between the purines studied and the material.

Besides  $\pi$  interactions, H-bonding and dispersive forces oxygen double bonds should be responsible for the diclofenac sodium affinity on  $[\text{Si}][\text{C}_3\text{C}_1\text{Im}]\text{Cl}$ <sup>108</sup>. Regarding the



chemical structure of adenine and adenosine, they haven't oxygen groups, therefore that could explain the adsorption failure.

Other works mentioned the importance of solutions' pH<sup>60</sup>. As pH decreases, purines are protonated and acquire a positive charge<sup>60</sup>. The nucleobases have several potential points of protonation, including ring nitrogen atoms and functional groups<sup>113</sup>. Cleaves *et al.* used rutile (TiO<sub>2</sub>) to adsorb nucleic acid components (adenine) and they suggest that adsorption is carried out by electrostatic interactions.

In this work, the pH used in purine adsorption assays was approximately water pH. At these conditions, all purines tested are neutral. For electrostatic interactions to occur, it is necessary that the molecules and materials have opposite charges. Analyzing Figure 32 and the potential zeta results (Chapter 3.1.3), it isn't possible promoting electrostatic interactions. In addition, at the pH of beer (4.8), purines maintain the neutral charge, and the synthesized SILs have a positive charge.

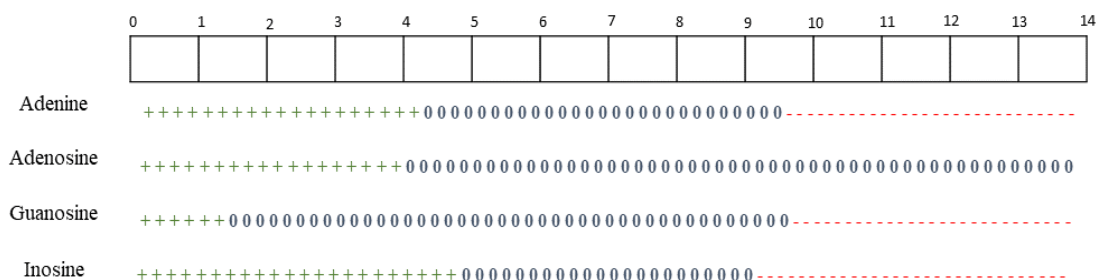


**Figure 32** – Charge of the compounds tested as a function of pH, based on  $pK_a$ , adapted from Cleaves *et al.* <sup>113</sup>

Such as referred in the introduction chapter, the precursor purines onto beer is the Yeast and Malt DNA<sup>24,25</sup>. Consequently, the idea is to remove DNA in the beer production process before it degrades into purines. Indirectly, the purine content could decrease.

In this way, DNA from *Saccharomyces* was extracted for posterior DNA adsorption assays.

### 3.1.8. DNA adsorption

As beer purines come from yeast and malt DNA, in this work, yeast DNA adsorption was also tested. Thus, instead of removing the purines, the idea would be to remove the DNA from the beer before it was catabolized into purines. To evaluate this possibility, 2.5 mg of each synthesized material was contacted with 250  $\mu\text{L}$  of DNA (27.25 mg/L) extracted from *Saccharomyces cerevisiae*. The results of the primary test are in Figure 33 and  $C_i$ ,  $C_f$  and  $q_t$  are in Table 14. and adsorption efficiency (% AE) in Figure 34,

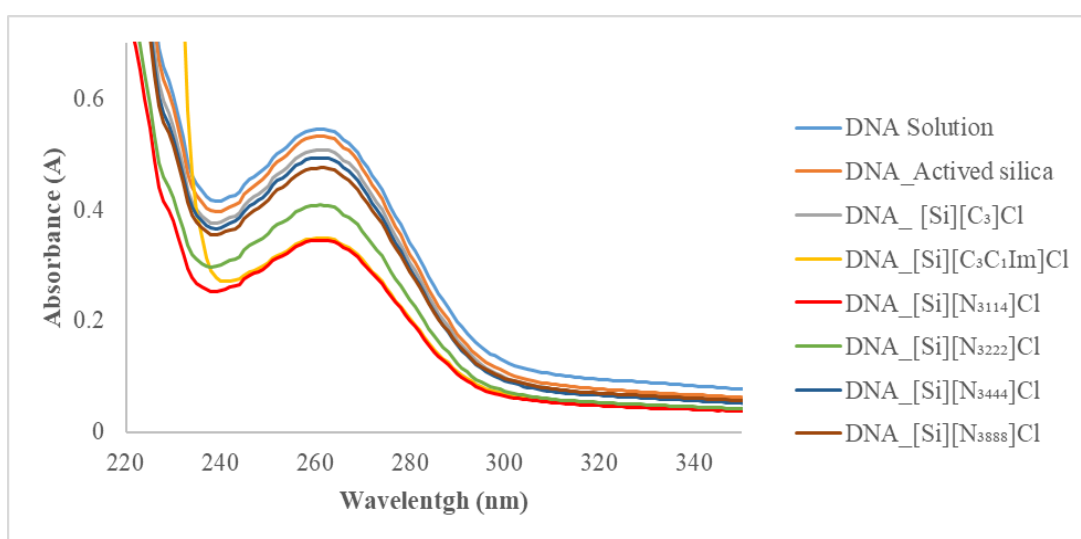


**Figure 33** – DNA adsorption assays, after 1 hour in contact with SILs.

**Table 14.**  $q_t$  values ( $\mu\text{g}/\text{mg}$ ) corresponding to the primary study of DNA adsorption.

Materials	$C_i$ ( $\mu\text{g}/\text{mL}$ )	$C_f$ ( $\mu\text{g}/\text{mL}$ )	$q_t$ ( $\text{mg}/\text{g}$ )
Activated Silica	27.25	26.55	0.06700
[Si][C <sub>3</sub> ]Cl		25.30	0.1970
[Si][C <sub>3</sub> C <sub>1</sub> Im]Cl		17.40	1.026
[Si][N <sub>3114</sub> ]Cl		17.20	0.9970
[Si][N <sub>3222</sub> ]Cl		20.35	0.6790
[Si][N <sub>3444</sub> ]Cl		24.60	0.2720
[Si][N <sub>3888</sub> ]Cl		23.70	0.320

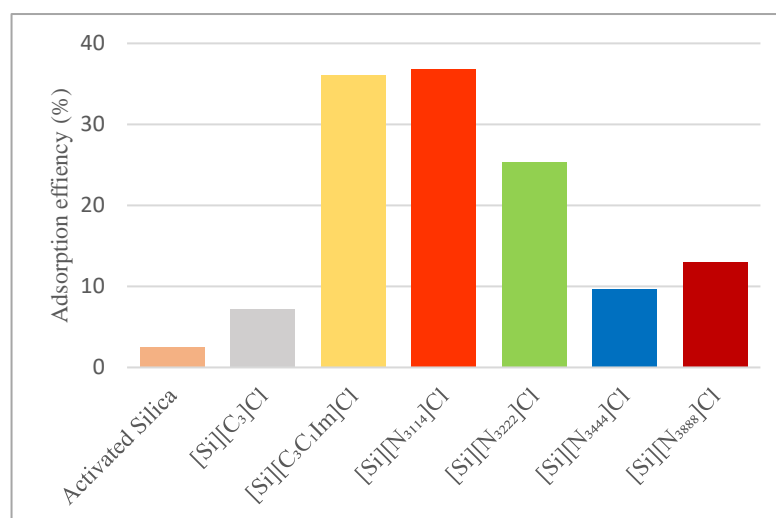


**Figure 34** – Adsorption efficiencies of DNA with different SILs, using an initial concentration of 27.25 µg/mL

Regarding the Figure 34 and  $q_t$  values in Table 14, it was observed that using the same initial conditions, the  $q_t$  value decreases in the following order: [Si][C<sub>3</sub>C<sub>1</sub>Im]Cl > [Si][N<sub>3114</sub>]Cl > [Si][N<sub>3222</sub>]Cl > [Si][N<sub>3888</sub>]Cl > [Si][N<sub>3444</sub>]Cl > [Si][C<sub>3</sub>]Cl > Activated Silica. It should be noted that silica functionalization is important, once with a higher specific surface area ( $S_{BET}$  of 434.545 m<sup>2</sup>/g) and a similar pore size diameter, even for a longer time (up to 30 minutes), the smallest percentage of adsorption of DNA was verified on silica (orange data in Figure 34), at least up to the detection limits of the analytical equipment used. On the other hand, the best materials for DNA removal are [Si][C<sub>3</sub>C<sub>1</sub>Im]Cl, [Si][N<sub>3114</sub>]Cl and [Si][N<sub>3222</sub>]Cl with an AE of 36.15; 36.78 and 25.78 %, respectively. Thus, these materials are used for adsorption assays with the aim of determine kinetics and equilibrium state.

### 3.1.8.1. Kinetics determination assays

Kinetic studies are important to understand the adsorption mechanisms in fluid-solid systems<sup>114,115</sup>. The data obtained from the kinetic tests give information about the time required to reach equilibrium and the time to complete the adsorption which determines the removal rate<sup>116</sup>. This data is important for choosing the optimal operating conditions for scaling up a large-scale batch process or even for a continuous process<sup>117,118</sup>.

The kinetic curves of DNA in SILs were determined in order to evaluate and establish the appropriate contact time for further studies on adsorption isotherms.

In this way, a DNA solution with a concentration of 34.50  $\mu\text{g/mL}$  was applied to 2.5 mg of  $[\text{Si}][\text{C}_1\text{C}_3\text{Im}]\text{Cl}$  during different times (the results are in Figure 32). Then, the models of pseudo-first (PFO) and second-order(PSO) (approached in chapter 2.6) was applied with the aim to describe kinetic behavior (Figure 35).

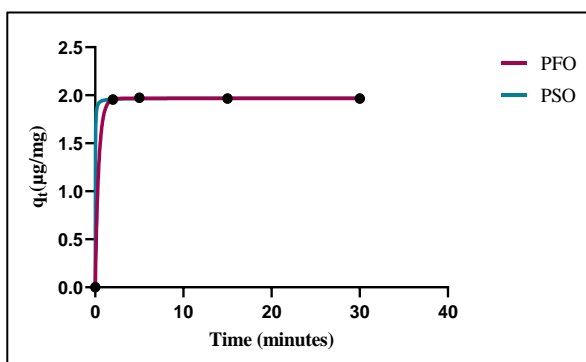


**Figure 35** – DNA adsorption assay with  $[\text{Si}][\text{C}_3\text{C}_1\text{Im}]\text{Cl}$  with representation of pseudo-first order (PFO) and pseudo-second order (PSO) kinetic models for  $[\text{Si}][\text{C}_3\text{C}_1\text{Im}]\text{Cl}$ .

For  $[\text{Si}][\text{C}_3\text{C}_1\text{Im}]\text{Cl}$ , equilibrium appears established into 2 minutes and remains for up to 30 minutes. DNA adsorption is almost instantaneous, which means quick adsorption of this molecule to the surface of the adsorbent. The maximum equilibrium concentrations of adsorbate in the solid phase ( $q_t$ ) were 1.97  $\mu\text{g}/\text{mg}$  at 5 minutes, which corresponds with a removal of 58%.

The same was performed with  $[\text{Si}][\text{N}_{3114}]\text{Cl}$ . The initial DNA concentration was 49.9  $\mu\text{g/mL}$ . The results for this material are in Figure 36.

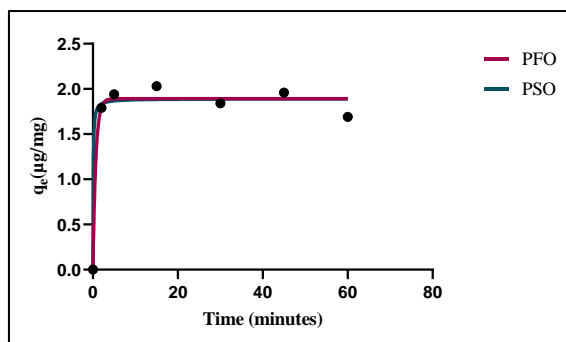


**Figure 36** - Experimental values of  $q_t$  ( $\mu\text{g}/\text{mg}$ ) of DNA as a function of time (min) and representation of pseudo-first order (PFO) and pseudo-second order (PSO) kinetic models for  $[\text{Si}][\text{N}_{3114}]\text{Cl}$ .

Regarding Figure 36, it was observed that the equilibrium for  $[\text{Si}][\text{N}_{3114}]\text{Cl}$  was established, also into 2 minutes and remains for up to 60 minutes. As  $[\text{Si}][\text{C}_3\text{C}_1\text{Im}]\text{Cl}$ , the adsorption also was instantaneous. Furthermore, was seen that the maximum equilibrium concentration of adsorbate in the solid phase ( $q_t$ ) was  $2.03 \mu\text{g}/\text{mg}$  (15 minutes), which coincides with the removal of 41.88 %.

The  $[\text{Si}][\text{N}_{3222}]\text{Cl}$  also was in contact with a DNA solution ( $32.2 \mu\text{g}/\text{mL}$ ). The experimental results of the  $q_t$  values ( $\mu\text{g}/\text{mg}$ ) of DNA as a function of time (min) and the same mathematics models applied are represented in Figure 37.

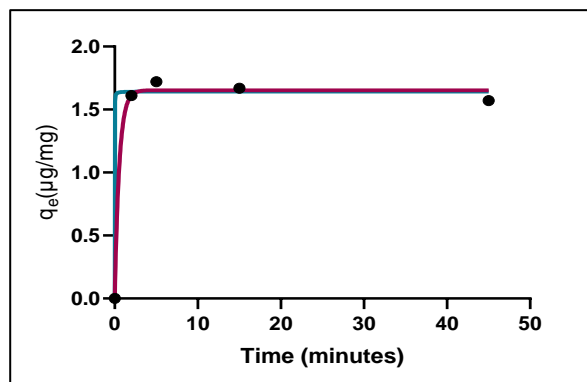


**Figure 37** - Experimental values of  $q_t$  ( $\mu\text{g}/\text{mg}$ ) of DNA as a function of time (min) and representation of pseudo-first order (PFO) and pseudo-second order (PSO) kinetic models for  $[\text{Si}][\text{N}_{3222}]\text{Cl}$ .

With [Si][N<sub>3222</sub>]Cl was noted the equilibrium at 5 minutes and then was remarked a decrease of  $q_t$  value. In this case, the maximum equilibrium concentration of adsorbate in the solid phase ( $q_t$ ) was 1.720  $\mu\text{g}/\text{mg}$  (52 %). Comparing with the other materials, the adsorption also occurred instantaneously.

The adjustment parameters obtained by applying the models can be found in Table 15.

**Table 15** - Kinetic parameters for the pseudo-first-order (PFO) and pseudo-second-order (PSO) models for the different synthesized SIL.

SIL	PFO			PSO		
	$q_e$ ( $\mu\text{g}/\text{mg}$ )	$k_1$ ( $\text{min}^{-1}$ )	$R^2$	$q_e$ ( $\mu\text{g}/\text{mg}$ )	$k_2$ ( $\text{g mg}^{-1}\text{min}^{-1}$ )	$R^2$
[Si][C <sub>3</sub> C <sub>1</sub> Im]Cl	1.968	2.511	1.000	1.969	46.33g	1.000
[Si][N <sub>3114</sub> ]Cl	1.892	1.468	0.9779	1.891	8.398	0.9755
[Si][N <sub>3222</sub> ]Cl	1.653	1.831	0.9946	1.643	274.5	0.9940

The choose of the best model is based on  $R^2$  (is the amount of adsorbate adsorbed by the adsorbent in equilibrium)<sup>115,119</sup>. Comparing the data, no significant differences were observed between the  $R^2$  and  $q_e$  values obtained from the two kinetics models. These results suggest that the adsorption process is a very fast process, almost instantaneous. Consequently, kinetics models are difficult to adjust to experimental data. However, a trend of  $q_e$  value decreases was observed in the following order: [Si][C<sub>3</sub>C<sub>1</sub>Im]Cl > [Si][N<sub>3114</sub>]Cl > [Si][N<sub>3222</sub>]Cl. These results corroborate with the preliminary test.

A supported ionic liquid (polymeric ionic liquid (PIL), poly(1-vinyl-3-(2-methoxy-2-oxyl ethyl)imidazolium)) was used to DNA Salmon removal for later application on plasmid DNA purification<sup>96</sup>. In this work, the equilibrium was achieved in one minute, with 95% of adsorption efficiency. This article didn't apply kinetics models studies; however, similar quick adsorption behavior was observed.

The instantaneous adsorption is advantageous for the purpose of this work, once that SILs should be faster than enzymatic activity in order to prevent DNA degradation into purines.

Relating with the results of purines, once that the synthesized SILs didn't have success as purines removal. This could mean that the interaction between DNA and materials happens perhaps due to the phosphate group of DNA<sup>28</sup>. So, this interaction could be electrostatic interaction<sup>96</sup>. In this work, DNA assays were performed at pH of water. Regarding Table 12 ( PZC of [Si][C<sub>3</sub>C<sub>1</sub>Im] Cl is 8.9, [Si][N<sub>3114</sub>]Cl is 9.3) and [Si][N<sub>3222</sub>]Cl (9.0)) and Figure 21, at this assays conditions, these materials have a positive charge. While with [Si][N<sub>3888</sub>]Cl and [Si][N<sub>3114</sub>]Cl, there could have repulsion forces.

For more conclusions, tests at different pH needs should be measured in the future.

### 3.1.8.2. Isothermal DNA assay

The adsorption isotherm is important from both theoretical and practical points of view<sup>120</sup>. In general, an adsorption isotherm is a curve that describes the phenomenon governing the retention (or release) or mobility of a substance from the aqueous media to a solid phase at the same conditions of temperature and pH<sup>97</sup>. Adsorption equilibrium is the ratio between the adsorbed amount with the remaining in the solution<sup>97</sup>. This equilibrium is established when an adsorbate containing phase has been contacted with the adsorbent for enough time, with its adsorbate concentration in the bulk solution is in a dynamic balance with the interface concentration<sup>97</sup>. Equilibrium equations are used to describe the experimental data, and the parameters obtained from the applied models give us information about the sorption mechanism, the surface properties, the affinity of the adsorbent and the interactions between adsorbate and adsorbent<sup>121</sup>. For this reason, it is important to establish the most appropriate correlations for each system, for proper interpretation of results and adsorption system optimization.

The experimental data on the adsorption isotherms were obtained at room temperature, the same pH (water) and time. The obtained isotherm seems to belong to the group of isotherms of type L or S<sup>122</sup>. In this sense the experimental data were adjusted to 3 models of isotherms that best describe this behavior - Langmuir isotherm (Eq.15), Freundlich isotherm (Eq.16), and Sips isothermal (Eq.17). Langmuir isotherm and Freundlich isotherm are two-parameter models and Sips isotherm is a model derived from the previous two models and it has 3 parameters<sup>97,102</sup>.

The initial concentrations of DNA extracted are ranging between 13.25 and 671.0  $\mu\text{g/mL}$  for [Si][C<sub>3</sub>C<sub>1</sub>Im] assays, 10.15 and 486.0  $\mu\text{g/mL}$  for [Si][N<sub>3114</sub>]Cl and 10.15 and 762.0  $\mu\text{g/mL}$  for [Si][N<sub>3222</sub>]Cl.

To guarantee that the equilibrium was reached, the contact time to carry out the adsorption isotherms studies was set to 30 minutes for [Si][C<sub>3</sub>C<sub>1</sub>Im]Cl, 15 minutes for [Si][N<sub>3114</sub>]Cl and 5 minutes for [Si][N<sub>3222</sub>]Cl (these times were established due to kinetic assay data).



The relation between DNA equilibrium concentrations on the solid and on liquid phases are shown in Figure 38 (detailed data are given in Tab.7 – Annex). In this figure, it is also possible to observe the isothermal models applied: Langmuir represented by the red curve, Freundlich by the blue curve and Sips by the green curve.

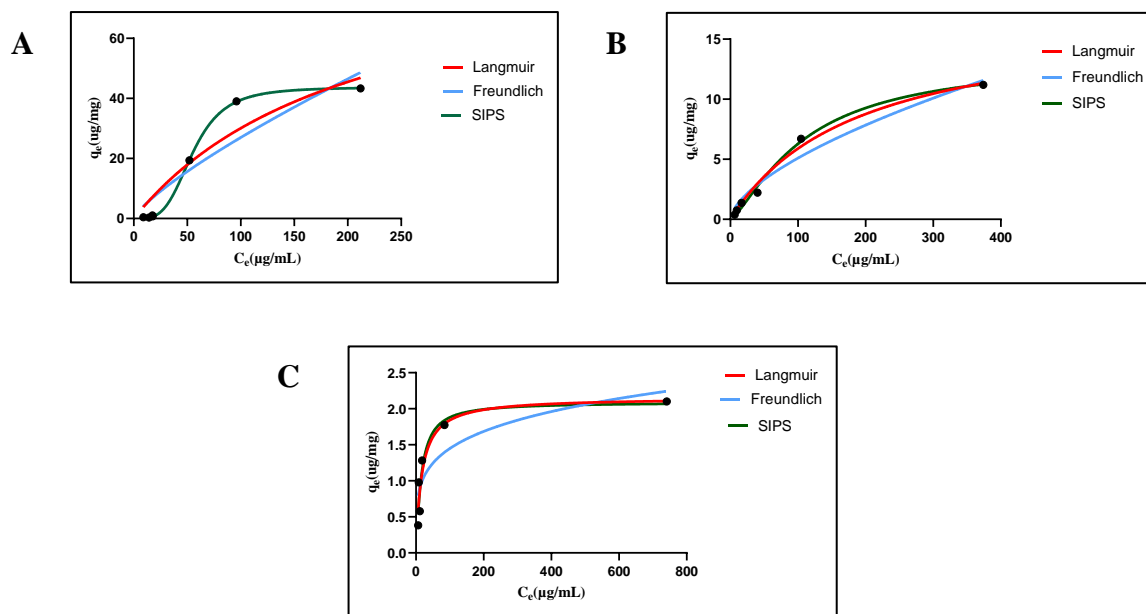


**Figure 38** - Adsorption isotherms of DNA onto SILs at room temperature: A)  $[\text{Si}][\text{C}_3\text{C}_1\text{Im}]\text{Cl}$ ; B)  $[\text{Si}][\text{N}_{3114}]\text{Cl}$  and C)  $[\text{Si}][\text{N}_{3222}]\text{Cl}$

Analyzing the isothermal graphics, it was observed that when initial concentration increases ( $C_0$ ), the DNA at equilibrium in water solution ( $C_e$ ) and the quantity of DNA adsorbed on SILs in equilibrium ( $q_e$ ) also increase. This means that the molecules are gradually being adsorbed on the surface until the equilibrium appears to be established. At this moment, a plateau is reached at around 100  $\mu\text{g} / \text{mL}$  for  $[\text{Si}][\text{C}_3\text{C}_1\text{Im}]\text{Cl}$  and  $[\text{Si}][\text{N}_{3222}]\text{Cl}$  and approximately around 400  $\mu\text{g} / \text{mL}$  for  $[\text{Si}][\text{N}_{3114}]\text{Cl}$  of an equilibrium concentration of adsorbate. However, more plots should be determined in the future. This wasn't possible in this work due to the difficulty of obtaining a high concentration of DNA in the extraction process.

According to the best experimental data of each SIL, the maximum quantity of DNA on the solid phase ( $q_{\text{máx}}$ ) was 43.32, 11.20 and 2.10  $\mu\text{g}/\text{mg}$  for  $[\text{Si}][\text{C}_3\text{C}_1\text{Im}]\text{Cl}$ ,  $[\text{Si}][\text{N}_{3114}]\text{Cl}$  and  $[\text{Si}][\text{N}_{3222}]\text{Cl}$ , respectively. The best material identified is  $[\text{Si}][\text{C}_3\text{C}_1\text{Im}]\text{Cl}$ , due to be capable of adsorbing more DNA per mg of material. These values corroborate with the primary test, present in chapter 3.1.8 of this dissertation.

Besides, the determination of the model parameters was performed using a nonlinear model and the Graphpad, with a 95% confidence. Table 16 provides the isotherms parameters and the correlation coefficients ( $R^2$ ) derived from Eqs 15, 16 and 17.

**Table 16** - Parameters and correlation coefficients obtained with the Langmuir, Freundlich and Sips models regarding the adsorption isotherms of DNA onto the three SILs.

<b>Langmuir model</b>					
<b>SIL</b>	$q_{\text{max}}$ ( $\mu\text{g}/\text{mg}$ )	$K_L$ ( $\text{mL}/\mu\text{g}$ )	$R^2$	$R^2$ adj	
$[\text{Si}][\text{C}_3\text{C}_1\text{Im}]\text{Cl}$	93.49	0.004740	0.8960	0.8752	
$[\text{Si}][\text{N}_{3114}]\text{Cl}$	17.38	0.005030	0.9880	0.9856	
$[\text{Si}][\text{N}_{3222}]\text{Cl}$	2.156	0.05851	0.8958	0.8698	
<b>Freundlich model</b>					
<b>SIL</b>	$K_F$ ( $\mu\text{g mg}^{-1}\text{mL}^{-1}$ )	$n_f$	$R^2$	$R^2$ adj	
$[\text{Si}][\text{C}_3\text{C}_1\text{Im}]\text{Cl}$	0.7262	1.274	0.8557	0.8268	
$r[\text{Si}][\text{N}_{3114}]\text{Cl}$	0.2573	1.556	0.9621	0.9546	
$[\text{Si}][\text{N}_{3222}]\text{Cl}$	0.5297	4.578	0.7603	0.7003	
<b>Sips model</b>					
<b>SIL</b>	$q_{\text{max}_s}$ ( $\mu\text{g}/\text{mg}$ )	$K_s$ ( $\text{mL } \mu\text{g}^{-1}$ )	$n_s$	$R^2$	$R^2$ adj
$[\text{Si}][\text{C}_3\text{C}_1\text{Im}]\text{Cl}$	43.71	0.01815	3.743	0.9998	0.9997
$[\text{Si}][\text{N}_{3114}]\text{Cl}$	13.36	0.009166	1.355	0.9944	0.9917
$[\text{Si}][\text{N}_{3222}]\text{Cl}$	2.090	0.06497	1.171	0.8984	0.8306

As mentioned before, the adjust of a model to adsorption isotherm data is evaluated by  $R^2$ . Once that the number of parameters of the Sips model is different from Langmuir and Freundlich models, it is necessary to use the  $R^2$  adjust for a confinable comparison between the three models.

The examination of plots of Figure 37 shows that the Langmuir and Freundlich models provide a poor-fitting across the concentration range studied, which can be confirmed by the determination coefficient adjusted ( $R^2$  adjust) for [Si][C<sub>3</sub>C<sub>1</sub>Im]Cl ( $R^2$  adjust<sub>Langmuir</sub>=0.8752 and  $R^2$ adjust<sub>Freundlich</sub>=0.8268). On the other hand, the Sips isotherm accurately describes the equilibrium behavior for DNA ( $R^2$ adjust<sub>Sips</sub>=0.9997) over the concentration ranges studied.

The same tendency was observed when the adsorbate is [Si][N<sub>3114</sub>]Cl. In this case the  $R^2$ adjust<sub>Sips</sub> =0.9917 >  $R^2$  adjust<sub>Langmuir</sub> =0.9856 >  $R^2$ adjust<sub>Freundlich</sub> =0.9546.

Across the concentration range used the adjustment of the experimental data in this study was accurately described by the Sips isotherm, which combines both Langmuir and Freundlich features. The obtained isotherms were S-type shape, in which the initial slope shows a concave trend, indicating that the sorption is unfavorable for lower DNA concentrations (below 25 µg/mL). For higher concentrations as the affinity of DNA to the surface of [Si][C<sub>3</sub>C<sub>1</sub>Im]Cl and [Si][N<sub>3114</sub>]Cl, the adsorption becomes significantly higher and an increment in the slope is observed. In general, this isotherm shape suggests the existence of cooperative sorption (the sorption becomes progressively easier as more sorbate is taken up) and it is indicative of a physical mechanism<sup>101,123</sup>.

The Sips isotherm provides a maximum adsorption capacity at monolayer coverage of 43.71 µg/mg for [Si][C<sub>3</sub>C<sub>1</sub>Im]Cl and of 13.36 µg/mg for [Si][N<sub>3114</sub>]Cl. The value  $q_{max}$ , obtained for [Si][C<sub>3</sub>C<sub>1</sub>Im]Cl highlights its higher capacity when compared with [Si][N<sub>3114</sub>]Cl. The deviation from the unity in the heterogeneity index values (Table 16) discloses the heterogeneity of the [Si][C<sub>3</sub>C<sub>1</sub>Im]Cl and [Si][N<sub>3114</sub>]Cl.

In the case of [Si][N<sub>3222</sub>]Cl, Langmuir was the model that better adjusts to experimental ( $R^2$  adjust<sub>Langmuir</sub>=0.8698), following Sips ( $R^2$ adjust<sub>Sips</sub>=0.8984) and finally Freundlich ( $R^2$ adjust<sub>Freundlich</sub>=0.7003). The Langmuir isotherm provides a maximum adsorption capacity of 2.090 µg/mg. This trend suggests that the adsorption of the molecule onto [Si][N<sub>3222</sub>]Cl, occurs through the formation of a monolayer adsorbate on the outer surface of the adsorbent, where no further adsorption takes place<sup>114</sup>.

Comparing the three synthesized materials, it was concluded that the best Yeast DNA removal is [Si][C<sub>3</sub>C<sub>1</sub>Im]Cl. That can be explained due to the functionalization of material. Regarding Table 11, the bounding amount of materials is 2.353, 1.261 and 0.4320  $\mu\text{mol}/\text{m}^2$  for [Si][C<sub>3</sub>C<sub>1</sub>Im]Cl, [Si][N<sub>3114</sub>]Cl and [Si][N<sub>3222</sub>]Cl and this means that at the begin [Si][C<sub>3</sub>C<sub>1</sub>Im]CL there is always a higher adsorption rate . In this way, in the future, the materials synthesis should be made with the same moles of cation percussor.

Regarding the bibliography, some investigations about DNA adsorption were performed. The results are in Table 17.

**Table 17** - The maximum capacities of DNA adsorption/extraction by various materials reported in the literature

Materials	$q_{\text{max}}$ ( $\mu\text{g}/\text{mg}$ )	Reference
Fe <sub>3</sub> O <sub>4</sub> nanoparticles	10.00	124
Aminosilane-modified Fe <sub>3</sub> O <sub>4</sub> nanoparticles	60.00	125
PEI-modified Fe <sub>3</sub> O <sub>4</sub> nanoparticles	70.00	126
Polyglycidyl methacrylate-modified Fe <sub>3</sub> O <sub>4</sub> nanoparticles	90.40	127
Poly(VMIIm)PF6 microspheres	190.7	96
[Si][C <sub>3</sub> C <sub>1</sub> Im]Cl	43.7	This work

Once that in the future, the aim should be included SILs in the brewing process, SILs would be placed in the malting phase of the process to remove the malt DNA. Also, these materials could be used in the clarification phase, in order to adsorb nucleic acids from yeast. In this way, the purine content of beer could be decreased.

It is known that there are 7.5  $\mu\text{g}/\text{mL}$  of nucleic acids in wort<sup>24</sup> and it was proved that 1 mg of [Si][C<sub>3</sub>C<sub>1</sub>Im]Cl is available to remove 43.7  $\mu\text{g}$  of DNA from water solution. So in industrial terms, 1 kg of [Si][C<sub>3</sub>C<sub>1</sub>Im]Cl could be used for treated 573.33 L of wort.

Although there are other materials with higher efficiency than [Si][C<sub>3</sub>C<sub>1</sub>Im]Cl, this material could be used and succeed if was selective.

In this way, a primary assay with an amino acid present in beer was performed.

### 3.1.9. Selective assays

In order to keep the flavors of beer, it is important that synthesized ionic liquids are selective, which means that these materials should be specific for the target molecule. To test this possibility, a preliminary assay was performed using one of the amino acids more abundant in the beer - tyrosine<sup>128</sup>. The choose of this specific amino acid is due to the chemical structure and its role in the flavor of beer<sup>128</sup>. This molecule is, also, present in barley<sup>128</sup>.

In this way, 2.5 mg of [Si][C<sub>3</sub>C<sub>1</sub>Im]Cl, [Si][N<sub>3114</sub>]Cl and [Si][N<sub>3222</sub>]Cl was contacted with 250  $\mu$ L of aminoacid solution (90 mg/L). This concentration was chosen because of the low limit of detection of equipment. The method of measurement of tyrosine concentration obeys Lambert-Beer law, therefore it was used UV-VIS spectrometry. These results are shown in Figure 39.

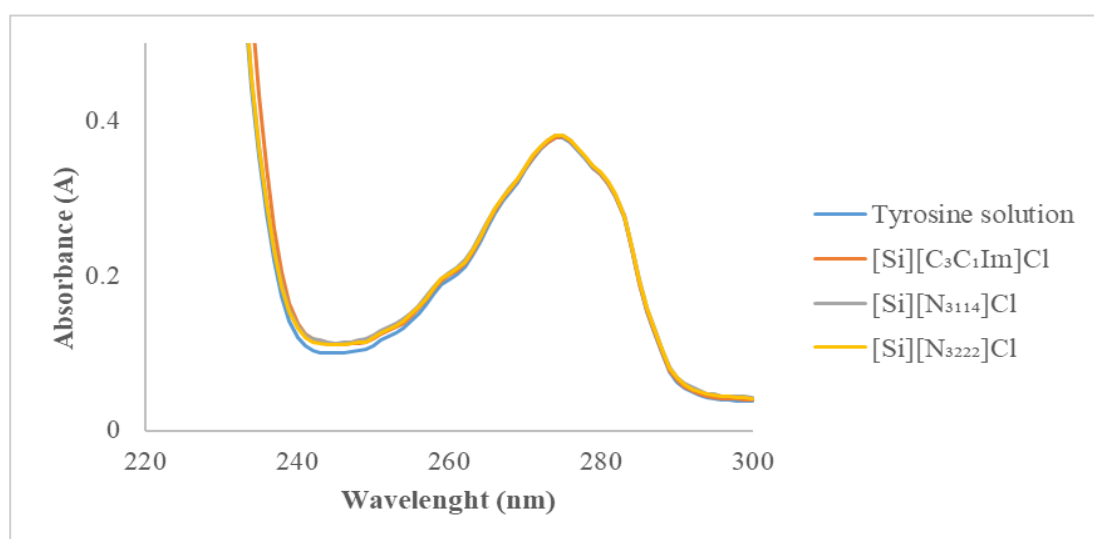


**Figure 39** – Tyrosine adsorption assays, after 30 minutes contact with SILs

Analyzing the results of Figure 39, it was observed that the absorbance of initial tyrosine solution doesn't decrease after 30 minutes of contact with the SILs, which means that the concentration of initial solutions was the same as tyrosine solution after contact with SILs. Consequently, this data suggests that the materials synthesized don't have capacity for tyrosine removal at the conditions, which the assays were performed.

As referred in chapter 3.1.8.1, DNA adsorption on [Si][C<sub>3</sub>C<sub>1</sub>Im]Cl, [Si][N<sub>3114</sub>]Cl and [Si][N<sub>3222</sub>]Cl are almost instantaneous. On the other hand, after 30 minutes of contact between tyrosine and SILs, the adsorption of this amino acid doesn't happen. So, this could suggest that the mentioned SILs are selective for DNA but they aren't specificity for tyrosine. This data gives a good perspective for the future. Besides this result, it is necessary to do more selective assays.

## **IV-Conclusions and future work**





The main objective of this dissertation was to study the adsorption of purines present in beer (adenine, adenosine, guanosine, and inosine) and Yeast DNA using silica-supported ionic liquids from water, aiming at the potential application of these materials in the beer process. Although the purine beer also comes from Malt DNA, the chemical structure is the same, consequently, only yeast DNA was tested.

Five SILS were synthesized and characterized for this purpose. The SILs are: [Si][C<sub>3</sub>C<sub>1</sub>Im]Cl; [Si][N<sub>3114</sub>]Cl, [Si][N<sub>3222</sub>]Cl [Si][N<sub>3444</sub>]Cl and [Si][N<sub>3888</sub>]Cl. The characterization, using several techniques, demonstrated that the synthesis was performed successfully.

In this way, those materials were used for purine adsorption assays.

SILs had not capacity for purine removal, in conditions that were performed the assays. So, another strategy for reducing purine content was to take DNA before this molecule was catabolized into purines by enzymes.

In this way, the DNA extracted from *Saccharomyces cerevisiae* was used to performed kinetics and isotherms adsorption assays. Considering the five SILS synthesized, only [Si][C<sub>3</sub>C<sub>1</sub>Im]Cl, [Si][N<sub>3114</sub>]Cl and [Si][N<sub>3222</sub>]Cl showed the ability to remove DNA. The kinetics data demonstrated that DNA adsorption is instantaneous, consequently, the models of kinetics are not applicable. Besides that, the adsorption data fit well with the Sips model for [Si][C<sub>3</sub>C<sub>1</sub>im]Cl and [Si][N<sub>3114</sub>]Cl and with the Langmuir model for [Si][N<sub>3222</sub>]Cl. The best DNA removal was [Si][C<sub>3</sub>C<sub>1</sub>Im]Cl. A maximum equilibrium concentration of DNA in the solid phase of 43.70 µg per mg of SIL was obtained.

With the aim to prove selective of [Si][C<sub>3</sub>C<sub>1</sub>Im]Cl, [Si][N<sub>3114</sub>]Cl and [Si][N<sub>3222</sub>]Cl, Tyrosine was used for adsorption assays. These SILs didn't demonstrate the capacity for amino acid removal, giving a little proof of selectivity.

Further studies are being carried out in order to identify more promising materials that can be used to remove purine compounds and DNA from beer to avoid beer restrictions due to hyperuricemia and gout conditions. As well, it is necessary for additional studies with synthesized SILs in other conditions of pH, temperature and medium complexity (amino acids and enzymes).

Later, the performance of these materials should be tested in wort (where Malt DNA is present before being catabolized into purines) and beer (after the fermentation).

Therefore, the results obtained in this work gives a good perspective to be applied in other areas, as DNA purification and chromatography.

## **V- Bibliography**



1. Holzapfel, W. *Advances in Fermented Foods and Beverages. Improving Quality, Technologies and Health Benefits* (British Library, 2015).
2. Gastineau, C., Darby, W. & Turner, T. *Fermented Food Beverages in Nutrition*. (Academic Press, 1979).
3. Magalhães, P. J., Carvalho, D. O., Cruz, J. M., Guido, L. F. & Barros, A. A. Fundamentals and health benefits of xanthohumol, a natural product derived from hops and beer. *Nat. Prod. Commun.* **4**, 591–610 (2009).
4. Wardencki, W. *Alcoholic Beverages. Encyclopedia of Analytical Science, 3rd Edition* (Elsevier Inc., 2018).
5. Ryan, R. Safety of Food and Beverages. *Encyclopedia of Food Safety* **3**, 364–3170 (2014).
6. Debebe, A., Redi-Abshiro, M. & Chandravanshi, B. S. Non-destructive determination of ethanol levels in fermented alcoholic beverages using Fourier transform mid-infrared spectroscopy. *Chem. Cent. J.* **11**, 1–8 (2017).
7. Yamamoto, T. & Moriwaki, Y. Purines in Beer. *Beer Heal. Dis. Prev.* 285–290 (2009).
8. Buiatti, S. & Science, F. Beer Composition : An Overview. *Beer in Health and Disease Prevention* 213–225 (2009).
9. Rodhouse, L. & Carbonero, F. Overview of craft brewing specificities and potentially associated microbiota. *Crit. Rev. Food Sci. Nutr.* 1–12 (2017).
10. Capece, A. *et al.* Use of *Saccharomyces cerevisiae* var. *bouardii* in co-fermentations with *S. cerevisiae* for the production of craft beers with potential healthy value-added. *Int. J. Food Microbiol.* **284**, 22–30 (2018).
11. Bamforth, C. W. Beer and health. in *Beer: A Quality Perspective* 229–253 (Academic Press, 2009).
12. Sohrabvandi, S., Mortazavian, A. M. & Rezaei, K. Health-related aspects of beer: A review. *Int. J. Food Prop.* **15**, 350–373 (2012).
13. Chen, W., Becker, T., Qian, F. & Ring, J. Beer and beer compounds: physiological effects on skin health. *J. Eur. Acad. Dermatology Venereol.* **28**, 142–150 (2014).
14. Diário da República. Lei 3/2001, 2001-02-23 - DRE. (2001). Available at: <https://dre.pt/pesquisa/-/search/386237/details/maximized>. (Accessed: 4th November 2018).

15. Li, Q., Wang, J. & Liu, C. *Beers. Current Developments in Biotechnology and Bioengineering: Food and Beverages Industry* (2016).
16. Harrison, M. A. & Albanese, J. B. Beer/Brewing. *Ref. Modul. Life Sci.* 1–11 (2017).
17. Cortacero-Ramírez, S., Hernáinz-Bermúdez De Castro, M., Segura-Carretero, A., Cruces-Blanco, C. & Fernández-Gutiérrez, A. Analysis of beer components by capillary electrophoretic methods. *TrAC - Trends Anal. Chem.* **22**, 440–445 (2003).
18. Bettenhausen, H. M. *et al.* Influence of malt source on beer chemistry, flavor, and flavor stability. *Food Res. Int.* **113**, 487–504 (2018).
19. Z. Yemataw, H. Mohamed, M. Diro, T. A. and G. B. Nitrogen compounds in brewing wort and beer : A review. *J. Brew. Distill.* **5**, 10–17 (2014).
20. Kunze, W. *Technology Brewing and Malting.* (VLB, 2004).
21. Bacha, K., Mehari, T. & Ashenafi, M. Microbiology of the fermentation of shamita, a traditional ethiopian fermented beverage. *Sinet:Ethiopian* **22**, 113–126 (1999).
22. Bokulich, N. A. & Bamforth, C. W. The microbiology of malting and brewing. *Microbiol. Mol. Biol. Rev.* **77**, 157–72 (2013).
23. Bamforth, C. *Grape vs grain.* **39**, (Cambridge university press, 2008).
24. MacWilliam, I. C. Wort Composition—a Review. *J. Inst. Brew.* **74**, 38–54 (1968).
25. Li, H., Liu, F., Hao, J. & Liu, C. Determination of Purines in Beer by HPLC Using a Simple and Rapid Sample Pretreatment. *Res. gate* **73**, 137–142 (2015).
26. Harris, G. & Parsons, R. Nitrogenous constituents of brewing materials. *J. Inst. Brew.* **63**, 227–236 (1957).
27. Shtogun, Y. V., Woods, L. M. & Dovbeshko, G. I. Adsorption of adenine and thymine and their radicals on single-wall carbon nanotubes. *J. Phys. Chem. C* **111**, 18174–18181 (2007).
28. Watson, J. D. & Crick, F. H. C. The structure of DNA. *Cold Spring Harb Symp Quant Biol* **18**, 123–131 (1953).
29. Ahmed, N. & James, T. *Fundamentals of Biomedical Science: Clinical Biochemistry.* (Oxford University Press, 2016).
30. Kumari, A. Purine Structures. in *Sweet Biochemistry: Remembering Structures, Cycles, and Pathways by Mnemonics.* 89–91 (Academic Press., 2018).
31. Keenan, R. T., Krasnokutsky, S. & Pillinger, M. H. Etiology and Pathogenesis of Hyperuricemia and Gout. *Kelley Firestein's Textb. Rheumatol.* 1597-1619.e6

- (2017).
32. Murray, R. *et al.* *Bioquímica ilustrada de Harper*. (AMGH Editora, 2014).
  33. Fam, A. G. Gout, diet, and the insulin resistance syndrome. *J. Rheumatol.* **29**, 1350–1355 (2002).
  34. Kaneko, K., Yamanobe, T. & Fujimori, S. Determination of purine contents of alcoholic beverages using high performance liquid chromatography. *Biomed. Chromatogr.* **23**, 858–864 (2009).
  35. Gibson, T., Rodgers, A. V., Simmonds, H. A. & Toseland, P. Beer drinking and its effect on uric acid. *Br. J. Rheumatol.* **23**, 203–209 (1974).
  36. Klampfl, C. W., Himmelsbach, M., Buchberger, W. & Klein, H. Determination of purines and pyrimidines in beer samples by capillary zone electrophoresis. *Anal. Chim. Acta* **454**, 185–191 (2002).
  37. Charalambous G, Bruckner KJ, Hardwick WA, L. A. Separation, identification and determination of beer flavour compounds by high pressure liquid chromatography. *Tech Q Master Brew Assoc Am* **11**, 150–154 (1974).
  38. de Oliveira, E. P. & Burini, R. C. High plasma uric acid concentration: causes and consequences. *Diabetol. Metab. Syndr.* **4**, 12 (2012).
  39. Roughley, M. *et al.* Risk of chronic kidney disease in patients with gout and the impact of urate lowering therapy: a population-based cohort study. *Arthritis Res. Ther.* **20**, 243 (2018).
  40. Maiuolo, J., Oppedisano, F., Gratteri, S., Muscoli, C. & Mollace, V. Regulation of uric acid metabolism and excretion. *Int. J. Cardiol.* **213**, 8–14 (2016).
  41. Kaneko, K., Aoyagi, Y., Fukuuchi, T., Inazawa, K. & Yamaoka, N. Total Purine and Purine Base Content of Common Foodstuffs for Facilitating Nutritional Therapy for Gout and Hyperuricemia. *Biol. Pharm. Bull* **37**, 709–721 (2014).
  42. Clarson, L. & Roddy, E. Epidemiology of Gout and Hyperuricemia. *Gout* 59–72 (2019).
  43. Yamamoto, T., Moriwaki, Y. & Takahashi, S. Effect of ethanol on metabolism of purine bases (hypoxanthine, xanthine, and uric acid). *Clin. Chim. Acta* **356**, 35–57 (2005).
  44. Lieber, C. S. Hyperuricemia induced by alcohol. *Arthritis Rheum.* **8**, 786–798 (1965).

45. Moriwaki, Y. & Yamamoto, T. *Effects of Beer Ingestion on Body Purine Bases. Beer in Health and Disease Prevention* (Elsevier Inc., 2009).
46. Martins, J., Jorge, E., Camolas, J. & Do Carmo, I. Estratégias para Intervenção Nutricional na Hiperuricemia e Gota. *Rev. Nutricias* **19**, 28–31 (2014).
47. Dalbeth, N., Merriman, T. R. & Stamp, L. K. Gout. *Lancet* **388**, 2039–2052 (2016).
48. Kuo, C.-F., Grainge, M. J., Zhang, W. & Doherty, M. Global epidemiology of gout: prevalence, incidence and risk factors. *Nat. Rev. Rheumatol.* **11**, 649–662 (2015).
49. Jankowska, D. A. *et al.* A novel enzymatic approach in the production of food with low purine content using *Arxula adenivorans* endogenous and recombinant purine degradative enzymes. *Bioeng. Bugs* **6**, 20–25 (2015).
50. Shibano, Y. *et al.* Process for producing beer. (1995).
51. Augusto, F., Hantao, L. W., Mogollón, N. G. S. & Braga, S. C. G. N. New materials and trends in sorbents for solid-phase extraction. *TrAC - Trends Anal. Chem.* **43**, 14–23 (2013).
52. Artioli, Y. The Chemistry of Adsorption. *Ecol. Process.* 60–65 (2008).
53. Tareq, R., Akter, N. & Azam, M. S. Biochars and Biochar Composites: Low-Cost Adsorbents for Environmental Remediation. *Biochar from Biomass Waste* 169–209 (2019).
54. Zhang, C., Xiao, Z., Qin, T. & Yang, Z. Mechanism and kinetics of uric acid adsorption on nanosized hydroxyapatite coating. *J. Saudi Chem. Soc.* (2018).
55. Liu, C. *et al.* Surface modification of pitch-based spherical activated carbon by CVD of NH<sub>3</sub> to improve its adsorption to uric acid. *Appl. Surf. Sci.* **254**, 6701–6705 (2008).
56. Marahel, F., Ghaedi, M. & Ansari, A. Zinc Oxide Nanoparticles Loaded on Activated Carbon and Its Application for Adsorption Removal of Uric Acid. *Synth. React. Inorganic, Met. Nano-Metal Chem.* **45**, 1387–1395 (2015).
57. Wang, P., Wu, H., Dai, Z. & Zou, X. Simultaneous detection of guanine, adenine, thymine and cytosine at choline monolayer supported multiwalled carbon nanotubes film. *Biosens. Bioelectron.* **26**, 3339–3345 (2011).
58. Abdullin, T. I., Nikitina, I. I. & Bondar', O. V. Adsorption and oxidation of purine bases and their derivatives on electrodes modified with carbon nanotubes. *Russ. J. Electrochem.* **44**, 1345–1349 (2008).



59. Kumar, A. S. & Shanmugam, R. Simple method for simultaneous detection of uric acid, xanthine and hypoxanthine in fish samples using a glassy carbon electrode modified with as commercially received multiwalled carbon nanotubes. *Anal. Methods* **3**, 2088–2094 (2011).
60. Marrubini, G., Castillo, B. E., Mendoza & Massolini, G. Separation of purine and pyrimidine bases and nucleosides by hydrophilic interaction chromatography. *J. Sep. Sci.* **33**, 803–816 (2010).
61. Hashizume, H. Adsorption of nucleic acid bases, ribose, and phosphate by some clay minerals. *Life* **5**, 637–650 (2015).
62. Gholami, S., Shokuhi Rad, A., Heydarinasab, A. & Ardjmand, M. Adsorption of adenine on the surface of nickel-decorated graphene; A DFT study. *J. Alloys Compd.* **686**, 662–668 (2016).
63. Manna, A. K. & Pati, S. K. Theoretical understanding of single-stranded DNA assisted dispersion of graphene. *J. Mater. Chem. B* **1**, 91–100 (2013).
64. Hughes, Z. E., Wei, G., Drew, K. L. M., Colombi Ciacchi, L. & Walsh, T. R. Adsorption of DNA Fragments at Aqueous Graphite and Au(111) via Integration of Experiment and Simulation. *Langmuir* **33**, 10193–10204 (2017).
65. Leshchinskaya, A. P., Ezhova, N. M. & Pisarev, O. A. Synthesis and characterization of 2-hydroxyethyl methacrylate-ethylene glycol dimethacrylate polymeric granules intended for selective removal of uric acid. *React. Funct. Polym.* **102**, 101–109 (2016).
66. Pedreira-Segade, U., Feuillie, C., Pelletier, M., Michot, L. J. & Daniel, I. Adsorption of nucleotides onto ferromagnesian phyllosilicates: Significance for the origin of life. *Geochim. Cosmochim. Acta* **176**, 81–95 (2016).
67. Gao, B., Jiang, P. & Lei, H. Studies on adsorption property of novel composite adsorption material PEI/SiO<sub>2</sub> for uric acid. *Mater. Lett.* **60**, 3398–3404 (2006).
68. Buday, A. Z. & Belleau, G. Use of Activated Carbon for Recovery and Concentration of Nucleic-Acid Derivatives and Other Compounds from Biological Samples. *Can. Inst. Food Sci. Technol. Journal-Journal L Inst. Can. Sci. Technol. Aliment.* **7**, 188–198 (1974).
69. Wilz, P. R. Adsorption Materials. (1976).
70. Fujino, S. & Sakuma, S. Process for producing fermented malt drink with reduced

- purine content. **1**, 1–26 (2004).
71. Shibata, J., Murayama, N. & Tateyama, M. Adsorption of Purine Compounds in Beer with Activated Carbon Prepared from Beer Lees. *Resour. Process.* **126**, 120–126 (2009).
  72. Wasserscheid, P. & Welton, T. *Ionic Liquids in Synthesis*. **7**, (2002).
  73. Xin, B. & Hao, J. Imidazolium-based ionic liquids grafted on solid surfaces. *Chem. Soc. Rev.* **43**, 7171–7187 (2014).
  74. Ventura, S. P. M. *et al.* Ionic-Liquid-Mediated Extraction and Separation Processes for Bioactive Compounds: Past, Present, and Future Trends. *Chem. Rev.* **117**, 6984–7052 (2017).
  75. Vidal, L., Parshintsev, J., Hartonen, K., Canals, A. & Riekkola, M. L. Ionic liquid-functionalized silica for selective solid-phase extraction of organic acids, amines and aldehydes. *J. Chromatogr. A* **1226**, 2–10 (2012).
  76. Lemus, J., Palomar, J., Gilarranz, M. A. & Rodriguez, J. J. Characterization of Supported Ionic Liquid Phase (SILP) materials prepared from different supports. *Adsorption* **17**, 561–571 (2011).
  77. Petkovic, M., Seddon, K. R., Rebelo, L. P. N. & Pereira, C. S. Ionic liquids: A pathway to environmental acceptability. *Chem. Soc. Rev.* **40**, 1383–1403 (2011).
  78. Han, D. & Row, K. H. Recent applications of ionic liquids in separation technology. *Molecules* **15**, 2405–2426 (2010).
  79. Toledo Hijo, A. A. C., Maximo, G. J., Costa, M. C., Batista, E. A. C. & Meirelles, A. J. A. Applications of Ionic Liquids in the Food and Bioproducts Industries. *ACS Sustain. Chem. Eng.* **4**, 5347–5369 (2016).
  80. Martins, P. L. G., Braga, A. R. & de Rosso, V. V. Can ionic liquid solvents be applied in the food industry? *Trends Food Sci. Technol.* **66**, 117–124 (2017).
  81. Wu, C. *et al.* Conversion of Xylose into Furfural Using Lignosulfonic Acid as Catalyst in Ionic Liquid. *J. Agric. Food Chem.* **62**, 7430–7435 (2014).
  82. Liang, R. *et al.* Feasibility of Ionic Liquids as Extractants for Selective Separation of Vitamin D<sub>3</sub> and Tachysterol<sub>3</sub> by Solvent Extraction. *J. Agric. Food Chem.* **61**, 3479–3487 (2013).
  83. Pereira, M. M. *et al.* Enhanced extraction of bovine serum albumin with aqueous biphasic systems of phosphonium- and ammonium-based ionic liquids. *J.*

- Biotechnol.* **206**, 17–25 (2015).
84. Magiera, S. & Sobik, A. Ionic liquid-based ultrasound-assisted extraction coupled with liquid chromatography to determine isoflavones in soy foods. *J. Food Compos. Anal.* **57**, 94–101 (2017).
  85. Zhang, C., Cagliero, C., Pierson, S. A. & Anderson, J. L. Rapid and sensitive analysis of polychlorinated biphenyls and acrylamide in food samples using ionic liquid-based in situ dispersive liquid-liquid microextraction coupled to headspace gas chromatography. *J. Chromatogr. A* **1481**, 1–11 (2017).
  86. Huang, L.-L. *et al.* Supported Ionic Liquids Solid-Phase Extraction Coupled to Electrochemical Detection for Determination of Trace Bisphenol A. *Chinese J. Anal. Chem.* **43**, 313–318 (2015).
  87. LiLi, Z., Lin, G., ZhenJiang, Z., Ji, C. & Min, Z. S. The preparation of supported ionic liquids (SILs) and their application in rare metals separation. *Sci. China Chem.* **55**, 1479–1487 (2012).
  88. Asefa, T. & Tao, Z. Biocompatibility of mesoporous silica nanoparticles. *TL - 25. Chem. Res. Toxicol.* **25** VN-r, 2265–2284 (2012).
  89. Liu, J. *et al.* Disposable ionic liquid coating for headspace solid-phase microextraction of benzene, toluene, ethylbenzene, and xylenes in paints followed by gas chromatography–flame ionization detection. *J. Chromatogr. A* **1066**, 27–32 (2005).
  90. Bi, W., Tian, M. & Row, K. H. Selective extraction and separation of oxymatrine from *Sophora flavescens* Ait. extract by silica-confined ionic liquid. *J. Chromatogr. B* **880**, 108–113 (2012).
  91. Bi, W., Zhou, J. & Row, K. H. Solid Phase Extraction of three phenolic acids from *Saliconia herbacea* L. by different ionic liquid-based silicas. *J. Liq. Chromatogr. Relat. Technol.* **35**, 723–736 (2012).
  92. Wang, Z. *et al.* Determination of phenolic acids and flavonoids in raw propolis by silica-supported ionic liquid-based matrix solid phase dispersion extraction high performance liquid chromatography-diode array detection. *J. Chromatogr. B* **969**, 205–212 (2014).
  93. Bi, W., Zhou, J. & Row, K. H. Solid phase extraction of lactic acid from fermentation broth by anion-exchangeable silica confined ionic liquids. *Talanta* **83**,

- 974–979 (2011).
94. Marwani, H. M., Bakhsh, E. M., Al-Turaif, H. A., Asiri, A. M. & Khan, S. B. Enantioselective separation and detection of D-phenylalanine based on newly developed chiral ionic liquid immobilized silica gel surface. *Int. J. Electrochem. Sci.* **9**, 7948–7964 (2014).
  95. Tian, M., Yan, H. & Row, K. H. Solid-Phase Extraction of Caffeine and Theophylline from Green Tea by a New Ionic Liquid-Modified Functional Polymer Sorbent. *Anal. Lett.* **43**, 110–118 (2009).
  96. Wang, X., Xing, L., Shu, Y., Chen, X. & Wang, J. Novel polymeric ionic liquid microspheres with high exchange capacity for fast extraction of plasmid DNA. *Anal. Chim. Acta* **837**, 64–69 (2014).
  97. Foo, K. Y. & Hameed, B. H. Insights into the modeling of adsorption isotherm systems. *Chem. Eng. J.* **156**, 2–10 (2010).
  98. Largitte, L. & Pasquier, R. A review of the kinetics adsorption models and their application to the adsorption of lead by an activated carbon. *Chem. Eng. Res. Des.* **109**, 495–504 (2016).
  99. Langmuir, I. The constitution and fundamental properties of solids and liquids. *J. Am. Chem. Soc.* **38**, 2221–2295 (1916).
  100. Allen, S. J., McKay, G. & Porter, J. F. Adsorption isotherm models for basic dye adsorption by peat in single and binary component systems. *J. Colloid Interface Sci.* **280**, 322–333 (2004).
  101. Rocha, L. S. *et al.* Simple and effective chitosan based films for the removal of Hg from waters: Equilibrium, kinetic and ionic competition. *Chem. Eng. J.* **300**, 217–229 (2016).
  102. Tan, K. L. & Hameed, B. H. Insight into the adsorption kinetics models for the removal of contaminants from aqueous solutions. *J. Taiwan Inst. Chem. Eng.* **74**, 25–48 (2017).
  103. Paul, R. & Genescà, E. The use of enzymatic techniques in the finishing of technical textiles. *Adv. Dye. Finish. Tech. Text.* 177–198 (2013).
  104. Tian, M., Bi, W. & Row, K. H. Solid-phase extraction of liquiritin and glycyrrhizic acid from licorice using ionic liquid-based silica sorbent. *J. Sep. Sci.* **32**, 4033–4039 (2009).

105. Tamboli, A. H., Chaugule, A. A., Sheikh, F. A., Chung, W.-J. & Kim, H. Synthesis, characterization, and application of silica supported ionic liquid as catalyst for reductive amination of cyclohexanone with formic acid and triethyl amine as hydrogen source. *Chinese J. Catal.* **36**, 1365–1371 (2015).
106. Galhotra, P., Navea, J. G., Larsen, S. C. & Grassian, V. H. Carbon dioxide (C16O2 and C18O2) adsorption in zeolite Y materials: effect of cation, adsorbed water and particle size. *Energy Environ. Sci.* **2**, 401 (2009).
107. Su, P., Wang, R., Yu, Y. & Yang, Y. Microwave-assisted synthesis of ionic liquid-modified silica as a sorbent for the solid-phase extraction of phenolic compounds from water. *Anal. Methods* **6**, 704–709 (2014).
108. Almeida, H. F. D., Neves, M. C., Trindade, T., Marrucho, I. M. & Freire, M. G. Supported ionic liquids: efficient materials to remove non-steroidal anti-inflammatory drugs from aqueous media. *Green Chem.* 122616 (2019).
109. Shah, S. N., Lethesh, K. C., Abdul Mutalib, M. I. & Mohd Pilus, R. B. Extraction and recovery of naphthenic acid from acidic oil using supported ionic liquid phases (SILPs). *Chem. Prod. Process Model.* **10**, 221–228 (2015).
110. Freitas, J. C. C., Cipriano, D. F., Zucolotto, C. G., Cunha, A. G. & Emmerich, F. G. Solid-State <sup>13</sup>C NMR Spectroscopy Applied to the Study of Carbon Blacks and Carbon Deposits Obtained by Plasma Pyrolysis of Natural Gas. *J. Spectrosc.* **2016**, 1–7 (2016).
111. Heurtault, B., Saulnier, P., Pech, B., Proust, J.-E. & Benoit, J.-P. Physico-chemical stability of colloidal lipid particles. *Biomaterials* **24**, 4283–4300 (2003).
112. nanoScience. Scanning Electron Microscopy - Nanoscience Instruments. Available at: <https://www.nanoscience.com/techniques/scanning-electron-microscopy/>. (Accessed: 3rd October 2019)
113. Cleaves, H. J., Jonsson, C. M., Jonsson, C. L., Sverjensky, D. A. & Hazen, R. M. Adsorption of nucleic acid components on rutile (tio<sub>2</sub>) surfaces. *Astrobiology* **10**, 311–323 (2010).
114. Yagub, M. T., Sen, T. K. & Ang, H. M. Equilibrium, kinetics, and thermodynamics of methylene blue adsorption by pine tree leaves. *Water. Air. Soil Pollut.* **223**, 5267–5282 (2012).
115. Russo, V., Tesser, R., Trifuoggi, M., Giugni, M. & Di Serio, M. A dynamic

- intraparticle model for fluid–solid adsorption kinetics. *Comput. Chem. Eng.* **74**, 66–74 (2015).
116. Sivashankar, R., Sathya, A. B., Vasantharaj, K. & Sivasubramanian, V. Magnetic composite an environmental super adsorbent for dye sequestration - A review. *Environ. Nanotechnology, Monit. Manag.* **1–2**, 36–49 (2014).
  117. Cooney, D. O. *Adsorption design for wastewater treatment*. (Lewis Publishers, 1999).
  118. Yagub, M. T., Sen, T. K., Afroze, S. & Ang, H. M. Dye and its removal from aqueous solution by adsorption: A review. *Adv. Colloid Interface Sci.* **209**, 172–184 (2014).
  119. Simonin, J. P. On the comparison of pseudo-first order and pseudo-second order rate laws in the modeling of adsorption kinetics. *Chem. Eng. J.* **300**, 254–263 (2016).
  120. Keyhanian, F., Shariati, S., Faraji, M. & Hesabi, M. Magnetite nanoparticles with surface modification for removal of methyl violet from aqueous solutions. *Arab. J. Chem.* **9**, S348–S354 (2016).
  121. Stephen Inbaraj, B. & Chen, B. H. Dye adsorption characteristics of magnetite nanoparticles coated with a biopolymer poly( $\gamma$ -glutamic acid). *Bioresour. Technol.* **102**, 8868–8876 (2011).
  122. Giles, C. H., Smith, D. & Huitson, A. A general treatment and classification of the solute adsorption isotherm. I. Theoretical. *J. Colloid Interface Sci.* **47**, 755–765 (1974).
  123. Yildirim, Z. E., Ilis, G. G., Mobedi, M. & Ülkü, S. Effect of isotherm shape on mass transfer in an adsorbent particle; An isothermal adsorption process. *Open Transp. Phenom. J.* **3**, 40–48 (2011).
  124. Davies, M. J., Taylor, J. I., Sachsinger, N. & Bruce, I. J. Isolation of Plasmid DNA Using Magnetite as a Solid-Phase Adsorbent. *Anal. Biochem.* **262**, 92–94 (1998).
  125. Nakagawa, T. *et al.* Capture and release of DNA using aminosilane-modified bacterial magnetic particles for automated detection system of single nucleotide polymorphisms. *Biotechnol. Bioeng.* **94**, 862–868 (2006).
  126. Chiang, C.-L., Sung, C.-S., Wu, T.-F., Chen, C.-Y. & Hsu, C.-Y. Application of superparamagnetic nanoparticles in purification of plasmid DNA from bacterial cells. *J. Chromatogr. B* **822**, 54–60 (2005).

127. Zhang, H.-P., Bai, S., Xu, L. & Sun, Y. Fabrication of mono-sized magnetic anion exchange beads for plasmid DNA purification. *J. Chromatogr. B* **877**, 127–133 (2009).
128. Fontana, M. & Buiatti, S. Amino Acids in Beer. *Beer Heal. Dis. Prev.* 273–284 (2009).
129. Wunderlich, S., Zürcher, A. & Back, W. Enrichment of xanthohumol in the brewing process. *Mol. Nutr. Food Res.* **49**, 874–881 (2005).

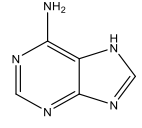
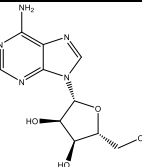
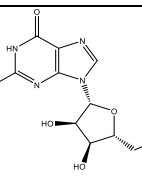
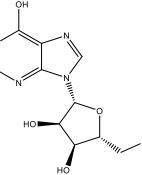




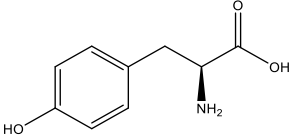
# **Annexes**

## A. Properties of molecules

**Tab. 1** – Purines properties (structure, molecular formula, and weight, CAS, Water solubility, melting point Log  $K_{ow}$  and pKa (Strongest acid and strongest basic)); adapted from pubchem.

Name	Structure	Molecular formula	Molecular weight (g/mol)	CAS	Water solubility (mg/L)	Melting point (°C)	Log Kow	pKa (Strongest acid)	pKa (Strongest basic)
Adenine		$C_5H_5N_5$	135.13	73-24-5	1030 (at 25 °C)	360	-	10.29	4.15
Adenosine		$C_{10}H_{13}N_5O_4$	267.24	58-61-7	5100 (at 25 °C)	234 – 236	-1.05	12.4	3.6
Guanosine		$C_{10}H_{13}N_5O_5$	283.24	118-00-3	700 (at 18 °C)	239	-1.90	10.16	1.79
Inosine		$C_{10}H_{12}N_4O_5$	268.23	58-63-9	15800 (at 20 °C)	218	-2.10	6.94	2.74

**Tab. 2** – Amino acids properties (structure, molecular formula, an weight, CAS, Water solubility, melting point Log  $K_{ow}$  and  $pK_a$  (Strongest acid and strongest basic)); adapted from pubchem.

Name	Structure	Molecular formula	Molecular weight (g/mol)	CAS	Water solubility (mg/L)	Melting point (°C)	Log $K_{ow}$	$pK_a$ (Strongest acid)	$pK_a$ (Strongest basic)
Tyrosine		$C_9H_{11}NO_3$	181.19	60-18-4	479 (at 25 °C)	343	-2.3	9.11	2.20

## B. Purine calibration curves

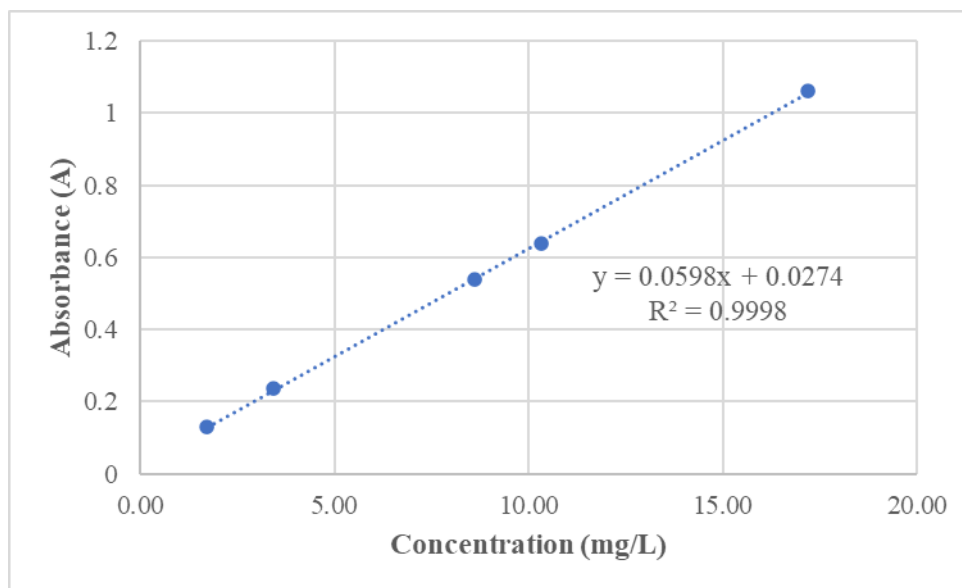


**Fig. 1** -Calibration curve for adenosine determined by UV-Vis spectroscopy at 260 nm.

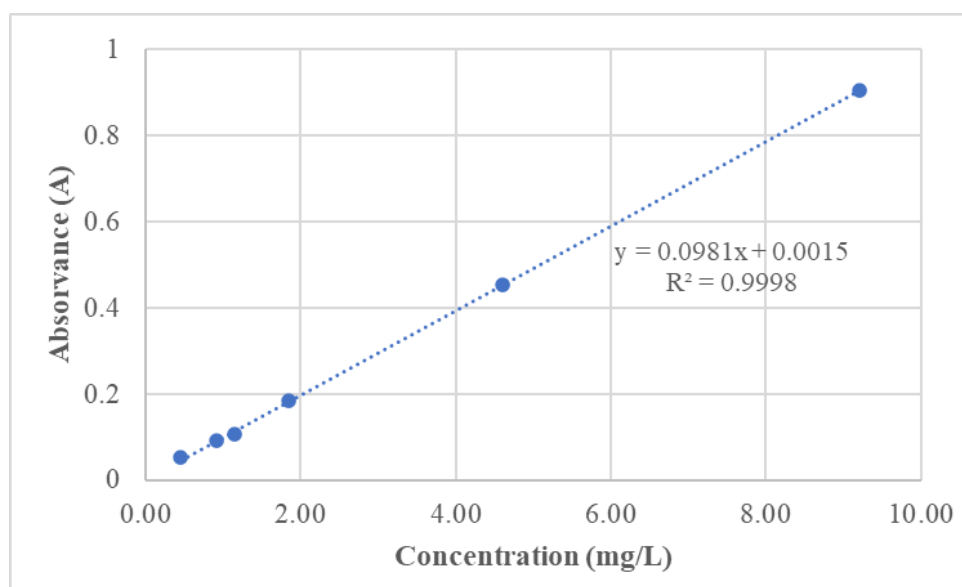


**Fig. 2**- Calibration curve for adenine determined by UV-Vis spectroscopy at 260 nm.

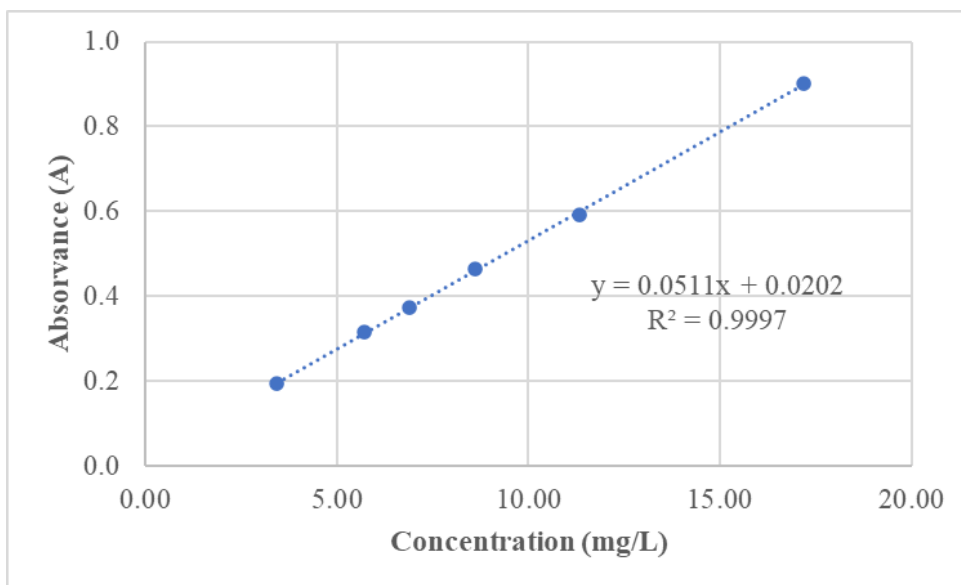


**Fig. 3** - Calibration curve of guanosine determined by UV-Vis spectroscopy at 252 nm

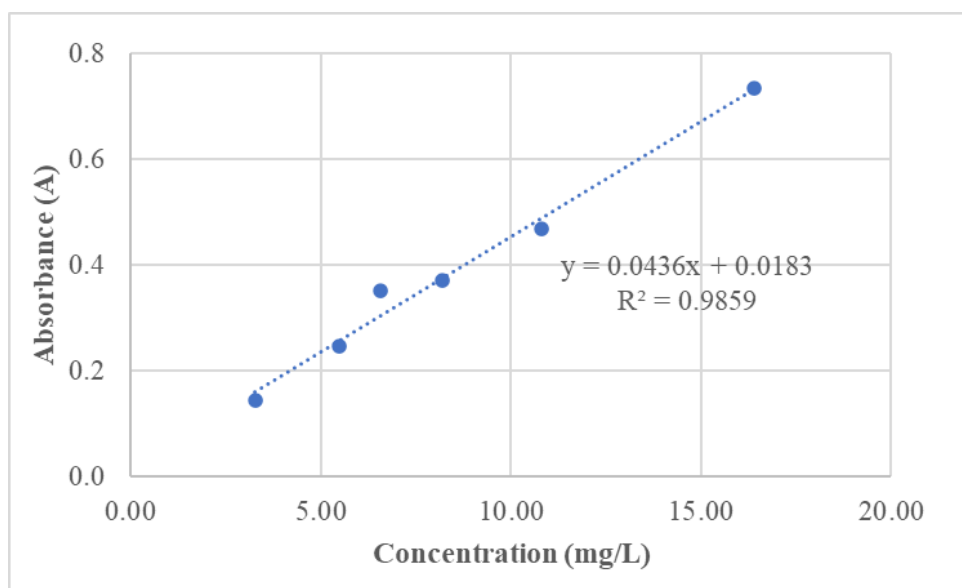


**Fig. 4** - Calibration curve for inosine determined by UV-Vis spectroscopy at 255 nm.

### C. Properties of cation precursor

**Tab. 3** - Values used of Volume (V), Molar mass (M), density and % of w/w.

Material	V (mL)	M (g/mol)	d (g/mL)	% (w/w)
[Si][C <sub>3</sub> ]Cl	5	198.72	1.07	0.98
[Si][C <sub>3</sub> C <sub>1</sub> Im]Cl	5	83.1	1.03	0.99
[Si][N <sub>3114</sub> ]Cl	5	101.19	0.72	0.99
[Si][N <sub>3222</sub> ]Cl	5	101.19	0.73	0.99
[Si][N <sub>3444</sub> ]Cl	5	185.35	0.78	0.99
[Si][N <sub>3888</sub> ]Cl	5	353.67	0.81	0.98

#### D. DNA Kinetic assays

**Tab. 4** – Adsorption time (minutes) used for kinetics assay with [Si][C<sub>3</sub>C<sub>1</sub>Im]Cl and respective results: absorbance obtained (with FD = 2),% removal efficient (%) and amount of ug DNA adsorbed per gram of material.

Time (minutes)	Abs <sub>260 nm</sub>	% AE	C <sub>e</sub> µg/mL	Q <sub>e</sub> (µg/mg)
0	0.345	0.00	34.5	0.00
2	0.144	58.26	14.4	1.96
5	0.142	58.84	14.2	1.97
15	0.143	58.55	14.3	1.96
30	0.143	58.55	14.3	1.96
50	0.15	56.52	15	1.90
90	0.152	55.94	15.2	1.88
120	0.162	53.04	16.2	1.78

**Tab. 5** - Adsorption time (minutes) used for kinetics assay with [Si][N<sub>3114</sub>]Cl and respective results: absorbance obtained (with FD = 2).% removal efficient (%) and amount of ug DNA adsorbed per gram of material.

Time (minutes)	Abs260 nm	% AE	Ce (µg/m L)	Qe (µg/mg)
0	0.499	0.00	49.9	0.00
2	0.315	36.87	31.5	1.79
5	0.3	39.88	30	1.94
15	0.29	41.88	29	2.03
30	0.31	37.88	31	1.84
45	0.298	40.28	29.8	1.96
60	0.325	34.87	32.5	1.69



**Tab. 6** - Adsorption time (minutes) used for kinetics assay with [Si][N<sub>3222</sub>]Cl and respective results: absorbance obtained (with FD = 2).% removal efficient (%) and amount of ug DNA adsorbed per gram of material.

Time (minutes)	Abs <sub>260 nm</sub>	% Remotion	C <sub>e</sub> µg/mL	Qe (µg/mg)
0	0.332	0	16.6	0.00
2	0.171	48.49	8.55	0.81
5	0.16	51.81	8	0.86
15	0.165	50.30	8.25	0.84
35	0.18	45.78	9	0.76
45	0.175	47.29	8.75	0.79
60	0.183	44.88	9.15	0.75
90	0.151	54.52	7.55	0.72

## E. DNA isotherms assays

**Tab. 7** - Equilibrium concentration of DNA after adsorption ( $C_e$ ), the concentration of adsorbate in the solid phase ( $q_e$ ), at room temperature.

[Si][C <sub>3</sub> C <sub>1</sub> Im]Cl				[Si][N <sub>3114</sub> ]Cl				[Si][N <sub>3222</sub> ]Cl			
C <sub>o</sub> (μg/mL)	C <sub>e</sub> (μg/mL)	q <sub>e</sub> (μg/mg)	AE (%)	C <sub>o</sub> (μg/mL)	C <sub>e</sub> (μg/mL)	q <sub>e</sub> (μg/mg)	AE (%)	C <sub>o</sub> (μg/mL)	C <sub>e</sub> (μg/mL)	q <sub>e</sub> (μg/mg)	AE (%)
13.25	8.90	0.40	32.83	10.15	6.35	0.38	37.44	10.15	6.35	0.38	37.44
17.25	14.20	0.31	17.68	16.70	9.40	0.74	43.71	16.60	8.00	0.98	51.81
25.15	17.40	1.02	36.03	22.20	14.50	0.77	34.68	16.70	11.20	0.58	32.93
27.2	17.75	0.71	29.42	29.90	16.60	1.37	44.48	29.90	17.80	1.28	40.47
245.2	52.00	19.40	78.79	61.30	40.00	2.22	34.75	102.40	84.30	1.77	17.68
486	96.00	39.00	80.25	174.60	104.60	6.70	40.09	762.00	741.00	2.10	2.76
671.2	212.00	43.32	68.41	486.00	374.00	11.20	23.05				